EARTHQUAKE INPUT MECHANISMS FOR DAM–FOUNDATION INTERACTION

by

MOHAMED BOUGHOUFALAH

Department of Civil Engineering and Applied Mechanics
McGill University
Montreal, Canada

February 1988

A thesis submitted to the Faculty of Graduate Studies and Research in partial fulfillment of the requirements for the degree of Master of Engineering

To My Parents

ABSTRACT

The seismic design of concrete dam–foundation–reservoir systems, must be able to ensure the survivability of these structures to extreme magnitude earthquakes. The need to represent non homogeneous geometrical and material foundation properties, and to predict damages which are generally due to non–linear effects implies that the solution must be determined in the time domain.

This study is concerned with the evaluation of four different earthquake input mechanisms that are suitable for time domain analysis of dam–foundation systems. These are:

A) the standard rigid base input model,

B) the massless foundation input model,

C) the deconvolved base rock input model,

D) the free-field dam–foundation interface input model,

The relative performances of various coordinates reduction techniques to solve the resulting time domain dynamic equilibrium equations have also been investigated. Parametric studies have been conducted from numerical experiments by applying the proposed earthquake input mechanisms to simplified 2–D finite element models of gravity dam–foundation systems. The principal parameters retained in the analyses were the ratio of the modulus of elasticity between the foundation rock and the concrete dam and the damping ratio of the foundation.

It has been found that the use of model A is not acceptable, producing significant artificial amplifications. Model C, which is theoretically the most accurate model, and model D produced results which were almost identical for the complete range of selected parameters. Model B although not as accurate as models C and D can be used for practical analyses if a proper modelling of the energy dissipation characteristics of the foundation is provided in the mathematical model. Coordinate reduction techniques

based on the derived load dependent Ritz transformation vectors have been shown to reduce very significantly the cost of the analysis without major loss in the accuracy of the response.

RÉSUMÉ

La conception parasismique de systèmes barrage–fondation–réservoir, doit assurer une performance adéquate de ces structures lorsque soumises à des séismes de magnitude extrême. La nécessité de représenter une géométrie et des propriétés non-uniformes de la fondation et de prédire d' éventuels dommages, dus généralement à des effets non-linéaires, implique que la solution soit déterminée dans le domaine du temps.

Cette étude se consacre à l'évaluation de quatre méthodes différentes d'application du chargement sismique, qui peuvent être utilisées pour l'étude dans le domaine du temps d'un barrage poids et de l'interaction avec sa fondation. Ces méthodes sont:

A) le modèle standard d'application à la base rigide du rocher,

B) le modèle de fondation sans masse,

C) le modèle d'application de l'accélérogramme déconvolué à la base du rocher,

D) le modèle d'application de l'accélérogramme enregistré au niveau de la surface à l'interface du barrage et de la fondation.

Une étude comparative de l'efficacité de différentes techniques de réduction du nombre de coordonnées pour la résolution des équations d'équilibre dynamique du système barrage-fondation a également été complétée. Des études paramétriques ont été menées à partir de simulations numériques qui ont consisté à appliquer les quatre méthodes proposées au modèle bidimensionnel d'éléments finis, utilisé pour la représentation du système barrage–fondation. Les paramètres retenus étaient le rapport des modules d'élasticité du barrage et de la fondation rocheuse et l'amortissement de la fondation.

Il a été montré que l'utilisation du modèle A est inacceptable, puisqu'il produit des amplifications artificielles très significatives. Le modèle C, qui est théoriquement le plus précis, et le modèle D ont produit des résultats presque identiques pour toutes les combinaisons de paramètres considérées. Le modèle B bien que moins précis que les

modèles C et D peut être utilisé en pratique si une idéalisation adéquate des mécanismes de dissipation d'énergie de la fondation est incluse dans le modèle mathématique. Il a été aussi montré que l'application des techniques de réduction de coordonnées basées sur les vecteurs de Ritz, dépendants du chargement, permettait de réduire d'une façon notable le coût de l'analyse sans pour autant sacrifier la précision des résultats.

ACKNOWLEDGMENTS

The author wishes to express his deepest gratitude to his supervisor, Professor P. Léger, for his guidance, valuable suggestions and constant encouragment during the course of this study and the writing of the thesis.

The support of the Ministry of Higher Education and Scientific Research of Algeria in granting the author a scholarship for his graduate studies is gratefully acknowledged.

The author is also grateful to the National Science and Engineering Research Council of Canada for their financial assistance.

Thanks are also due to all the members of my familly for their encouragment and morale support.

Finally the author wishes to express his gratitude to the staff members and his fellow graduate students in the Civil Engineering Department at McGill University for providing helpful and constructive criticism.

TABLE OF CONTENTS

LIST OF FIGURES

LIST OF TABLES

CHAPTER 1

INTRODUCTION

1.1 Overview and Objectives

Dynamic analysis of concrete dams, subjected to earthquake ground motions, has been the subject of much research since the mid sixties. Although there are no documented failures of concrete dams subjected to earthquakes, there are however, some cases where this type of dams have suffered major structural damages. Some of the concrete dams which experienced such severe damages due to earthquakes, include the Ponteba dam in Algeria, in 1954, the Hsinfengkiang dam in China, in 1962, and the Koyna dam in India, in 1967[1].

The consensus was that the method used to analyze these dams had some major flaws in predicting their structural response when subjected to seismic loading. The method used in the earthquake response was the pseudo-static method. This method consists of determining the structural behavior of the dam subjected to a set of static loads obtained from average horizontal and vertical ground accelerations of a specified seismic zonal map. The hydrodynamic forces are determined using Westergaard's approximation[2] for an equivalent mass of water to move with the dam. The pseudo-static method does not consider the dynamic response characteristics of the dam–foundation–reservoir system, nor the characteristics of the earthquake ground motions. Studies on the earthquake performance of Koyna dam[3] have shown that stresses in gravity dams found by applying the pseudo-static method, have little resemblance to the dynamic response of such dams when subjected to earthquake ground motions.

The development of the finite element method and recent advances in dynamic analyses, as well as the progress in the field of computer science, make the use of realistic analysis of the seismic response of dams possible. This has led to the development of new regulations concerning the analysis and design of concrete dams. In the United States several agencies such as the "U.S. Bureau of Reclamation", the "U.S Corps of Engineers" and the "U.S. Commission on Large Dams", have had an ongoing interest in the safety of dams since the early seventies[4,5,6]. These agencies have been involved in an extensive program aimed at determining the safety of existing dams and also in formulating new design criteria for dams. In contrast to the pseudo-static method of analysis previously used, the new regulations consider in more realistic terms the dynamic properties of the dam, the local seismicity of the site and the interaction among the dam, reservoir and foundation rock.

The three basic steps in a realistic analytical evaluation of the seismic safety of a dam are as follows[7]:

1– Estimation of the maximum expected earthquake excitation.

2– Analysis of the response to this dynamic input.

3– Comparison of predicted response with the strength and deformation capacity of the structure.

The selection of the design earthquake may well be the most important part of this total procedure. The first step in this process is to investigate the geologic and seismic conditions in the region of the intended site, the consequences of failure and hazards associated with the facility. The second step is to select the operating basis earthquake (OBE) and the maximum design earthquake (MDE), on the basis of an integrated evaluation of the previously defined earthquake factors. The OBE represents the maximum level of ground shaking that can be expected to occur at the site during the economic life of the dam. The MDE is the most severe earthquake associated with the region, it is generally equated to the maximum credible earthquake (MCE). The dam should be able to resist the OBE without any significant damages. In the case of the MDE however, the main criterion is to avoid any release of the water contained in the reservoir. To remain economical the design of the dam subjected to the MDE should not prevent all damages possibilities, but control what can be considered as an acceptable level of damage.

This design philosophy admits that stresses exceeding the linear elastic range can be acceptable and will thus indicate a non-linear behavior of the structure. These non-linearities may take the form of concrete cracking, opening of joints between adjacent monoliths or uplift at the dam foundation-interface and cavitation at the dam-reservoir interface. Numerical techniques to treat the dam-foundation-reservoir dynamic interaction problem have been mainly concerned with frequency domain methods. However, frequency domain techniques can not solve non-linear problems and are relatively inefficient for three dimensional problems. The other alternative to solve the dam- foundation-reservoir interaction problem, is the solution in the time domain. This will require a proper mathematical modeling of the reservoir, the dam and the foundation.

Specific earthquake input mechanisms can be associated with particular foundation models and it will be obviously questionable to put a great deal of effort in defining the characteristics of ground motions if the way in which they are applied can influence the structural response significantly.

The work presented in this report is the first part of a research program aimed at developing efficient numerical techniques in the time domain that can solve the soil-fluid-structure interaction problem in two and three dimensions and at the same time leave the door open for the practical solution of locally non-linear problems such as the uplift and relative slip at the interface of the structure foundation system.

The principal objectives of this study are:

a- To assess the influence of various earthquake input models, such as;

  - the standard rigid base rock input model,
  - the massless base rock input model,
  - the deconvolved base rock input model,
  - the free-field concrete rock interface model,

on the time domain structural response of a dam–foundation–reservoir system, in order to get an appreciation of the significance of the effort to be put in the definition of the intensity and frequency properties of a design earthquake.

b- To determine a specific range of parameters such as the ratio of modulus of elasticity between the foundation and the structure and the damping ratio in the foundation rock, for which particular input mechanisms are more suitable to be used in order to get an accurate time domain seismic response of the dam- foundation-reservoir system.

c- To develop efficient time-domain coordinate reduction procedure, to compute the earthquake response of a dam-foundation-reservoir system.

1.2 Review of Past Work

The earthquake analysis of concrete dams has come a long way, progressing from simple pseudo-static methods for computing design forces, to sophisticated dynamic analysis. The system represented by the dam-foundation-reservoir subjected to an earthquake, can be solved by either a frequency domain solution in the linear range or by a time domain solution in the linear or the non-linear range. The frequency domain approach has the advantage to include the frequency-dependent properties of the interacting soil and fluid systems.

The dam–foundation–reservoir system can obviously be partitioned into three substructures: the dam, the reservoir and the foundation rock, to evaluate the seismic response. The problem is compounded by the fact that these three substructures do not behave independently. Early works, investigated the effect of the dam–reservoir interaction[8,9] and the dam–foundation rock interaction[10] separately.

Chopra and Chakrabarti[11] developed over a period of several years, a technique whereby a two dimensional reservoir–dam system is divided into two substructures. The flexible dam substructure is represented as an assemblage of finite elements and the reservoir substructure is represented as a semi–infinite continuum governed by the wave equation. The response of the total system is computed by combining the complex frequency response function of the hydrodynamic forces with modal frequency response functions of the dam and calculating the response to arbitrary excitation through Fourier integration. The water impounded in the reservoir could also be idealized as a finite region of irregular geometry adjacent to the dam, connected to a channel of uniform cross section extending to infinity in the upstream direction[12].

The other important effect influencing the earthquake response of dam-foundation-reservoir systems, is the interaction between the dam and the foundation rock. A lot of work related to that problem has been done under the heading soil-structure interaction, and a lot has been gained from seismic studies of nuclear power plants in the recent years[13].

The methods of treating the soil-structure interaction problem in the frequency domain can be divided into three categories :

(i) Complete methods[14]

(ii) Hybrid methods[15]

(iii) Substructure methods[16]

For massive structures such as concrete dams, the substructure method was mostly used to treat the dam–foundation interaction problem. Chopra and Perumalswami[10] used the idea of separately analyzing the foundation rock system, idealizing it as an elastic half–space, and then using its frequency dependent compliance characteristics in the determination of the structural behavior. Throughout the last two decades the substructure method to treat the dam–foundation–reservoir system subjected to an earthquake loading, has been refined. This has led recently to the development of realistic frequency domain procedures and related computer programs, for the linear earthquake response analysis of concrete gravity dams idealized as two–dimensional systems[17,18] and also for concrete dams in general treated as three dimensional systems[19].

The major drawback of the frequency domain approach, is that it can not solve non–linear problems; these can only be treated effectively in the time domain. Numerical techniques to solve the earthquake response of a dam–foundation–reservoir system in the time domain received very little attention. Wilson[20] solved the problem of a dam on a layered foundation by constructing a large planar finite element mesh through the entire system and solving for a base rock seismic excitation using the step–by–step integration procedure. However this approach was relatively expensive due to the large number of degrees–of–freedom (d.o.f) of the discretized model. Methods to treat the soil–structure interaction problem in the time domain can be divided into three main groups:

(i) Complete methods[21,22]

(ii) Boundary methods[21,23]

(iii) Volume methods[21]

The problem inherent for all these three methods is the cost of the analysis. Recently Léger and Wilson[24], Bayo and Wilson[25], and Clough and Wilson[26] presented some coordinate reduction procedures suitable for time domain analysis of soil–structure problems.

In current practice in engineering offices, the complete method is the one that is used most conveniently for Canalysis of the earthquake response of concrete gravity dams. A finite element discretization is used for both the dam and the foundation rock. The hydrodynamic forces are computed by the added mass approach originated by

Westergaard[2]. The input earthquake motions, generally a free-field recorded accelerogram, can then be introduced according to one of the following input mechanisms:

A- The standard rigid base input model[20,27], where the free field motions recorded at the ground surface are applied directly at the base of the deformable foundation rock.

B- Massless foundation rock model[28,29,30], which is the same as the previous model but with the deformable foundation rock assumed to be massless to reduce the number of dynamic d.o.f.

C- Deconvolved base rock input model[29,31], where the base rock motions at the deformable foundation rock are derived from the free–field motions by the deconvolution process.

D- The free field concrete rock interface model[21,22,7], where the equations of motion of the complete dam–foundation rock system are rewritten so that the effective seismic input is expressed directly in terms of the free field motions.

Clough and Chang[32] discussed the possibility of combining some of these input mechanisms to develop appropriate cross–canyon seismic excitation of arch dams. Although no quantitative conclusions could be reached, it was pointed out that the use of different input assumptions can lead to significant variations in the structural response.

1.3 Scope of the Present Study

In this report, the four proposed earthquake input mechanisms are applied to a simplified two-dimensional finite element model representing a gravity dam–foundation–reservoir system and the response is computed in the time domain. Comparative studies of the resulting response quantities are carried out for the various controlling parameters such as, the ratio of moduli of elasticity of the foundation rock and the concrete dam and the level of damping provided by the foundation rock. The earthquake structural response is measured in terms of the acceleration levels, structural displacements and related stresses at representative locations.

In a second phase coordinate reduction techniques to solve the time domain dynamic equilibrium equations of the dam-foundation-reservoir system are investigated. The damping levels provided by the dam and the foundation rock are usually different, as a consequence the modal equations of motion are coupled, which corresponds to a condition of non–proportional damping. Various solution strategies including the non–proportional damping effect are presented.

In Chapter 2, the formulations of the four proposed earthquake input mechanisms models are presented. The advantages and drawbacks of each model are also discussed. The mathematical model representing the dam-foundation-reservoir system for the actual numerical applications is presented in Chapter 3. The structural behavior of this model for free vibration response is investigated and a preliminary earthquake analysis is carried out. In Chapter 4, the relative performance of the four proposed models of earthquake input mechanisms are investigated in terms of typical response quantities of interest which are derived for various range of controlling parameters. In Chapter 5, coordinate reduction techniques suitable for the time domain solution of the dam–foundation–reservoir system subjected to earthquake ground motions, are presented. The response is expressed in terms of the superposition of a truncated vector basis, using either the eigenvectors of the free vibration eigenproblem or the derived load dependent Ritz transformation vectors. The performance of different solutions strategies to compute the earthquake response of the non–proportionally damped dam–foundation system, is also investigated. Finally the conclusions, recommendations and some remarks concerning the needs for future research on the time domain solution of dam–foundation–reservoir systems are presented in Chapter 6.

CHAPTER 2

MODELS FOR THE EARTHQUAKE INPUT MECHANISMS

2.1 Introduction

In this chapter, the equations of dynamic equilibrium for the four models of earthquake input mechanisms described in Chapter 1 (Section 1.2) are examined. A typical concrete gravity dam is chosen to formulate these different models. Although the dam is considered to be constructed from a homogeneous, elastic and isotropic material, its foundation is generally heterogeneous and anisotropic. The system considered is idealized by a two-dimensional linear elastic, finite element model which includes the entire concrete dam, plus a portion of the rock on which the dam is founded. The hydrodynamic effect is implicitly included by the added mass approach. The seismic loading is represented by a free-field recorded accelerogram time history $\ddot{\underline{v}}_g(t)$, acting in the horizontal direction, perpendicular to the longitudinal axis of the dam. The problem is simplified by assuming that the motions in the free–field could be described by vertically propagating waves.

The earthquake input mechanisms considered, and the related dam–foundation rock models, are shown in Figure 2.1. The idealization of the dam–foundation rock system is essentially the same for the four models, except for model B where the foun-

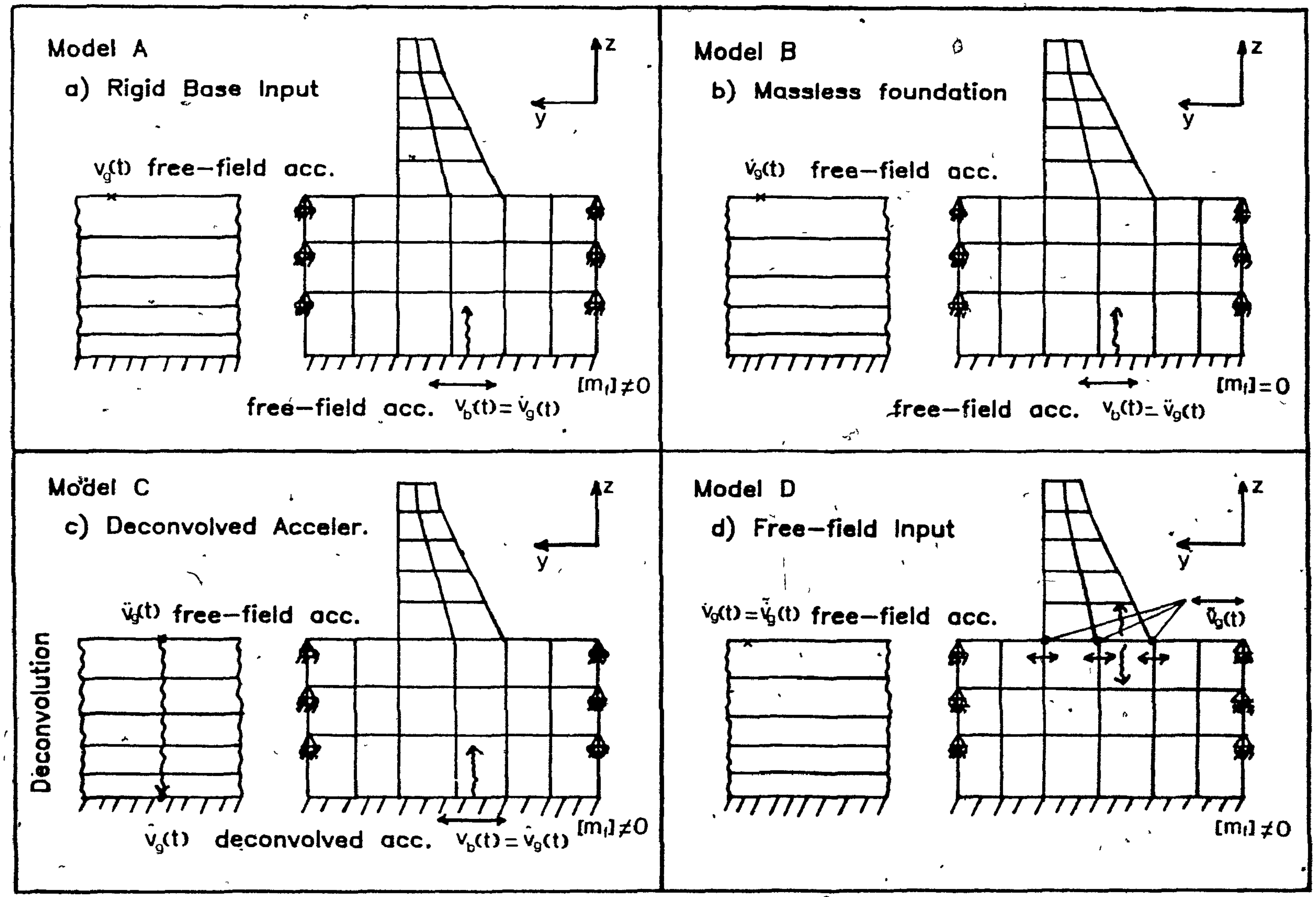

Figure 2.1 Representation of the Four Proposed Earthquake Input Mechanisms.

dation rock is considered to be massless. Note that appropriate supports are employed at all vertical boundaries at the dam-foundation rock system shown in Figure 2.1, to model its response to the horizontal earthquake motions.

2.2 Model A: Rigid Base Input

In this model the specified free-field accelerogram time history, is applied at the rigid base rock of the finite element model (Fig. 2.1a)). These base motions propagate vertically through the deformable foundation rock, by elastic wave mechanisms. The earthquake that reaches the interface between the concrete dam and the foundation rock, will thus be different, in frequency content and in intensity, as compared with the motions produced by the real rigid base input which has its focus beneath the local base rock.

The equations of motion for the finite element model of Figure 2.1a) subjected to a single horizontal earthquake component may be written as:

$$[M]\ddot{\underline{v}} + [C]\dot{\underline{v}} + [K]\underline{v} = -[M]\underline{r}_v \ddot{\underline{v}}_b(t) \tag{2.1}$$

in which [M], [C] and [K] are the finite element mass, damping and stiffness matrices for the complete dam–foundation–reservoir system, $\underline{v}$, $\dot{\underline{v}}$ and $\ddot{\underline{v}}$ are respectively the displacement, velocity and acceleration vectors of the nodal points, $\ddot{\underline{v}}_b(t)$ is the specified base earthquake acceleration time history and $\underline{r}_v$ is the influence coefficient vector, expressing the nodal displacements resulting from a uniform horizontal unit value of the base rock displacement, $\underline{v}_b = \underline{1}$.

The application of this rigid base input model is relatively simple, because no modifications have to be made to the recorded accelerogram and also because the matrices representing the physical properties of the complete dam–foundation–reservoir system, and the specified seismic loading can be used directly. This makes possible the application of standard finite element program for the earthquake response analysis, in which the system properties are expressed in terms of global matrices.

The rigid base input model is not expected to give very accurate results, since the earthquake applied at the base rock has been actually recorded at the ground surface. This is a crude assumption knowing that when these free-field motions are applied at the base rock level they are modified firstly by propagation through the deformable foundation rock and secondly by the interaction between the dam and the foundation rock.

2.3 Model B: Massless Foundation Rock

This model has been proposed in the late seventies[33] and has been used extensively for seismic analysis of concrete dams since then[30,34,35]. The only difference with model A, is that the idealized foundation rock model is assumed to be massless. This results firstly, in a reduction in the number of dynamic d.o.f of the system. Secondly, the absence of mass makes the foundation rock function as a spring, in other words only the flexibility of the foundation rock is taken into account. Thus, the rigid base rock input motions are transmitted instantaneously through the foundation rock to the base of the dam, without any wave propagation effects. This will eliminate the problem of artificial amplification of the free–field accelerogram, as discussed for model A. If there were no dam-foundation interaction effects, the same free-field motions, applied at the base rock, would be observed at the surface of the foundation rock. It is thus appropriate to apply the free-field surface motions as the earthquake input at the base rock in this model.

The damping of the foundation rock in absence of mass is usually taken as zero, but this neglects the radiation damping of the foundation. Thus to assess the extent of this effect, two cases can be considered in the analysis: massless foundation rock including damping and massless foundation neglecting damping.

Basically the advantages of model A can be restated for model B, which are the simplicity of its application and the possibility of using standard finite element programs, for the earthquake response analysis. Furthermore, the dam vibrations will not be affected by the mass of the foundation. If a large volume of foundation rock with mass is included in the model, it is possible that the vibration modes of the foundation may tend to dominate the dynamic response of the dam such that the numerical solution can become more costly and ~~difficult to~~ implement.

Model B is expected to give better results than model A, however, the idealized foundation rock without mass does not totally model the dam–foundation interaction mechanism and it is not certain that the system frequencies given by this model will be valid.

2.4 Model C: Deconvolved Base Rock Input

A more realistic approach to the problem of the earthquake input mechanism, is to define more appropriate rigid base rock motions in equation (2.1). This can be achieved by performing a deconvolution analysis[31] to the recorded free–field accelerogram. This is equivalent to compute the base rock accelerogram which might have produced the free–field accelerogram, after propagation through the deformable foundation. This analysis requires the application of specialized computer programs to the free–field system. A program called "SHAKE" designed for the earthquake response analysis of horizontally layered sites[30], can be used to perform the deconvolution analysis. In this program, the foundation rock is assumed to be uniformly layered and extending to infinity in the horizontal direction. Then a shear beam model is used to idealize the deformable foundation, reducing the problem to a one-dimensional system. The deconvolved accelerogram is determined by the inverse application of the one-dimensional wave propagation equation. In order to verify the accuracy of the computed base rock accelerogram, a separate analysis has to be carried out. It consists in applying the computed deconvolved accelerogram at the base of the two–dimensional finite element model, representing the foundation rock and deriving the corresponding free-field accelerogram. The computed and the original free-field accelerograms are then compared by means of the corresponding pseudo-acceleration spectra (PSa). The two PSa should exhibit a close match especially at the periods of modes contributing significantly to the dynamic response of the dam–foundation–reservoir system. The complete procedure of the deconvolved base rock input mechanism is summarized in Figure 2.2.

The deconvolution analysis is a complex task to be achieved and the assumptions made in the program "SHAKE" illustrate some limitations to its general applicability. Indeed, the assumption of uniformly layered system can not be applied to any site. Furthermore, some adjustments may have to be made to the foundation rock properties, or to the parameters controlling the numerical stability of the procedure such that the deconvolved accelerogram obtained from the one-dimensional analysis will produce, after propagation through the two-dimensional finite element model representing the foundation, a free-field accelerogram for which the PSa coincides with the PSa of the original free–field accelerogram. It should be noted that this requirement might be theoretically avoided by assuming that the deconvolved accelerogram applied at the rigid base, beneath the deformable foundation rock was obtained by a one–dimensional deconvolution analysis of a specified free–field earthquake motions. This deconvolved accelerogram can then be arbitrarily applied to a two–dimensional model which includes different geological features than those retained in the deconvolution analysis. The actual computer implementation of the deconvolution analysis retained for this study will be discussed in more details in Chapter 4.

The results obtained from model C, will be obviously dependent upon the quality of the deconvolution process. Typical structural response quantities of interest found by applying the deconvolved accelerogram at the rigid base rock, should theoretically be more accurate than those obtained by applying models A and B. The main disadvantage

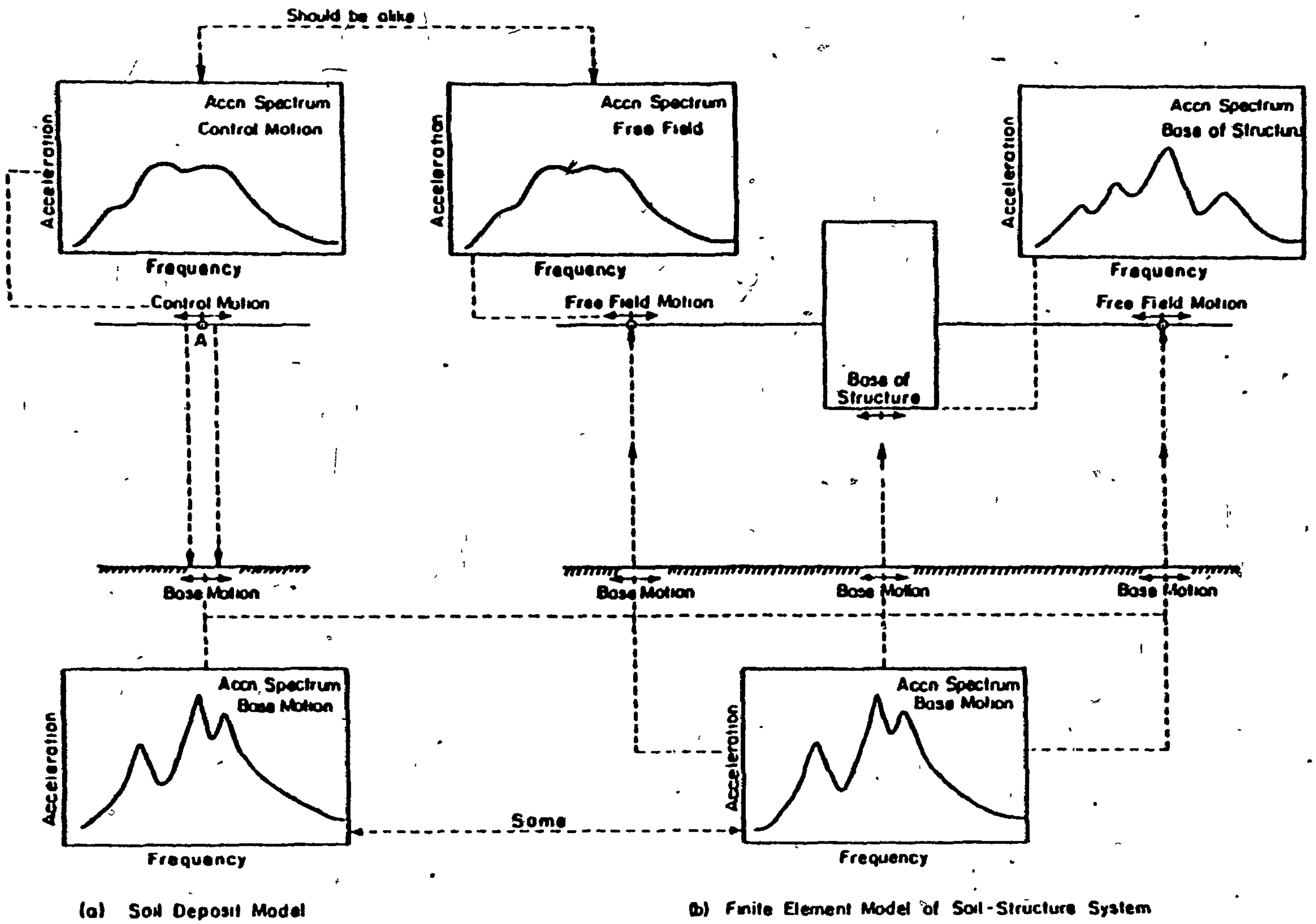

Figure 2.2 Representation of the Deconvolved Base Rock Input Process Adapted from Reference 13.

of model C is that the complete response analysis is rather tedious, since it involves two separate analyses. The first one, the deconvolution analysis, requires a specific computer program and some form of sensitivity analysis in order to be implemented reliably. The main advantages are that the dam–foundation interaction mechanisms will be well represented and the earthquake input motions will be treated in a more realistic manner.

2.5 Model D: Free–Field Input

An alternative approach to the problem of defining an appropriate earthquake input mechanism, is to express the effective seismic input in the equation of motion of the dam-foundation rock system directly in terms of the free-field motions recorded at the ground surface[7,21,22].

The formulation of this free-field input is presented in this section, Figure 2.3 illustrates the system considered and the corresponding properties.

The free-field response to the base rock excitation is expressed as follows[22]:

$$[\tilde{m}_f]\ddot{\underline{\tilde{v}}}_f + [\tilde{c}_f]\dot{\underline{\tilde{v}}}_f + [\tilde{k}_f]\underline{\tilde{v}}_f = -[m_b]\ddot{\underline{v}}_b - [c_b]\dot{\underline{v}}_b - [k_b]\underline{v}_b = \underline{F}_b \tag{2.2}$$

in which $[\tilde{m}_f]$, $[\tilde{c}_f]$ and $[\tilde{k}_f]$ represent the properties of the existing foundation rock before the dam is constructed and $\underline{\tilde{v}}_f$ represents the corresponding free–field motions of the system. The vector $\underline{F}_b$ represents the force exerted by the basement rock on the finite element model, $[m_b]$, $[c_b]$ and $[k_b]$ are the coupling terms expressing forces in the foundation material, due to motions of the basement rock $(\underline{v}_b)$.

The corresponding equation after construction of the dam may be written as:

$$[\tilde{m}_f + m_d]\{\ddot{\underline{\tilde{v}}}_f + \ddot{\underline{v}}^t\} + [\tilde{c}_f + c_d]\{\dot{\underline{\tilde{v}}}_f + \dot{\underline{v}}^t\} + [\tilde{k}_f + k_d]\{\underline{\tilde{v}}_f + \underline{v}^t\} = \underline{F}_b \tag{2.3}$$

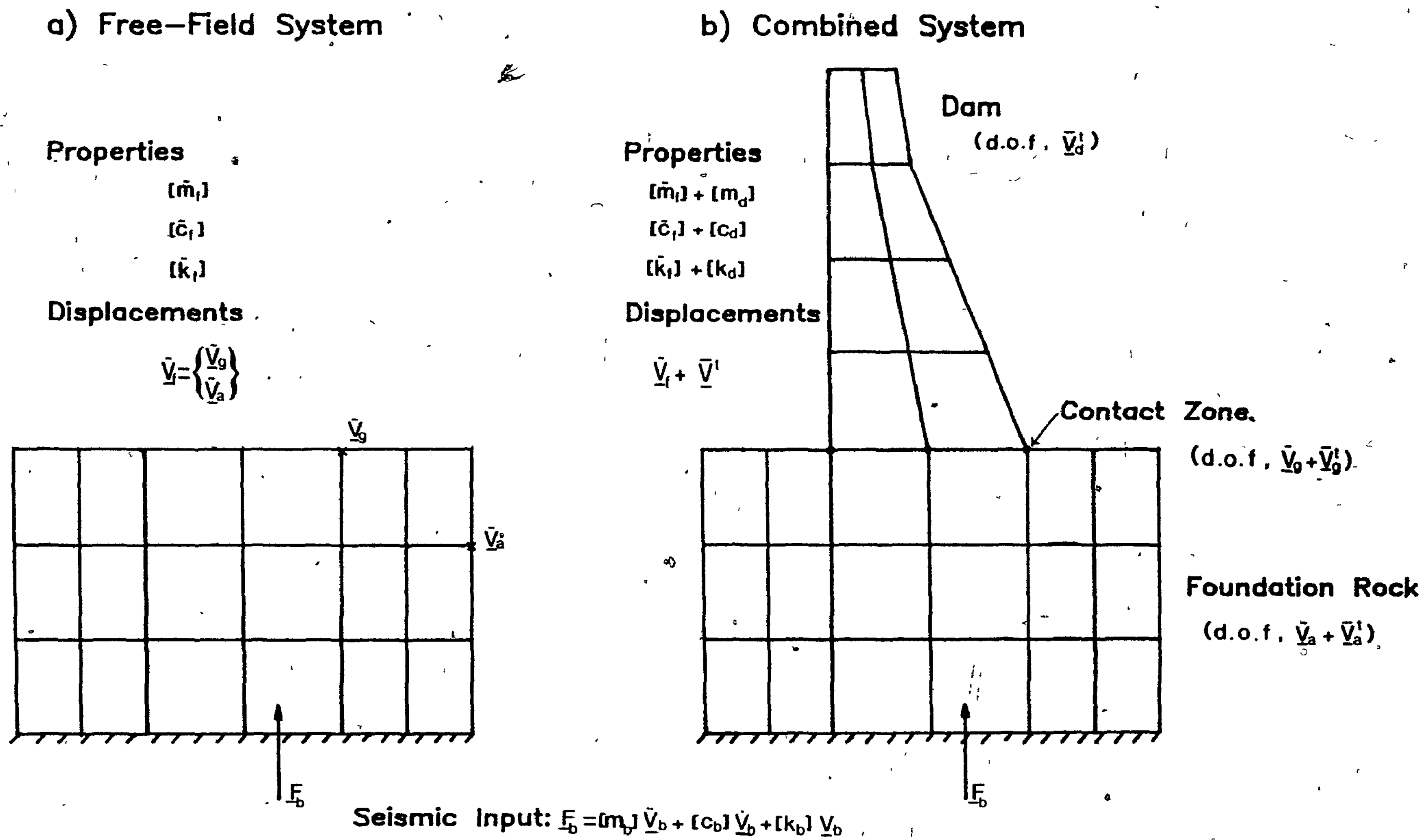

Figure 2.3 Formulation of the Free–Field Input Mechanism (Model D).

in which $[m_d]$, $[c_d]$ and $[k_d]$ are the dam properties and $\underline{v}^t$ represents the added response resulting from superimposing the dam on the free–field system. Substituting equation (2.2) into equation (2.3) one can reduce equation (2.3) to:

$$[\tilde{m}_f + m_d]\ddot{\underline{v}}^t + [\tilde{c}_f + c_d]\dot{\underline{v}}^t + [\tilde{k}_f + k_d]\underline{v}^t = -[m_d]\ddot{\tilde{\underline{v}}}_f - [c_d]\dot{\tilde{\underline{v}}}_f - [k_d]\tilde{\underline{v}}_f \tag{2.4}$$

Equation (2.4) could be further simplified, by partitioning the added and the free–field displacements as follows:

$$\underline{v}^t = \begin{Bmatrix} \underline{v}_d^t \\ \underline{v}_g^t \\ \underline{v}_a^t \end{Bmatrix} \qquad \tilde{\underline{v}}_f = \begin{Bmatrix} \underline{0} \\ \tilde{\underline{v}}_g \\ \tilde{\underline{v}}_a \end{Bmatrix} \tag{2.5}$$

in which the three partitions refer respectively to the d.o.f, in the dam, d.o.f at the dam–foundation interface, and the non–contact d.o.f in the foundation-rock (Fig. 2.3b)).

All physical property matrices are then partitioned accordingly, such that the dam and foundation mass matrices can be written as:

$$[m_d] = \begin{bmatrix} m_{dd} & m_{dg} & 0 \\ m_{gd} & m_{gg} & 0 \\ 0 & 0 & 0 \end{bmatrix} \qquad [\tilde{m}_f] = \begin{bmatrix} 0 & 0 & 0 \\ 0 & \tilde{m}_{gg} & \tilde{m}_{ga} \\ 0 & \tilde{m}_{ag} & \tilde{m}_{aa} \end{bmatrix} \tag{2.6}$$

Similar expressions can be written for the damping and stiffness matrices. Using the partitions of equations (2.5) and (2.6), one can rewrite equation (2.4) as follows:

$$\begin{gathered}[\tilde{m}_f + m_d]\ddot{\underline{v}}^t + [\tilde{c}_f + c_d]\dot{\underline{v}}^t + [\tilde{k}_f + k_d]\underline{v}^t = \\ -\begin{bmatrix} m_{gd} \\ m_{gg} \\ 0 \end{bmatrix}\ddot{\tilde{\underline{v}}}_g - \begin{bmatrix} c_{gd} \\ c_{gg} \\ 0 \end{bmatrix}\dot{\tilde{\underline{v}}}_g - \begin{bmatrix} k_{gd} \\ k_{gg} \\ 0 \end{bmatrix}\tilde{\underline{v}}_g\end{gathered} \tag{2.7}$$

These equations of motion can be cast in a simpler form by expressing the added response $\underline{v}^t$ as the sum of a dynamic component $\underline{v}$ and a pseudo-static component $\underline{v}^s$.

The pseudo-static component may be derived from equation (2.7) by eliminating the dynamic terms. Hence,

$$[\tilde{k}_f + k_d]\underline{v}^s = -\begin{bmatrix} k_{gd} \\ k_{gg} \\ 0 \end{bmatrix} \underline{\tilde{v}}_g$$

or

$$\underline{v}^s = [\tilde{r}]\,\underline{\tilde{v}}_g \tag{2.8}$$

in which

$$[\tilde{r}] = -[\tilde{k}_f + k_d]^{-1}\begin{bmatrix} k_{gd} \\ k_{gg} \\ 0 \end{bmatrix} \tag{2.9}$$

Thus

$$\underline{v}^t = \underline{v} + [\tilde{r}]\underline{\tilde{v}}_g \tag{2.10}$$

In principle, any desired spatial variation of the free–field components could be considered, however there seldom is sufficient information to specify such variation. If we assume the same free-field input motion at each contact point, equation (2.10) will reduce to:

$$\underline{v}^t = \underline{v} + [\tilde{r}]\underline{1}\tilde{v}_g$$

$$\underline{v}^t = \underline{v} + \underline{\tilde{r}}\tilde{v}_g \tag{2.11}$$

Equation (2.7) can thus be simplified to:

$$[\tilde{m}_f + m_d]\underline{\ddot{v}} + [\tilde{c}_f + c_d]\underline{\dot{v}} + [\tilde{k}_f + k_d]\underline{v} = -\left\{[\tilde{m}_f + m_d]\underline{\tilde{r}} + \begin{bmatrix} m_{gd} \\ m_{gg} \\ 0 \end{bmatrix}\right\}\ddot{\tilde{v}}_g \tag{2.12}$$

It can be noticed that the effective force vector on the right hand side of equation (2.12) is in terms of the free–field accelerations only. The stiffness dependent term has dropped out because the pseudo–static displacements were defined so that

$$[\tilde{k}_f + k_d][\tilde{r}] + \begin{bmatrix} k_{gd} \\ k_{ga} \\ 0 \end{bmatrix} = [0] \tag{2.13}$$

The damping dependent term due to support motions has also been omitted in equation (2.12), these forces being usually negligible either because the damping matrix is proportional to the stiffness matrix which would impose a condition similar to the one given by equation (2.13) or because these damping coefficients are themselves negligible.

The free–field input model (model D) can be seen as an improved version of the massless foundation model (model B). In both models B and D the original free–field accelerogram would be observed in the absence of the dam. In model B this is achieved by neglecting the inertial effect of the foundation rock whereas in model D this is done simply by rewriting the equations of motion in terms of the free–field motions. Thus the improvement in model D is that the mass of the foundation rock is taken into account in the analysis so that it will represent the dam–foundation interaction in a relatively more realistic manner. The formulation of model D is based on some basic assumptions. The first one was that the input motion at the level of the base rock is not modified when the dam is superimposed on the free–field system (equation 2.3). This is due to the fact that far from the structure the input is not considered to be affected by the presence of the dam[7]. The other basic assumption is to neglect the damping dependent term in equation (2.12) which suppose that, either the damping matrix is proportional to the stiffness matrix or that the damping coefficients are themselves negligible for a practical implementation of this formulation. The last assumption is that all interface nodes are subjected to the same free–field accelerogram. It is believed that this assumption will be reasonable for the contact surface at the base of a gravity dam. However for an arch dam where the free–field motions are not uniform along the canyon wall contact surface, such an assumption can be seriously questioned[7].

The free–field input mechanism if compared with the deconvolved input model, is advantageous in the sense that the analysis can be carried in one step since no preliminary analysis is required to define the base rock input because the equation of motion (equation 2.12) is expressed directly in terms of the free–field accelerogram. The comparative study between the free–field input model and the deconvolved input model will allow us to assess to what extent the assumptions made in the formulation of the free–field input model will affect the response quantities of interest. Comparisons between the free–field input model and the massless foundation model will illustrate the importance of the mass of the foundation rock on the dynamic behaviour of the dam–foundation–reservoir system.

2.6 Exploitation of the Response Quantities in the Analysis

In the seismic analysis of a dam–reservoir–foundation system, typical response quantities of engineering interest can be defined in terms of the displacements, the accelerations and the related stresses.

To illustrate the different displacement components resulting from applying a rigid base rock input (models A, B and C) using equation (2.1) and a free–field input (model D) using equation (2.12), let us consider the simple cantilever beam of Figure 2.4. This cantilever beam has three nodes, each one with a single d.o.f (lateral displacement). Node 3 represents the displacements of the dam, node 2 represents the displacements of the dam–foundation interface and node 1 represents the foundation displacements.

As can be seen in Figure 2.4 the dynamic displacements $\underline{v}$ derived from equation (2.1) and $\bar{\underline{v}}$ obtained from equation (2.12), are not computed with respect to the same location. To be able to make a comparative study between the four proposed earthquake input mechanisms, these response quantities should be expressed according

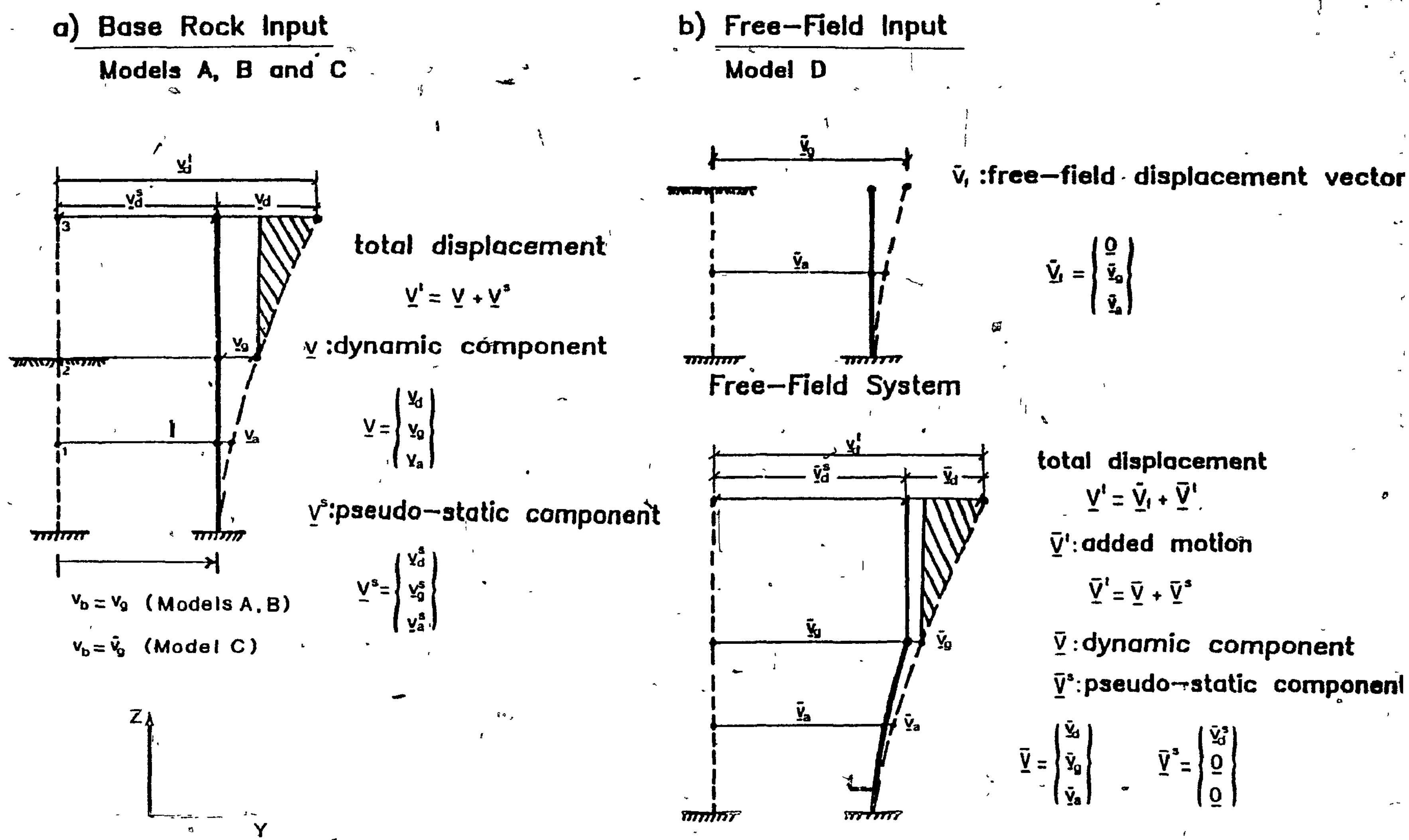

Figure 2.4 Displacement quantities Resulting from the Application of the Four Input Mechanisms

to a common reference. One way to do this will be to express the displacements in terms of total motions with respect to the initial position before the occurrence of the earthquake. For models A, B and C, the total dam displacements can be expressed as:

$$\underline{v}_d^t = \underline{v}_d + \underline{r}_y \underline{v}_b \tag{2.14}$$

in which $\underline{v}_d$ is the dynamic displacement vector found by solving equation (2.1) and $\underline{r}_y$ is the influence coefficient vector expressing nodal displacements due to a uniform unit horizontal displacement of the base rock. For model D the total displacements of the dam are given as:

$$\underline{v}_d^t = \underline{\bar{v}}_d + \underline{\tilde{r}\tilde{v}}_g \tag{2.15}$$

where $\underline{\bar{v}}_d$ is the dynamic displacement vector computed from equation (2.12) and the product $\underline{\tilde{r}\tilde{v}}_g$ is the pseudo–static displacement vector. Note that the pseudo-static displacements in model D are different from those of models A, B and C. Indeed $\underline{\tilde{r}}$ in equation (2.15) is the influence coefficient vector expressing the nodal displacements of the dam due to a uniform unit displacement applied at the base of the dam (not the base rock) $\underline{\tilde{v}}_g = \underline{1}$.

Expressing the displacements in total quantities has the inconvenient of requiring the application of the displacements corresponding to the input accelerogram, which are often not directly available. This procedure can be avoided by computing relative displacements quantities in the dam with respect to the displacements of the dam–foundation rock interface. Thus for models A, B and C these displacements can be written as:

$$\underline{v}_{rd} = \underline{v}_d - [\tilde{r}]\underline{v}_g \tag{2.16}$$

in which $\underline{v}_g$ is the dynamic displacement vector of the interface nodes (Fig. 2.4), $\underline{v}_d$ is the vector of nodal dam displacements computed from equation (2.1) and $[\tilde{r}]$ is defined in equation (2.9).

For model D, displacements relative to the dam–foundation interface can be expressed as:

$$\underline{v}_{rd} = \underline{\bar{v}}_d - [\tilde{r}]\underline{\bar{v}}_g \quad (2.17)$$

where $\underline{\bar{v}}_g$ is the dynamic component of the added displacement vector corresponding to the interface nodes found by solving equation (2.12) and $\underline{\bar{v}}_d$ is the dynamic displacement vector of the structural system, found from the same equation.

In this study, the dam displacements are computed relative to the displacements of the dam-foundation rock interface for all of the considered earthquake input mechanisms in order to make comparative analyses on a consistent basis.

CHAPTER 3

MATHEMATICAL MODELLING OF THE DAM–FOUNDATION–RESERVOIR SYSTEM

3.1 Introduction

The structural system considered in this report represents a section of the Koyna Dam in India, a typical concrete gravity dam which was subjected to an earthquake in 1967[3]. The system is idealized by a two–dimensional finite element model which includes the entire concrete dam, along with a portion of the rock on which the dam is founded.

The behavior of the dam structure during large amplitude motions depends on the extent to which the inertia forces can be transmitted across the joints. For concrete gravity dams with straight contraction joints, the inertia forces that develop during large amplitude motions are much greater than the shear forces that the joint can transmit. Therefore the joints would slip and the individual monoliths would vibrate independently. This was one of the observations from the study of the damages of the Koyna dam[3]. For such gravity dams, a two–dimensional plane stress model of the individual monoliths is an acceptable assumption for predicting the earthquake response. However, for dams with keyed contraction joints the above assumption is inappropriate and a two–dimensional plane strain system is more suitable.

For the concrete gravity dam selected for this study a plane stress model has been used, a unit slice taken normal to the longitudinal axis of the dam is considered representative of the behavior of the entire structure. The foundation rock is also assumed to be in a state of generalized plane stress. This assumption, is also dictated by the relatively small longitudinal volume of foundation rock expected to participate in the earthquake response of a single dam monolith[37]. The hydrodynamic effect is included by the added mass approach originated by Westergaard[2].

Several finite element models using coarser to finer meshes were considered in a series of preliminary static and dynamic analyses in order to select a system with a reasonable number of d.o.f for ease of manipulation, but still providing a representative structural behavior in terms of the response quantities of interest. Two finite element meshes representative of the different meshes analyzed are shown in Figure 3.1. The mesh that was finally selected for further numerical applications is the finer mesh (Fig. 3.1b)), in which the dam is idealized as an assemblage of 8–nodes linear isoparametric elements with a total of 178 d.o.f. The foundation block is represented by an assemblage of 4–nodes linear isoparametric elements with a total of 80 d.o.f.

3.2 Finite Element Model of the Dam–Foundation–Reservoir System

3.2.1 Computational Procedure

The methodology used to evaluate the influence of the four proposed earthquake input models on the time domain structural response of the dam–foundation–reservoir system is somewhat similar to the technique used to construct response spectra. The dynamic properties of the dam (mass, damping, stiffness) were assumed constant for all analyses. The critical parameters were selected as:

1- the modulus of elasticity of the foundation rock,

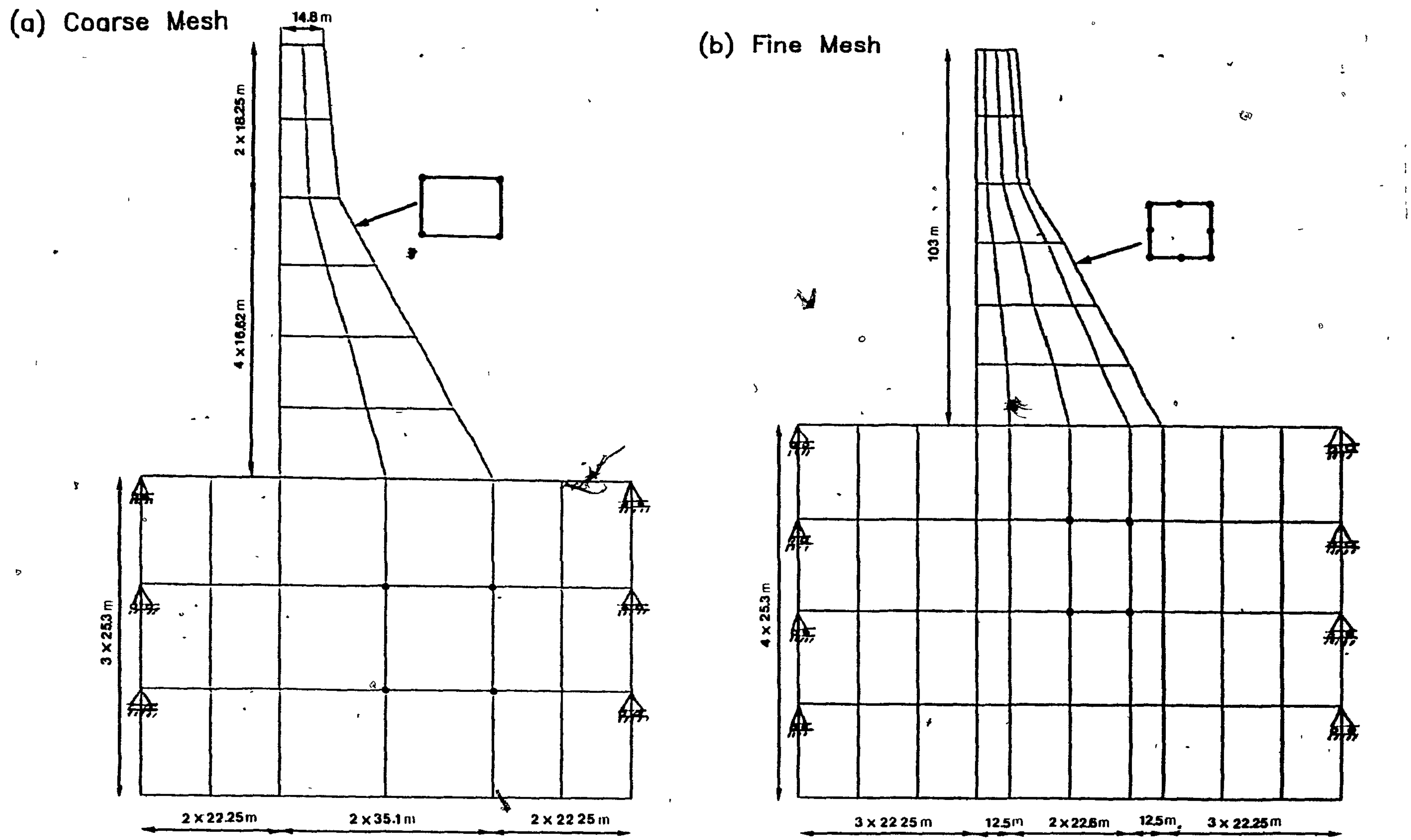

Figure 3.1 Finite Element Meshes Used for Analysis.

2- the inertial properties of the foundation rock,

3- the energy dissipation characteristics of the foundation rock,

4- the frequency content of the specified free-field input accelerogram.

It should be noted that variations in the stiffness and material properties of the foundation will in fact result in changes in the natural periods of vibration of the combined system.

Time domain analyses were carried out for selected range of the above critical parameters and the intensity of the response of typical quantities of engineering interest were computed from the equations of dynamic equilibrium derived in Chapter 2, to compare the relative performance of the four earthquake input models.

3.2.2 System Properties and Ground Motions

The mass concrete in the dam is assumed to be a homogeneous, isotropic, linear elastic solid with the following properties: modulus of elasticity, $E_d = 2.4 \times 10^4$ MPa mass density, $\rho_d = 2640$ kg/m^3 and Poisson's ratio, $\nu_d = 0.20$. Energy dissipation in the dam is represented by a constant viscous damping ratio ($\xi_d = 5\%$) for all vibration modes. The foundation rock region supporting the dam monolith is idealized as a homogeneous, isotropic, linear elastic system. For the foundation rock, the modulus of elasticity, E_f, is varied such that E_f/E_d =4, 2, 1, 1/2, 1/4, 1/8. The mass density is taken as $\rho_f = 2643$ kg/m^3 and the Poisson's ratio, $\nu_f = 0.33$. The damping ratio for the foundation rock, ξ_f, is specified as 5, 10 and 15 percent of critical. An example of a possible range of the elastic properties of soft foundation rock of a typical finite element model developed for the static analysis of a dam foundation system is shown in Figure 3.2.

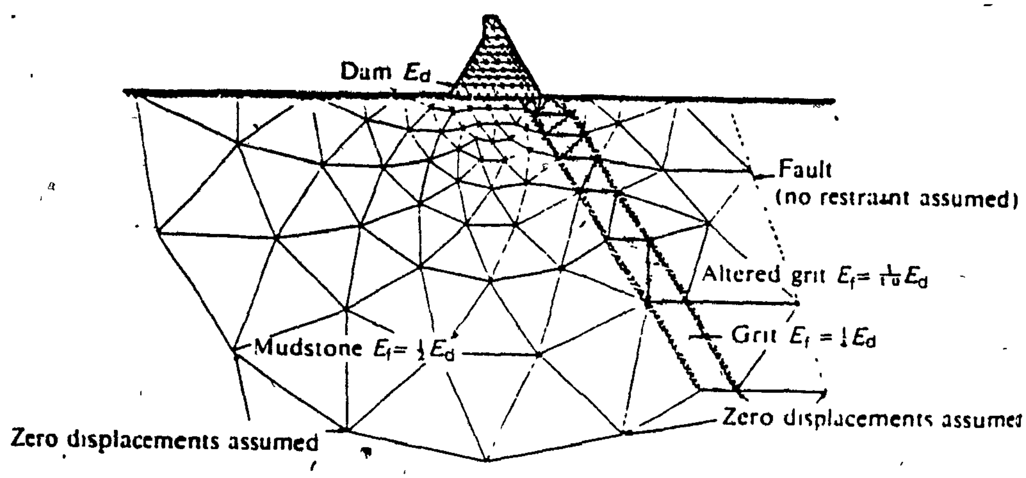

Figure 3.2 Example of a Dam–Foundation System Properties Adapted from Reference 38.

The ground motions selected for this study are the horizontal components of:

- the 1940 El Centro earthquake (NS component),
- the 1971 San-Fernando earthquake recorded at Pacoima (SW component),
- the 1966 Parkfield, California earthquake (NW component).

Figures 3.3 to 3.5 show the considered time history accelerograms and the corresponding spectral accelerations. It should be noted that the Pacoima and the Parkfield accelerograms were scaled to 0.35g, which represents the maximum acceleration of the EL Centro earthquake.

3.2.3 Stiffness Matrix

The stiffness matrix of the combined system is found by direct assembly of the stiffness matrices of the concrete dam and the foundation rock evaluated using the specified values of the moduli of elasticity. These matrices can be written respectively

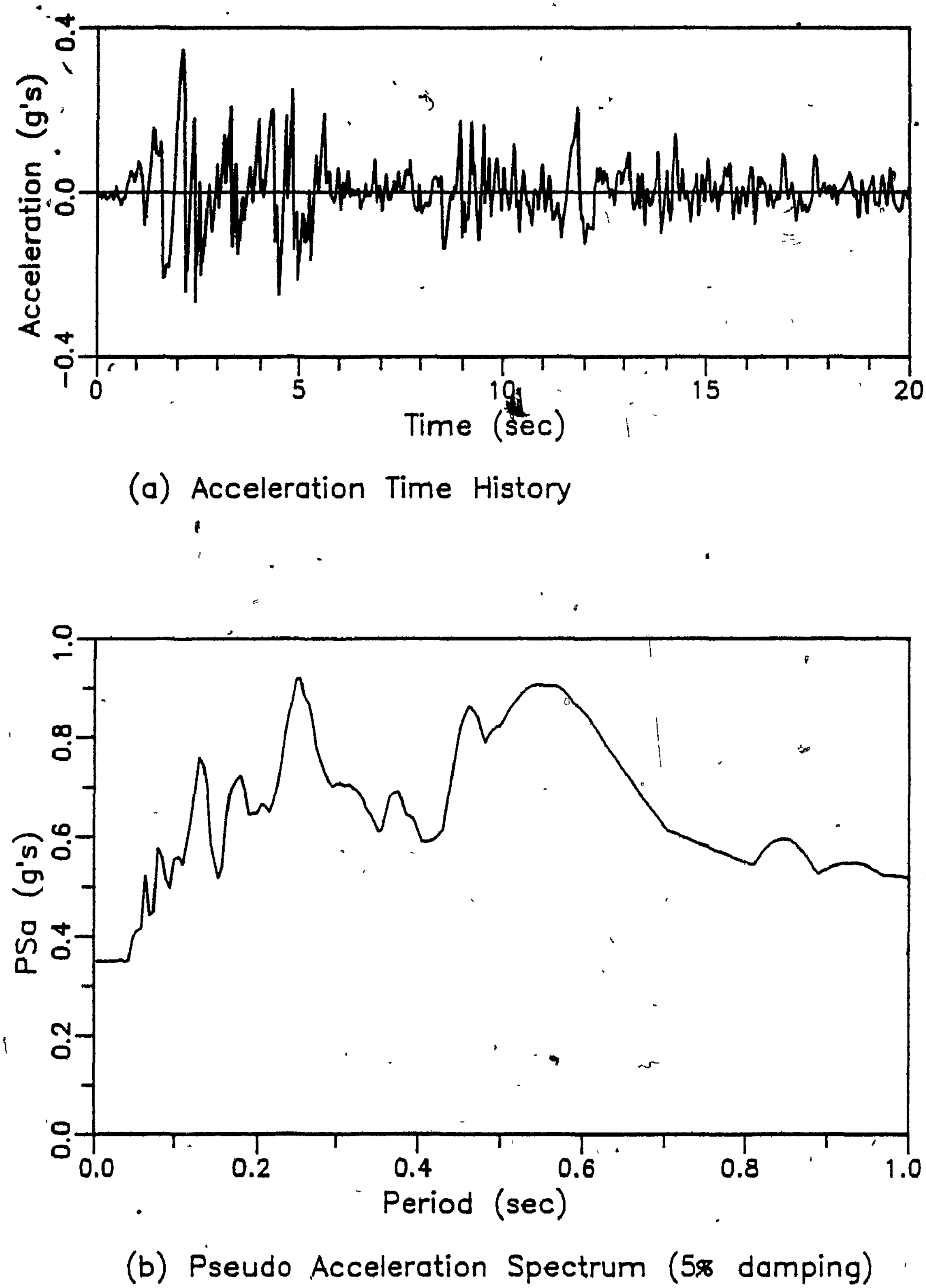

Figure 3.3 El Centro Earthquake, May18, 1940 (NS component).

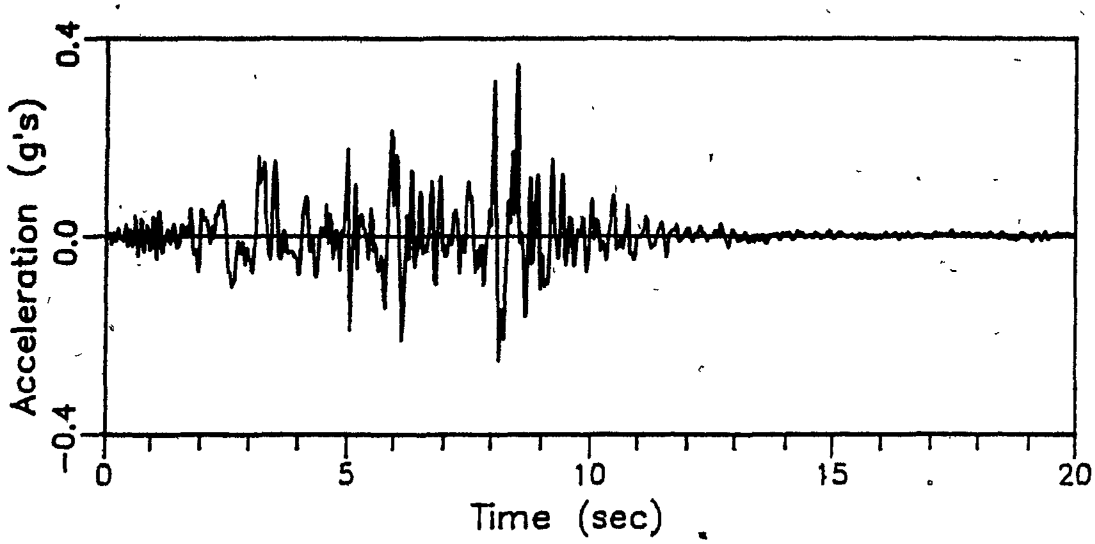

(a) Acceleration Time History

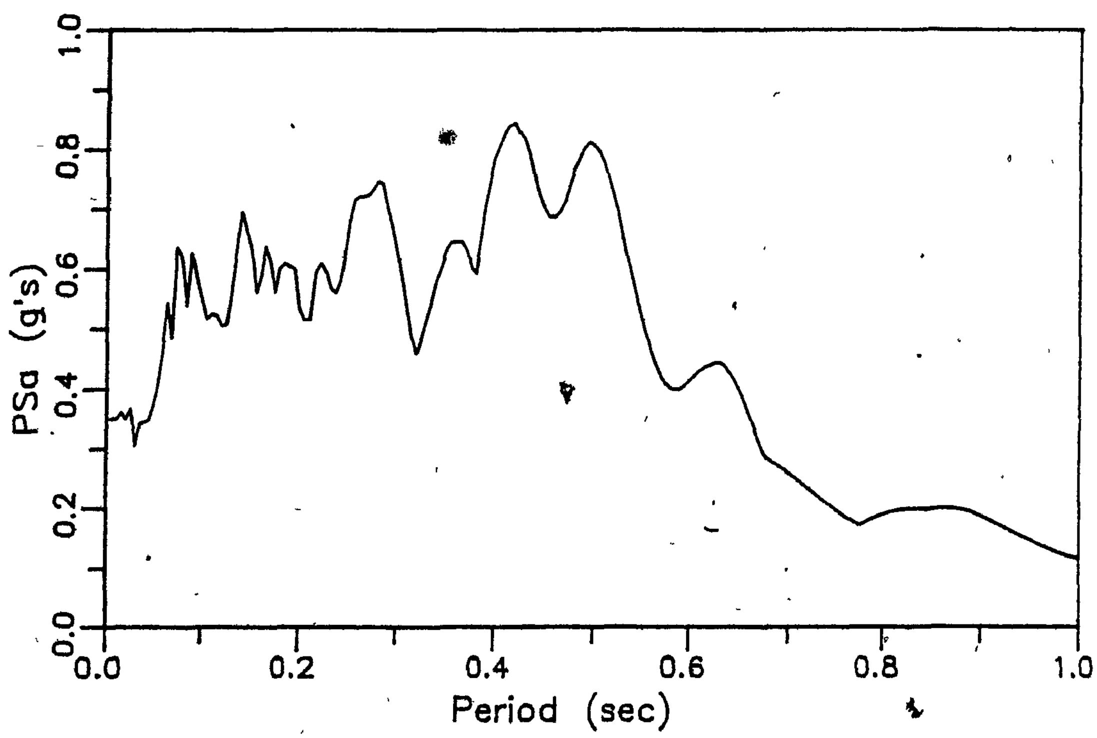

(b) Pseudo Acceleration Spectrum (5% damping)

Figure 3.4 San-Fernando Earthquake Recorded at Pacoima, February 9, 1971, (SW component) Scaled to 0.35g.

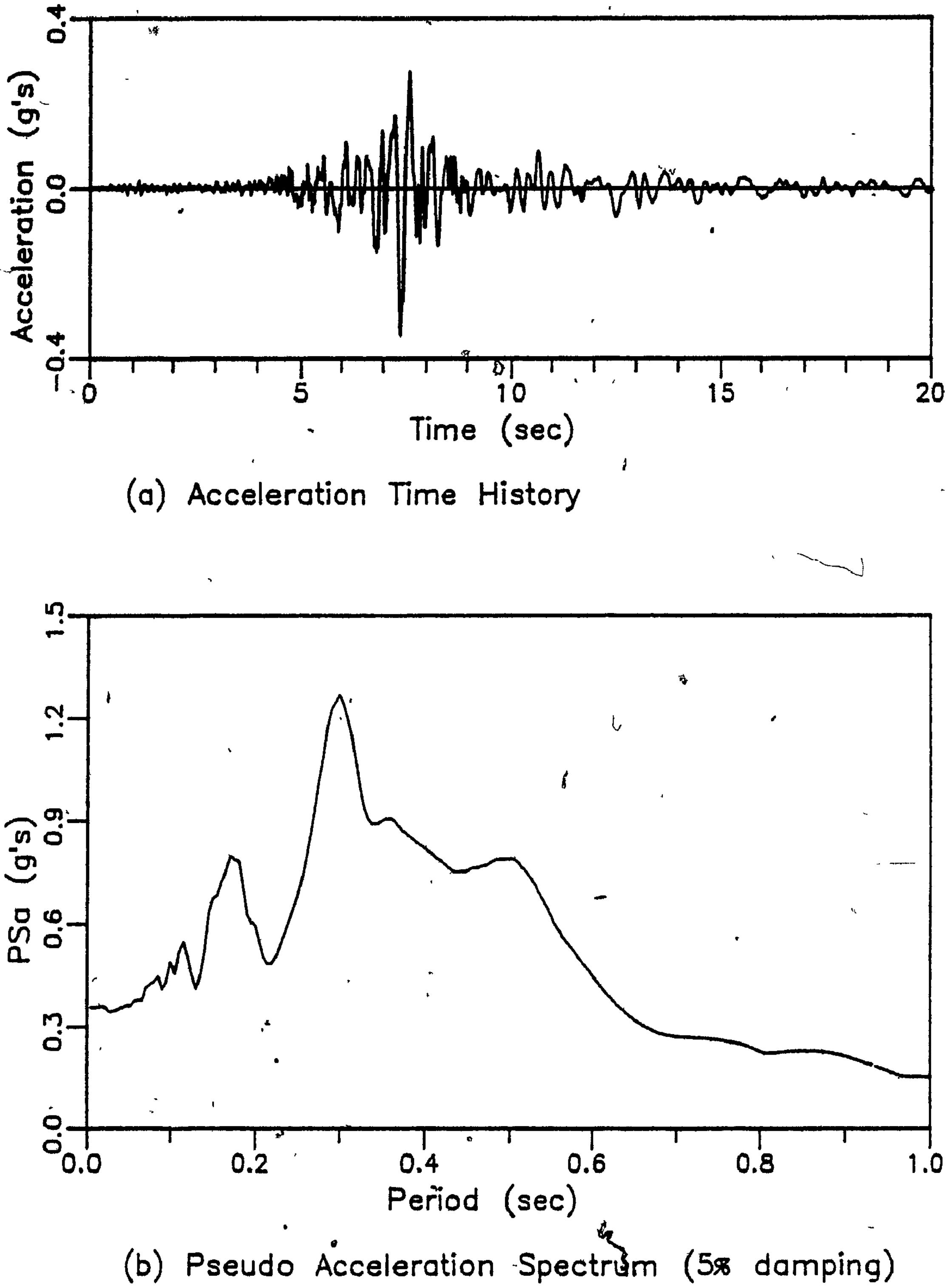

Figure 3.5 Parkfield, California Earthquake, June 27, 1966, (NW component) Scaled to 0.35g.

as:

$$[K_d] = \begin{bmatrix} k_{dd} & k_{dg} & 0 \\ k_{gd} & k_{gg} & 0 \\ 0 & 0 & 0 \end{bmatrix} \qquad [\tilde{k}_f] = \begin{bmatrix} 0 & 0 & 0 \\ 0 & \tilde{k}_{gg} & \tilde{k}_{ga} \\ 0 & \tilde{k}_{ag} & \tilde{k}_{aa} \end{bmatrix} \tag{3.1}$$

The global stiffness matrix of the dam-foundation system will be of dimension 248× 248. In order to reduce the size of the global stiffness matrix of the system, a static condensation of the mid-side element nodes in the dam substructure has been performed; the size of the global stiffness matrix was thus reduced to 140 × 140.

3.2.4 Mass Matrix

The global mass matrix is contributed by the dam, the foundation and the reservoir. For the dam and the foundation block, a lumped mass formulation was used, leading to a diagonal mass matrix having the same dimension as the stiffness matrix.

The mass that is contributed by the reservoir is supposed to represent the hydrodynamic effect, this is called the "added mass" approach and was originated by Wetergaard[2]. The basic assumptions of this method are:

1- the dam is rigid,

2- the upstream face is a vertical plane,

3- the liquid is incompressible,

4- the dam is located in a broad canyon so that a 2-D model is valid,

5- the reservoir extends to infinity in the upstream direction.

Westergaard stated that for a gravity dam subjected to a horizontal acceleration, the only significant reservoir pressures are acting at the dam face (Fig. 3.6a)) and could be evaluated by the following formula:

$$P(y=0) = \frac{7}{8}\, \rho_w\ H\ (1 - \frac{z}{H})^{\frac{1}{2}}\ \ddot{v}_g(t) \tag{3.2}$$

which represents a parabolic pressure distribution.

The same effect can be obtained if a block of water is attached to the upstream face of the dam. According to Westergaard, this block should have a parabolic shape with the base width equal to 7/8 H as shown in Figure 3.6b). The masses $(m_1, \ldots, m_6)$ attached to the nodes of the upstream face (Fig 3.3b)) are computed proportionally to their respective tributary area of water and are only activated by horizontal ground motion.

3.2.5 Damping Matrix

The global damping matrix is found by assembling the damping matrices of the dam and the foundation. The damping ratio specified for the concrete dam was 5 percent of critical and the damping ratios specified for the foundation rock were set at 5, 10 and 15 percent of critical for a parametric evaluation of the corresponding earthquake response.

In the case where, the damping ratios of the concrete dam and the foundation rock are not equal, the modal coordinates equations of motion are coupled, this is called non-proportional damping[39]. Non-proportional damping may be expected in any structure-foundation system in which significant interaction is developed and where the damping properties of the structure and the foundation medium are quite different. Non-proportional damping can be expressed only in terms of an explicit matrix [C]. The methods to construct such a matrix are numerous, but the most efficient approach from a computer implementation standpoint is the concept of Rayleigh damping which is widely used in practice. The popularity of this method is due to the fact that the damping matrix of each substructure is given by a linear combination of the mass and the stiffness matrices of the subsystem considered, and therefore, no additional storage in the computer memory is needed for the damping matrix. If more than two proportionality constants are used, the matrix [C] will in general be full. Since the cost of the analysis is increased by a very significant amount if a full [C] matrix has to be

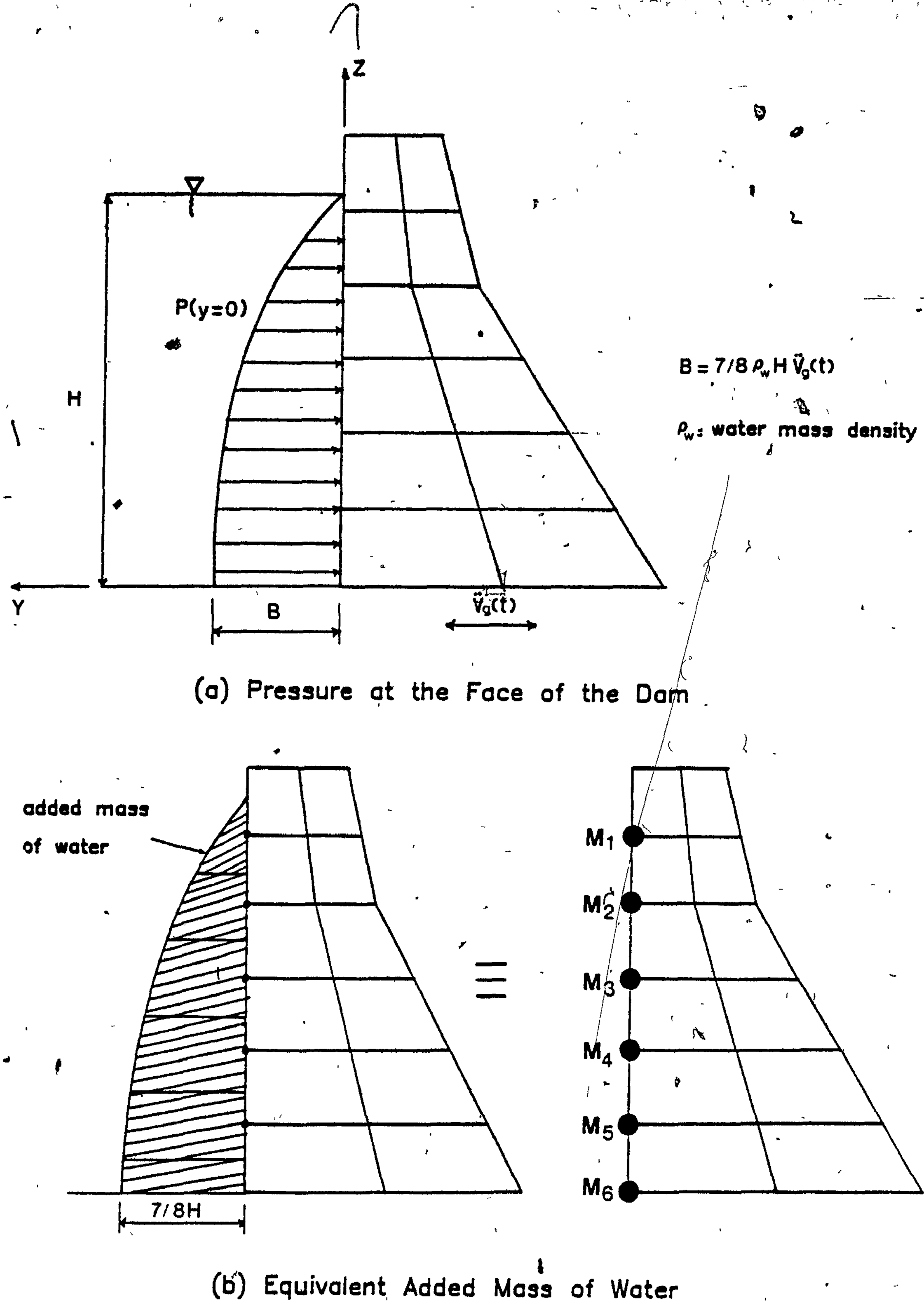

Figure 3.6 Representation of the Hydrodynamic Effect by Westergaard's Approach.

used, in most practical analyses using direct integration, Rayleigh damping is assumed. The damping matrix of each substructure can thus be expressed as:

$$[C_i] = a_{0_i}[M_i] + a_{1_i}[K_i] \tag{3.3}$$

in which a_{0_i} and a_{1_i} are proportionality constants specified for the ith substructure. In order to select the coefficients a_{0_i} and a_{1_i} the following formula can be used if the same damping ratio, ξ, is specified for mode 1 and mode r:

$$\begin{Bmatrix} a_{0_i} \\ a_{1_i} \end{Bmatrix} = \frac{2\xi}{\omega_1 + \omega_r} \begin{Bmatrix} \omega_1 \, \omega_r \\ 1 \end{Bmatrix} \tag{3.4}$$

The frequencies ω_1 and ω_r are generally chosen as the undamped frequencies of the lowest and the highest modes of the entire structure which are expected to contribute significantly to the response; damping ratios of other important modes will then receive a reasonable value.

In the case where the foundation is assumed to be massless (Model B), the damping matrix of the foundation is proportional to the corresponding stiffness matrix only, that is:

$$[C_f] = a_{1_f}[k_f] \tag{3.5}$$

in which a_{1_f} is the proportionality constant and is given by:

$$a_{1_f} = \frac{2\xi_f}{\omega_j} \tag{3.6}$$

in which ω_j is generally chosen as the undamped frequency of the mode of vibration of the entire structure (with massless foundation), that is expected to contribute most significantly to the response.

For the dam–foundation system considered in this study, the damping matrix of the dam substructure will be computed from equation (3.3). For the foundation, the damping matrix is computed from equation (3.3) in the case where the mass of the foundation rock is taken into account (Models A, C and D) and from equation (3.5) in the case of a massless foundation (Model B). The global damping matrix for the complete structure will be obtained by assembling the damping matrices of the dam and the deformable foundation using standard structural property assembly procedures.

$$[C_d] = a_{0_d}[M_d] + a_{1_d}[K_d]$$

$[C] =$ 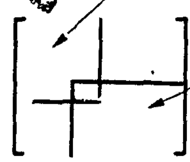

$$[C_f] = a_{0_f}[M_f] + a_{1_f}[K_f]$$

or

$$[C_f] = a_{1_f}[K_f]$$

The major disadvantages of the Rayleigh damping method are:

- the higher modes are considerably more damped than the lower modes,
- the damping is controlled at only two modes of vibration (in the case where the damping matrix is proportional to both the mass and stiffness matrices) in between these two modes the values of the damping ratio are less than the assigned value,
- in the case of a damping matrix proportional only to the stiffness matrix, the damping ratio is controlled at only one mode, generally the fundamental mode, therefore the higher modes will be much more damped than the first one.

In order to illustrate the above remarks, the variation of the damping ratio of the foundation rock in the different modes of vibration for the case where a value of ξ_f = 15% has been assigned to the foundation medium, is shown in Figure 3.7. Two cases have been considered: a foundation model with mass (Fig. 3.4a)) and a massless foundation model, for two values of the moduli ratio E_f/E_d, 1/8 and 4, which represent respectively a flexible and a rigid foundation rock. Figure 3.7a) shows that when the damping is controlled at two modes (mode 1 and 6 in this case), the variation of the damping ratio versus the circular frequencies of vibration is of a parabolic shape. Therefore, the values of the damping ratio in the other modes expected to contribute significantly to the total response (modes 2 to 5 in this case) are less than the assigned value of damping ratio ($\xi_f = 15\%$). For the flexible foundation case ($E_f/E_d = 1/8$), the decrease in the damping ratio for modes 2 to 5 is not as important as in the case of a rigid foundation ($E_f/E_d = 4$). For the massless foundation case, the damping is controlled at only the first mode of vibration. The variation of the damping ratios of the foundation with the circular frequencies of the system (with massless foundation) is linear, this leads to a very significant augmentation of the damping ratios in the higher modes as shown in Figure 3.7b). Indeed for both cases, $E_f/E_d = 1/8$ and 4, the second mode of vibration receives a damping ratio value of 36%. This shows that the actual value of damping corresponding to the massless foundation system that is effectively used in the analysis, depends to a large extent on the contribution of the higher modes to the total response.

The most obvious method to analyze a structure with non-proportional damping is to integrate directly the coupled equations of motion expressed in original geometric coordinates as performed in this study. The important disadvantage of this procedure is that all of the equations of motion must be included in the analysis requiring a larger computational effort. Alternate strategies for a more effective solution of non-proportional damped systems will be presented in Chapter 5.

3.2.6 Influence of Boundaries Location

One of the critical issues in the process of mesh selection is the location of the boundaries of the foundation block which should be included in the finite element model, to reflect the flexibility of the foundation. The process of locating the foundation block boundaries in the finite element model is in fact divided in two parts. First is the

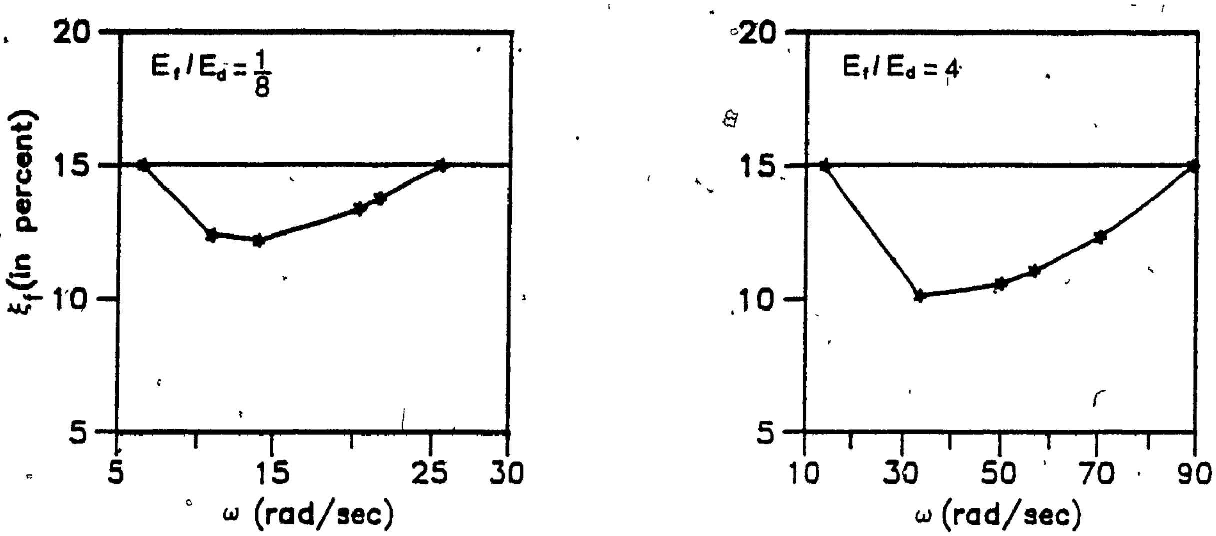

(a) Mass Foundation (Models A, C, D)

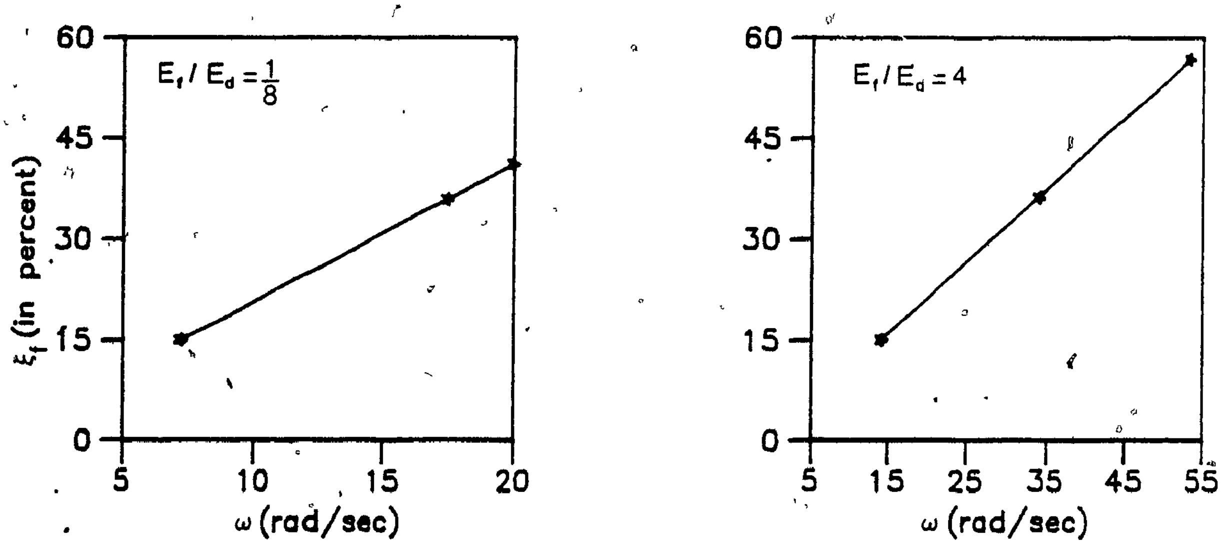

(b) Massless Foundation (Model B)

Figure 3.7 Variation of the Damping Ratios in the Different Modes of Vibration as Given by the Rayleigh Method.

determination of the location of the rigid boundary at the bottom of the foundation and second is the determination of the location of the lateral boundaries. Since this study was restricted to the application of horizontal ground motions, antisymmetric lateral boundary conditions were used to minimize the horizontal dimensions of the foundation block model.

The rigid lower boundary has the effect of trapping energy radiating away from the foundation, thus potentially introducing artificial resonance conditions. Therefore to minimize this effect, this lower boundary should be located at a reasonable depth. The lateral boundaries if placed too close to the structure will reflect the incident waves which will also interfere with the response of the structure.

In the current practice, there are no precise rules for the location of the foundation boundaries, the only method available is the trial and error procedure. This means that, the boundaries of the foundation block are moved away from the dam in both the lateral and vertical directions and the dynamic response characteristics of the corresponding system are evaluated. If a certain stabilization in the response is reached, the model can then be accepted as representative of the behavior of the physical system. It should be noted that a smaller foundation block could be used in the finite element model if transmitting boundaries are used. The most frequently used transmitting boundaries are of the simple viscous type[40], and they are usually more appropriate for a frequency domain analysis.

For the finite element mesh selected for this study, the lateral boundaries were displaced by 22 meters on either side of the base of the dam and the depth of the rigid boundary was displaced downward by 25 meters. The characteristics of the dynamic response were evaluated in terms of the free-vibration properties and displacements of preliminary transient analysis with specified E_f/E_d value of 1 and $\xi_f = 5\%$. The fundamental period of the enlarged system increased by 1.2% and the maximum displacement in the Y-dir increased by 8% as compared with the original model. These differences were judged to be sufficiently small to justify the use of the selected model.

3.2.7 Dynamic Analysis Procedure

The development of appropriate mathematical models, for complete earthquake response analysis of a typical structural system requires the application of the following procedures:

- static analysis,
- study of the free vibration response,
- spectral analysis,
- linear time history analysis,
- non-linear time history analysis.

In the free-vibration study, the natural periods and the associated mode shapes of the mathematical model are computed. The periods indicate possible resonant conditions with maximum dynamic amplification. The mode shapes are useful to visualize the deformed shape of the structure in the different modes of vibration, indicating which regions of the structure are most flexible. The mode shapes are also needed to compute the effective modal mass in order to identify modes which are contributing significantly to the dynamic response of the system (see Section 3.3). Natural periods of vibrations of the system will also provide indications to select an appropriate time step for the transient response analysis.

The spectral analysis is performed in order to get an appreciation of the magnitude of the probable maximum displacements and stresses in the structure. If these values are acceptable, no further analyses are generally required. On the other hand, if they are excessive, a linear or non–linear time history analysis of the critically stressed elements can be performed to determine the length of time over which unacceptable stresses occur. This type of analysis will also allow to determine the magnitude of stresses which occur at these locations immediately before and after the occurrence of the critical values, and the number of repetitions during the earthquake of values close to critical ones. Such an indepth analysis can be a basis for a judgment decision of the actual structural significance of unacceptable stresses since such factors as time, span and stress recurrence can be considered. The volume of computations involved in the transient analysis is much more significant than in the spectra analysis.

3.3 Structural Behavior of the Mathematical Model in Free–Vibration

3.3.1 Effective Modal Mass

The effective modal mass can be used to identify the modes that contribute significantly to the total structural behavior. The effective modal mass for mode i in the Y-direction can be expressed as[22,24]:

$$EMM_y = \frac{p_{i,y}^2}{M_i} \tag{3.7}$$

in which $p_{i,y}$ is the earthquake participation factor in the Y-direction for mode i given by:

$$p_{i,y} = \underline{X}_i^T \, [M] \, \underline{r}_y \tag{3.8}$$

and M_i is the generalized mass for mode i

$$M_i = \underline{X}_i^T \, [M] \, \underline{X}_i \tag{3.9}$$

X_i is a transformation vector (eigenvector or derived Ritz vector) corresponding to mode i, $\underline{r}_y$ is defined in equation (2.1). The generalized mass M_i is often normalized to unity to simplify the computations. The total mass of the system, in the horizontal direction can be expressed as:

$$M_T = r_y^T [M] r_y \tag{3.10}$$

The percentage of effective modal mass in the Y-direction (PEMMy) which represents the fraction of the total mass participating in the response in this direction by the direct superposition of a truncated vector basis can then be expressed as:

$$PEMM_y = \sum_{i=1}^{r} \frac{P_{i,y}^2}{M_T} \times 100 \tag{3.11}$$

for r modes retained in the summation. In this analysis, the procedure used to identify the modes which are contributing significantly to the total structural response was to fix a required percentage of effective modal mass in the Y-direction where the structure is excited, to a value of 95 percent and to compute the number of modes necessary to reach this value.

3.3.2 Ratio of Foundation Rock Elastic Modulus to Concrete Elastic Modulus

The dam–foundation interaction effect, is basically controlled by the ratio of foundation rock modulus to concrete modulus (E_f/E_d) and therefore the behavior of the dam–foundation-reservoir system in free–vibration, will also be dependent on the ratio E_f/E_d. The periods of the combined system as a function of the foundation flexibility are presented in Table 5.1 for a mass foundation system and Table 5.2 for a massless foundation system.

It can be noticed from these tables that the periods of vibration lengthen with the increase of the foundation flexibility. Furthermore, neglecting the mass of the foundation reduces the periods of the system. Figure 3.8 shows the displacements of the dam-foundation system in the first two modes of vibration as a function of the flexibility of the foundation rock for the modes with mass foundation. It should be observed that for the case $E_f/E_d = 4$ which represents a relatively rigid foundation, the foundation

Table 3.1 Periods (in sec) of Dam-Foundation System, Foundation with Mass (Models A, C, D).

E_f/E_d	1/8	1/4	1/2	1	2	4
T_1	0.948	0.718	0.579	0.504	0.467	0.448
T_2	0.582	0.440	0.338	0.262	0.212	0.189
T_3	0.451	0.325	0.237	0.184	0.153	0.126
T_4	0.309	0.242	0.205	0.168	0.133	0.111
T_5	0.290	0.221	0.159	0.115	0.098	0.089
T_6	0.247	0.177	0.131	0.109	0.082	0.067

Table 3.2 Periods (in sec) of Dam-Foundation System, Massless Foundation (Model B).

E_f/E_d	1/8	1/4	1/2	1	2	4
T_1	0.867	0.680	0.565	0.500	0.465	0.447
T_2	0.362	0.292	0.250	0.220	0.199	0.186
T_3	0.316	0.245	0.190	0.153	0.131	0.118
T_4	0.165	0.146	0.129	0.115	0.105	0.099
T_5	0.086	0.082	0.077	0.073	0.070	0.068
T_6	0.071	0.070	0.067	0.064	0.059	0.056

block remains almost undeformed during the dam vibrations. Figure 3.9 shows the effect of the foundation flexibility on the periods of the first three modes of vibration of the dam-foundation- reservoir system. Two cases are considered: foundation block with mass and massless foundation block. Results indicate that for the flexible foundation rock with mass, the periods of vibration increase considerably as compared to those of infinitely rigid foundation. For the massless foundation case, the increase is relatively less than in the mass foundation case. Thus, the massless foundation model is less affected by the flexibility of the foundation rock.

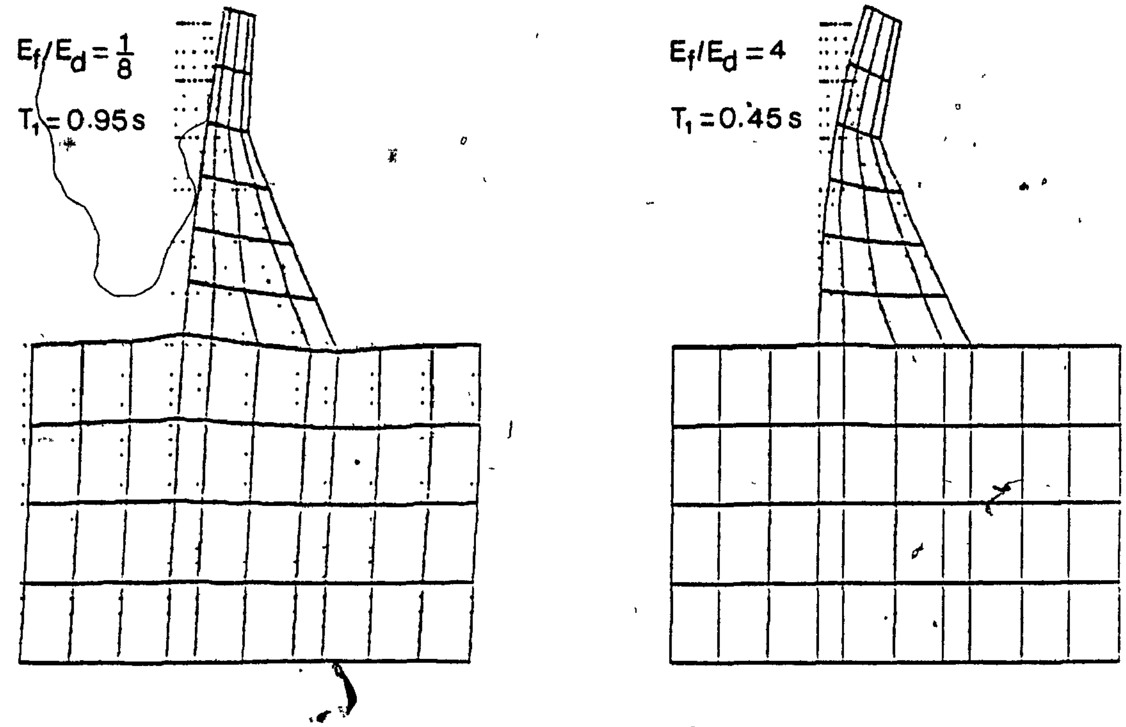

(a) First Mode of Vibration

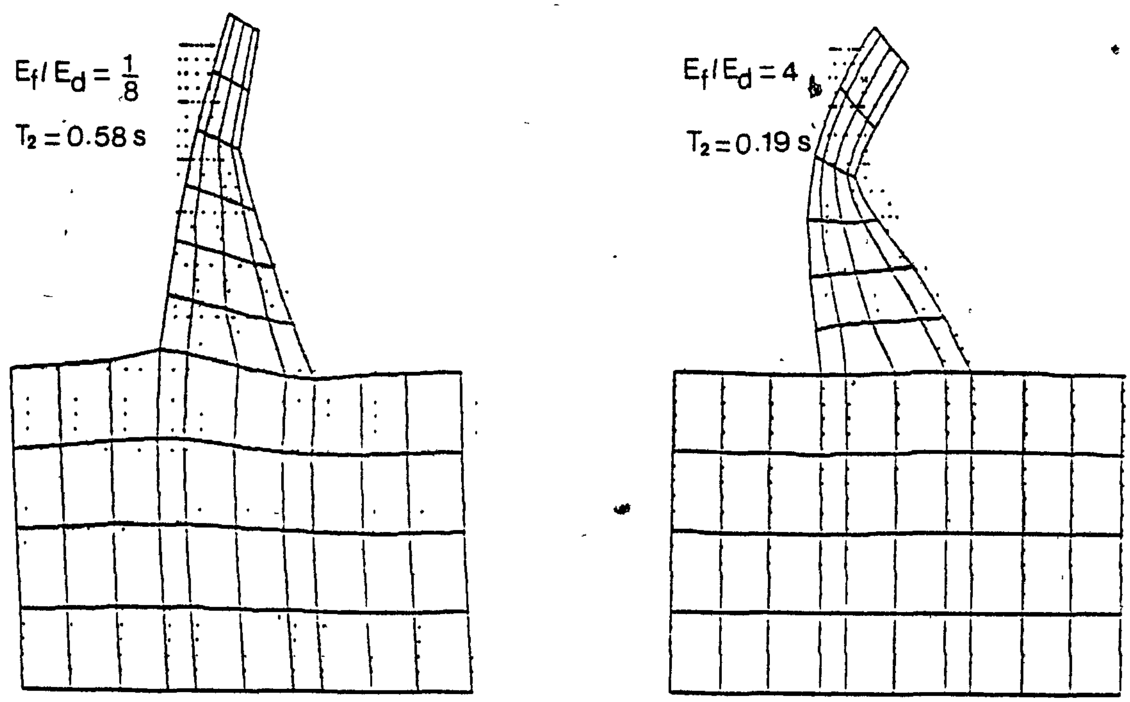

(b) Second Mode of Vibration

Figure 3.8 Effect of Dam–Foundation Interaction on the First Two Modes of Vibration of the Models with Mass Foundation (A, C, D).

The effective modal mass is also affected by the ratio of moduli E_f/E_d. Figure 3.10 shows the variation of the number of modes required to reach 95 percent of the effective modal mass in the Y-direction (EMM_y), as a function of the ratio E_f/E_d. The results indicate that the number of modes required to reach the imposed value for the EMM_y, increase with the augmentation of the stiffness of the system as given by the ratio E_f/E_d. For a gravity dam with a flexible foundation, a relatively small number of low frequency modes is thus able to represent adequately the dynamic response of the system.

It should also be observed that for any specified value of E_f/E_d the number of modes required to reach a horizontal effective modal mass of 95% is significantly less for the massless foundation earthquake input model than for the input models with non zero mass foundation (models A, C, D). This is due to the fact that in model B there is no need to represent the inertial vibration characteristics of the foundation by the truncated eigenbasis.

This will also represent a significant computational advantage for model B as compared to models A, C, D, if the time history response analysis is to be carried out from a reduced system of dynamic equilibrium equations expressed in generalized coordinates.

3.3.3 Hydrodynamic Interaction Effect

The hydrodynamic effect which was included by the added mass approach, as mentioned previously will produce an increase in the periods of vibration of the system.

The periods of vibration for the selected finite element model neglecting the added mass of water have also been computed. Comparison with the model in which the added mass of water was included shows that for the case $E_f/E_d = 1/8$ which represents a relatively flexible foundation rock, the increase in the periods of vibration due to the added mass of water was of 15% for the first mode and 5% for the second mode. For

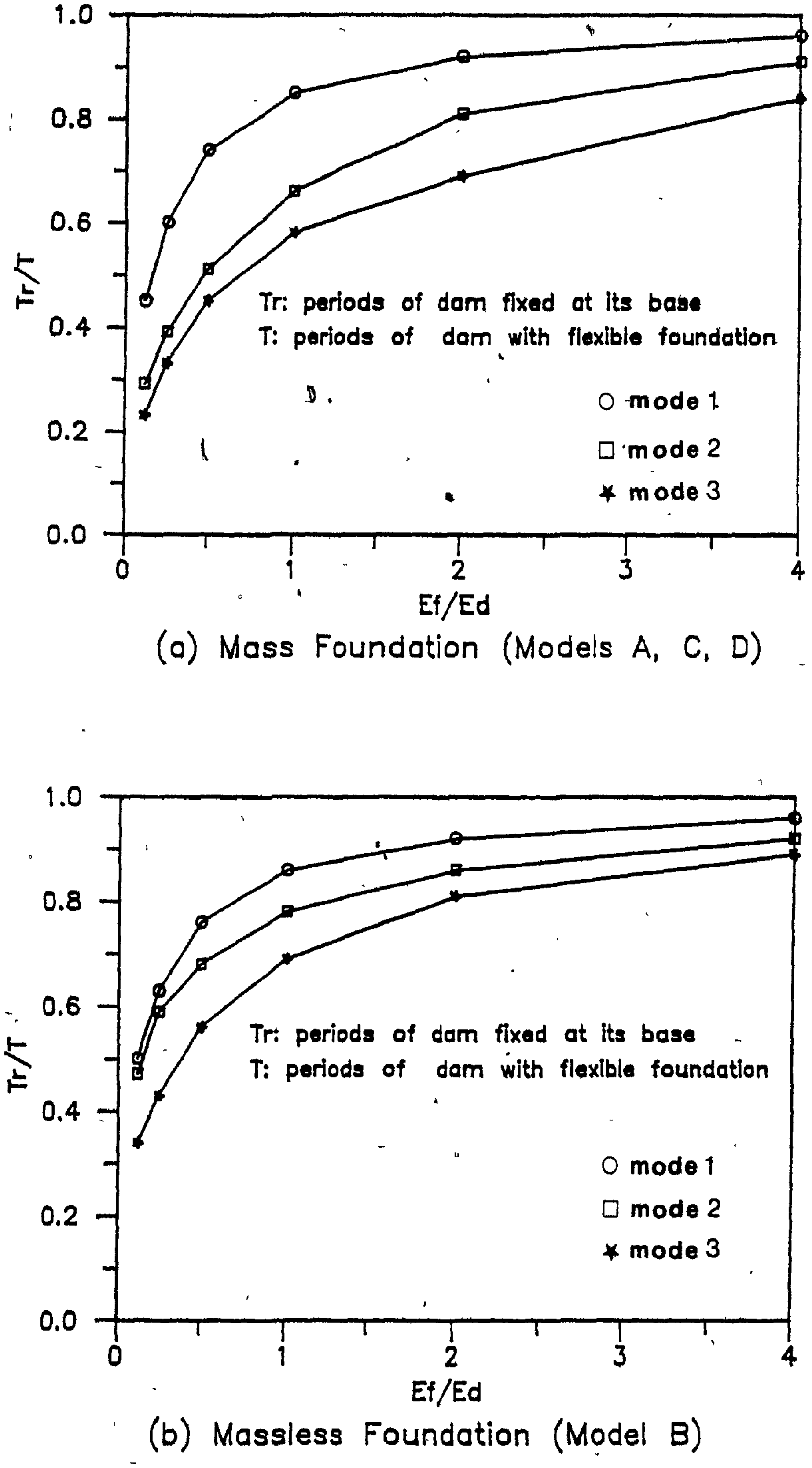

Figure 3.9 Effect of Foundation Flexibility on the First Three Periods of Vibration of the Combined System.

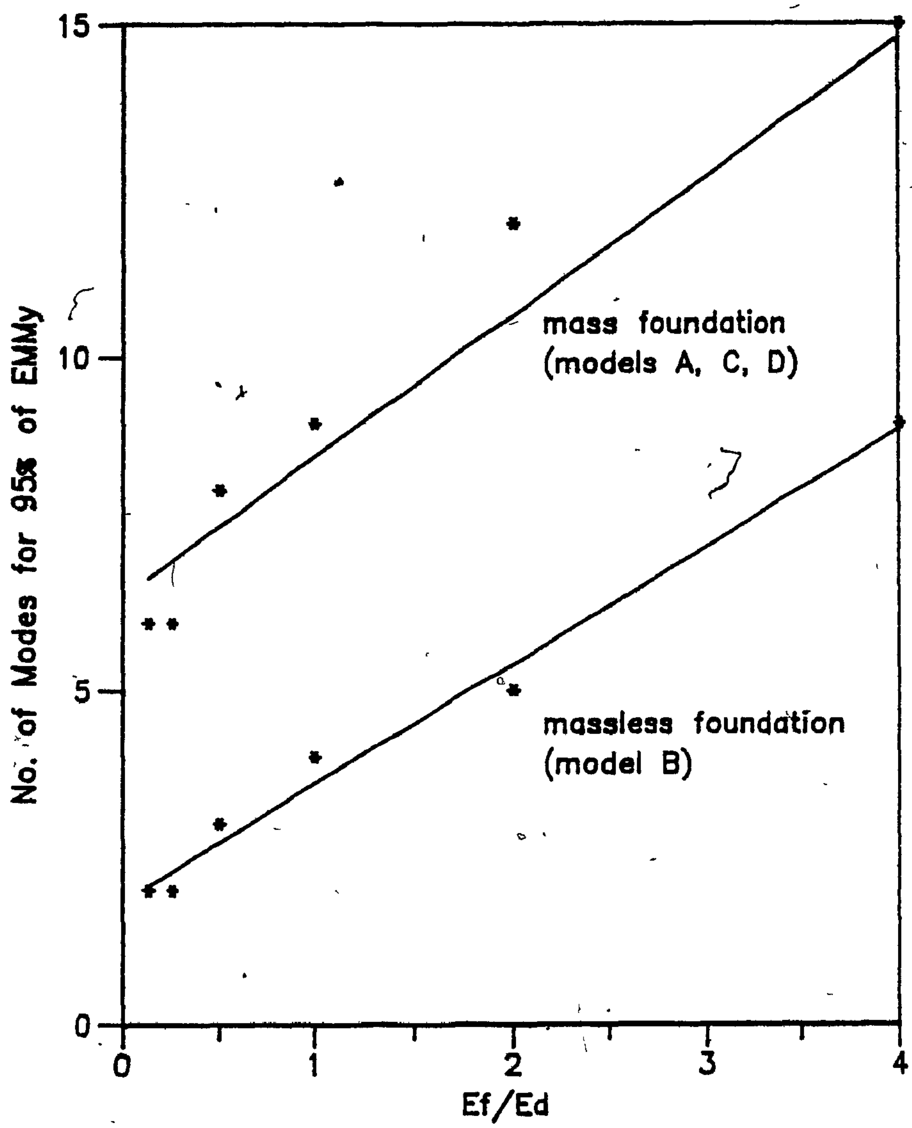

Figure 3.10 Effect of Foundation Flexibility on the Effective Modal Mass.

the ratio $E_f/E_d = 4$, the increase was of 16% and 19% for the first and second mode, respectively. This shows that the hydrodynamic effect when represented by the added mass approach, will cause a greater perturbation of the vibration modes for a rigid foundation than for a flexible foundation.

3.4 Preliminary Earthquake Analysis

Preliminary earthquake analyses were performed in order to get a general idea of the behavior of the selected dam–foundation–reservoir system.

The first step consisted of performing a spectral analysis, using the PSa shown in Figure 3.3b). The finite element program SAP 80[41] was used to perform the spectral analyses. A number of modes varying from 7 to 15, depending on the flexibility of the foundation, was included in the response. Results showed that there is a concentration of high stresses in the vicinity of the reentrant corner in the upper part of the dam section, and at the base of the dam. The maximum displacements in the Y-dir occurred at the top of the dam.

The second step in the preliminary earthquake analyses was to perform a transient analysis to obtain a time history of the structural response for the El Centro earthquake. The transient analysis consists of a step–by–step integration of the equation of motion expressed in geometrical coordinates. Thus, a proper numerical integration scheme as well as a time step had to be selected. The first consideration in selecting a numerical integration method, is its stability. Usually, it is desirable to use a method that is unconditionally stable. For linear systems, the errors associated with the numerical integration result in elongation of the free–vibration periods and in decrease of the vibration amplitudes. In this study, the Newmark average acceleration method has been selected, it is unconditionally stable and it produces no amplitude decay. The cost of a transient analysis as well as its accuracy relate directly to the size of the time step (Δt) chosen. A value of Δt=0.01 second was selected for the analysis, it can be observed that the earthquake loadings that are represented by the recorded accelerograms have been discretized at t=0.02 second interval and therefore they will be well represented by the chosen Δt. To ensure that the selected time step will lead to accurate results, a smaller time step equal to 0.001 second has been used in the transient analysis of the retained finite element model. The foundation rock was chosen to be rigid, $E_f/E_d = 4$, so that the periods of vibration will be the smallest in the range of the considered parameters. The chosen Δt=0.001 second represents 1/66 of the period of the highest mode expected to contribute significantly to the total response. The results of the analysis using Δt=0.001 second were very close to those using a larger time step Δt=0.01 second. As an example the maximum displacement in the horizontal direction at the dam crest varied by only 2.8 percent. Therefore, the chosen Δt=0.01 second is sufficiently small to lead to accurate results.

The preliminary transient analyses indicated also that the maximum structural response occurs around t=2 and t=5 seconds for that particular earthquake. In order to reduce the numerical effort involved in this study, it was decided to conduct the parametric response analyses of the four proposed earthquake input models using the first six seconds of the El Centro earthquake to obtain a complete set of results. The Pacoima and Parkfield accelerograms (scaled to 0.35g) were then used to validate the observations and conclusions obtained from the El Centro earthquake by performing some complementary analyses. A detailed description and interpretation of the quantitative results obtained is presented in the next chapter.

CHAPTER 4

COMPUTER IMPLEMENTATION AND NUMERICAL ANALYSES

4.1 Introduction

In this chapter, numerical solutions of dynamic behavior obtained from applying the four proposed earthquake mechanisms to the dam-foundation-reservoir system considered in Chapter 3, are presented. In Section 4.2 the computer implementation of the deconvolution process is discussed. The different cases analyzed and parameters selected for the analyses are presented in Section 4.3. In Section 4.4, typical response quantities of engineering interests resulting from applying the NS component of the El Centro earthquake accelerogram, according to each specific input model, are discussed and compared. The effect of the damping ratio of the foundation on the massless foundation model is examined in Section 4.5. The effect of using different ground motions, is investigated in Section 4.6. For that purpose the time domain earthquake responses of the dam-foundation-reservoir system are computed by applying the four proposed input models, considering two additional earthquake loadings represented by the Pacoima and the Parkfield accelerograms.

The computations in the different analyses have all been carried out on microcomputers. The computer programs that have been used are:

a- CALDAM which is a modified version of the computer program CAL-86[42] specially developed for this study in order to evaluate the static and dynamic behavior of small structural systems that can be modeled using two-dimensional finite elements. CALDAM uses a macro language operating on a data base which allow the user a complete control on the sequence of operations required for the solutions.

b- SHAKE[36], a computer program designed for the earthquake response analysis of horizontally layered sites, used to perform the deconvolution analysis.

c- SPECTR [43], a program to evaluate dynamic response spectra.

A special interface program has also been developed to produce graphic display of the numerical results produced by these programs using the plotting package Grapher[44].

4.2 Computer Implementation of the Deconvolution Process

The deconvolution process is performed in order to compute the base rock accelerogram which might have produced the free-field accelerogram. This process is in fact divided into two parts. First, the foundation block is idealized as a simple shear beam, then the program SHAKE can be used to compute the accelerogram at any level of the layered foundation block. The parameters that control the analysis in the program SHAKE are: the shear modulus and the equivalent viscous damping ratio of the foundation rock and to a lesser degree the maximum frequency that should be transmitted through the foundation rock. The second step consists in analyzing the two-dimensional finite element model representing the foundation block subjected to the deconvolved accelerogram applied at the base of the model. From this analysis, the new free-field accelerogram will be derived and compared to the original one by means of the corresponding PSa, computed by the program SPECTR. This process has been summarized in Figure 2.2. If the match between the two PSa's is satisfactory then the computed deconvolved accelerogram will be retained for the transient analysis of the dam-foundation system. If the match between the two PSa is not satisfactory, then the deconvolution process should restart at the first step and some adjustments have to be made to the controlling parameters in the program SHAKE in order to reduce the differences between the two PSa's, the target and the computed.

Figure 4.1 shows the comparison of the PSa for the cases of a flexible and a rigid foundation. It can be observed that for the rigid foundation case (Fig. 4.1b)), the difference between the two PSa's is very small. This was achieved easily by inputting the actual values of the shear modulus, G_f, and damping ratio, ξ_f, corresponding to the foundation rock in the program SHAKE. In other words for a rigid foundation rock the one-dimensional representation used in the program SHAKE is not too sensitive to the controlling parameters and is very close to the two-dimensional finite element representation used in CALDAM. For the flexible foundation case, as can be seen in Figure 4.1a), the two PSa's do not exhibit a close match throughout the whole period range. It is very difficult to improve the situation, because the responses are now very sensitive to the values of G_f and ξ_f retained for the computations. It should however be recognized that to obtain a satisfactory response by this method it is only required to achieve a close match at the periods of modes of vibration which are contributing significantly to the dynamic response of the dam-foundation-reservoir system. As the flexibility of the foundation is increased, the periods of the important modes lengthen. For example considering the case $E_f/E_d = 1/8$, it was still possible to obtain an average relative error of the order of 3% between the computed and the target PSa for the first three modes representing 90% of horizontal effective modal mass.

4.3 Cases Analyzed and Selected Parameters

The earthquake response of a gravity dam-foundation-reservoir system is affected by the following factors:

a- frequency content and intensity of the specified accelerogram,

b- dam-foundation interaction,

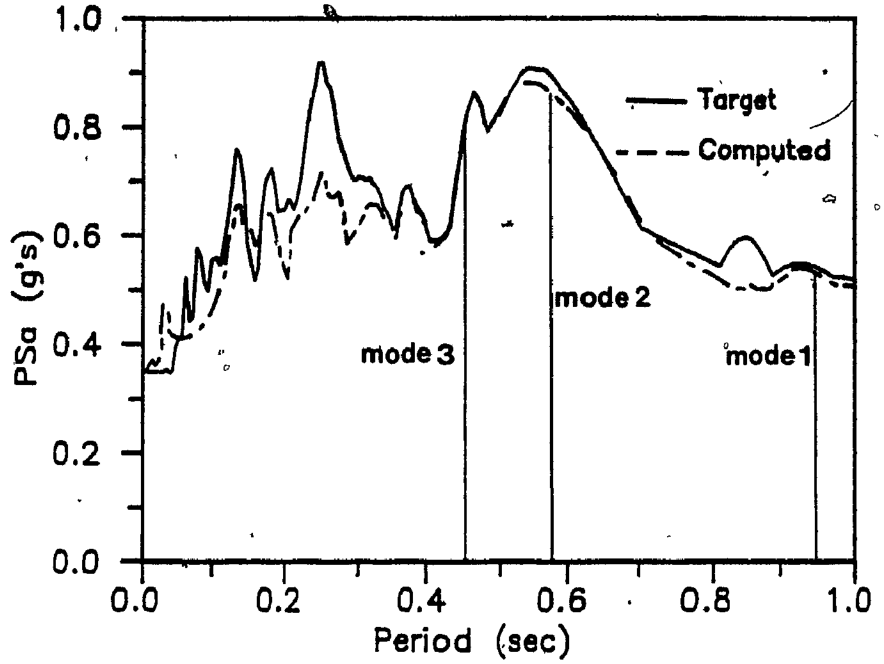

(a) Flexible Foundation Case (Ef/Ed=1/8)

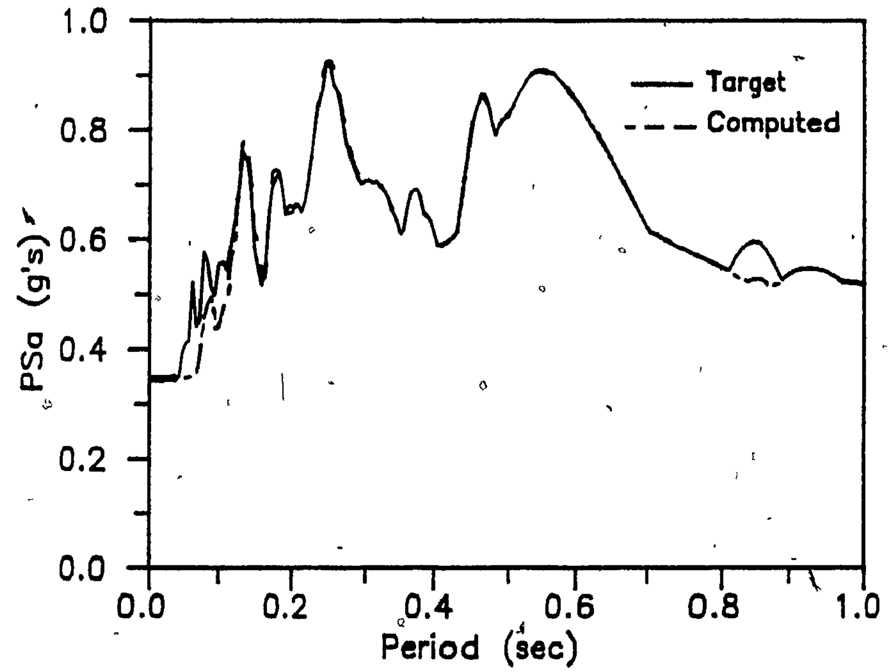

(b) Rigid Foundation Case (Ef/Ed=4)

Figure 4.1 Comparison of the Computed PSa and the Target PSa.

c- dam-water interaction,

d- reservoir bottom absorption,

e- water compressibility.

In this study, only the first three factors have been taken into account, in order to simplify the analysis. It should be noted that a rigorous treatment of water compressibility is only possible in the frequency domain. The dam-water interaction has been included by the added mass approach. For the dam-foundation interaction, two parameters have been selected to cover a wide range of foundation materials and different site conditions. These two parameters are the ratio of moduli of elasticity between the dam and the foundation and the equivalent viscous damping ratio of the foundation rock. The values assigned to these two parameters have been presented in Section 3.2. It should be noted that when the damping ratio of the foundation, ξ_f, is assigned a value of 5 percent of critical, the damping levels provided by the concrete dam and the foundation rock are the same. This corresponds to a condition of proportional damping. In the cases where ξ_f is not equal to 5 percent, the damping matrix of the combined dam–foundation system will be non–proportional.

For the massless foundation input model (Model B), in the case of a proportional damping, the damping matrix of the dam-foundation system can be established in two different ways that yield different results. The first procedure, which is the most commonly used in practice consists of applying directly the Rayleigh method to the combined dam–foundation system. The second procedure consists of establishing separately the damping matrices of the dam and the massless foundation and then assembling them to get the global damping matrix. In this last procedure the fact that the damping matrix corresponding to the massless foundation rock is proportional only to the stiffness matrix of the foundation is taken into account. A value of zero damping for the massless foundation rock has also been considered in the analyses, in order to assess the effect of the damping when the inertial effect of the foundation rock is neglected. Table 4.1 summarizes the cases analyzed using the El Centro earthquake as the input motion.

Table 4.1 Cases Analyzed Using the El Centro Earthquake as the Input Motion.

Input Mechanism Model	Moduli Ratio E_f/E_d	Damping Ratio of the Foundation
Model A		5%
Model C	4, 2, 1, 1/2, 1/4, 1/8	10%
Model D		15%
		0%
Model B	4, 2, 1, 1/2, 1/4, 1/8	5%
		10%
		15%

The time domain earthquake response of the system has been measured in terms of the displacements, the acceleration levels and the stresses developed in the structure. A preliminary transient analysis was performed in order to study the intensity of the response in the complete model and to select representative nodes and elements in the mathematical model, for which the results of the various analyses will be examined. For the displacements and the accelerations nodes 1, 11 and 31 as shown in Figure 4.2 have been selected. The three nodes are located on the upstream face of the dam, the maximum displacements and accelerations occur at node 1, nodes 11 and 31 were chosen in order to cover the height of the dam. The stress results will be retained for elements 1 and 5 at points a, b and c which have the same coordinates as the Gauss quadrature points.

The results of the computer analyses consist of the response history of horizontal and vertical displacements and accelerations at the nodal points of the finite element

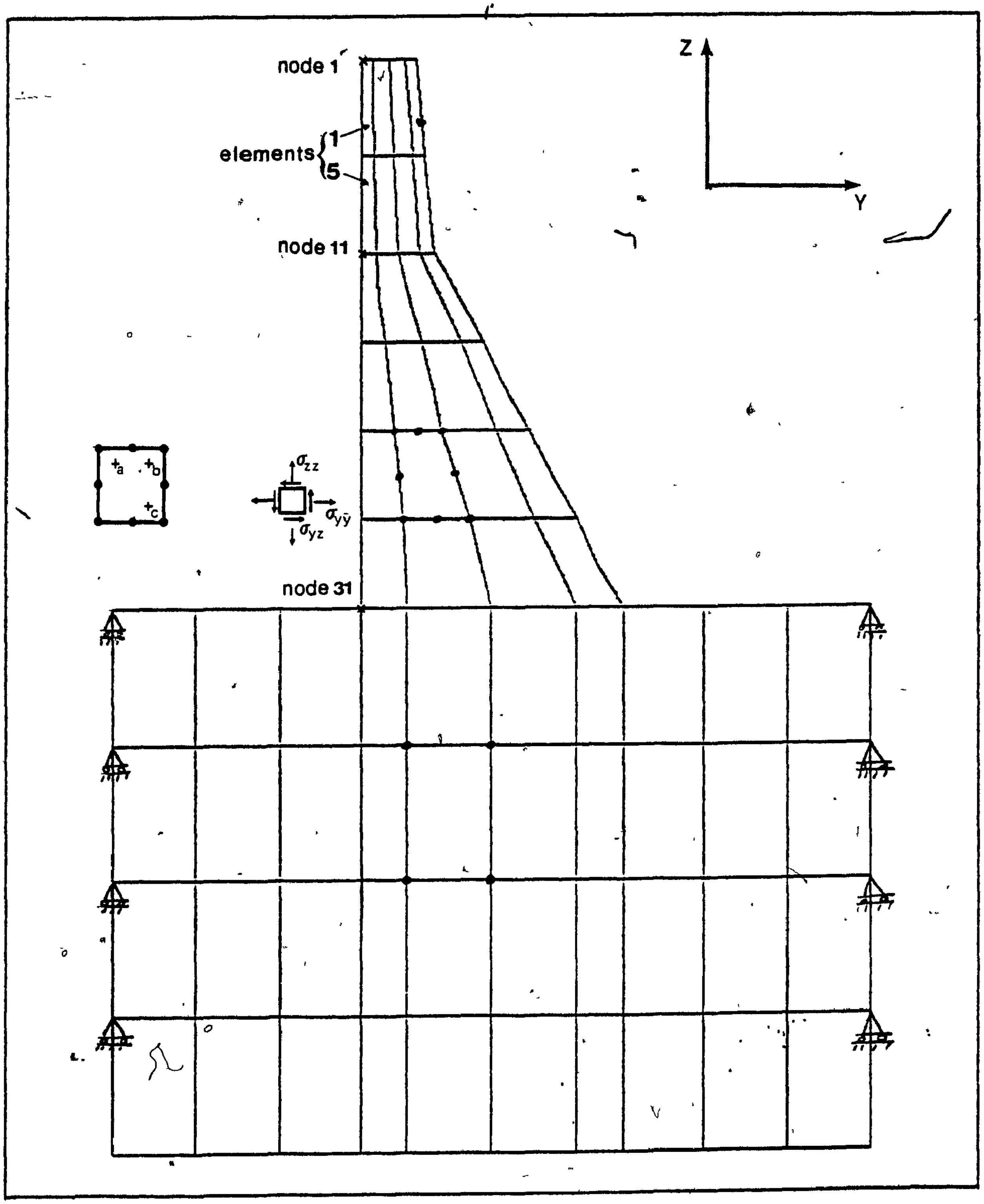

Figure 4.2 Nodes and Elements Selected for Presentation of Results.

mesh and the three components of plane stress (σ_{yy}, σ_{zz}, σ_{yz}) at the Gauss points of the finite elements. Comparing directly these response quantities given as time histories is not very practical. Thus, there is a need to define some measure of the intensity of these response quantities. The first measure of intensity to consider in the comparison of the results is the maximum that occurs during the time of excitation. This maximum value is an interesting indicator especially from a design point of view. The maximum value can not be used alone as an indication of the intensity of the response quantity of interest because it is a local measure and might not be representative of the general trend of the specified response quantity. The root mean square (R.M.S) value of a given time history can be considered as a global measure of the intensity and as an indicator of the general trend. For example the R.M.S.D, root mean square of the displacements will be given as:

$$R.M.S.D = \left(\sum_{i=1}^{n} v^2 \left(t_i \right) \right)^{1/2} \qquad (4.1)$$

where t_i represents the cumulative time achieved after every two time steps and n is the total number of time steps for which results were output. Therefore, the response quantities computed in the various analyses are compared in terms of their maximum (Max) and the corresponding root mean square (R.M.S) values.

4.4 Numerical Results from the Four Input Models

The response quantities under consideration have been computed for all the cases shown in Table 4.1. It should be noted that for the proportionally damped case, ξ_f = 5%, the global damping matrix [C] was established by applying the Rayleigh damping method for the complete system, unless otherwise specified. Due to the large amount of data, only important numerical results are presented in order to illustrate the relative performance of the four proposed earthquake input models. A more complete set of results in terms of the Max and the R.M.S values is presented in the Appendix.

4.4.1 Displacements

4.4.1.1 Time Histories

The responses time histories of horizontal displacements at node 1, resulting from the application of the El Centro accelerogram according to the four proposed input mechanisms are presented in Figures 4.3 and 4.4 for E_f/E_d=1/8, 4 and ξ_f = 5 and 15 percent of critical, representing the lower and the upper limits of the range of the selected parameters. First let us consider the case $E_f/E_d = 1/8$ with $\xi_f = 5\%$ which represents a flexible foundation rock with low damping. From Figure 4.3a) it can be observed that the results given by model A, the rigid base input model, are considerably larger than those derived from the other models. The second observation that can be made is that the responses given by model C, the deconvolved input model and model D, the free-field interface input model, are almost identical. The displacement time history corresponding to model B, the massless foundation input model, is larger than those obtained from models C and D, but the frequency content is very similar for these three models. The displacements time histories derived from models B, C and D can be approximated by harmonic functions with periods close to 1 second. Considering Figure 4.3b) in which the damping ratio of the foundation has been increased from 5 to 15 percent, shows that the frequency content of the displacements histories is not affected by the increase of the damping ratio of the foundation. However, the amplitudes of the responses diminish when the damping ratio, ξ_f, is increased. Furthermore, the amplitude of the displacements derived from models B, C and D are quite close.

Figure 4.4a) presents the displacements histories corresponding to $E_f/E_d = 4$, which represents a rigid foundation rock, the damping ratio of the foundation is set equal to 5 percent. In this case, the displacements derived from model A are still the largest but the difference with respect to the displacements derived from the other

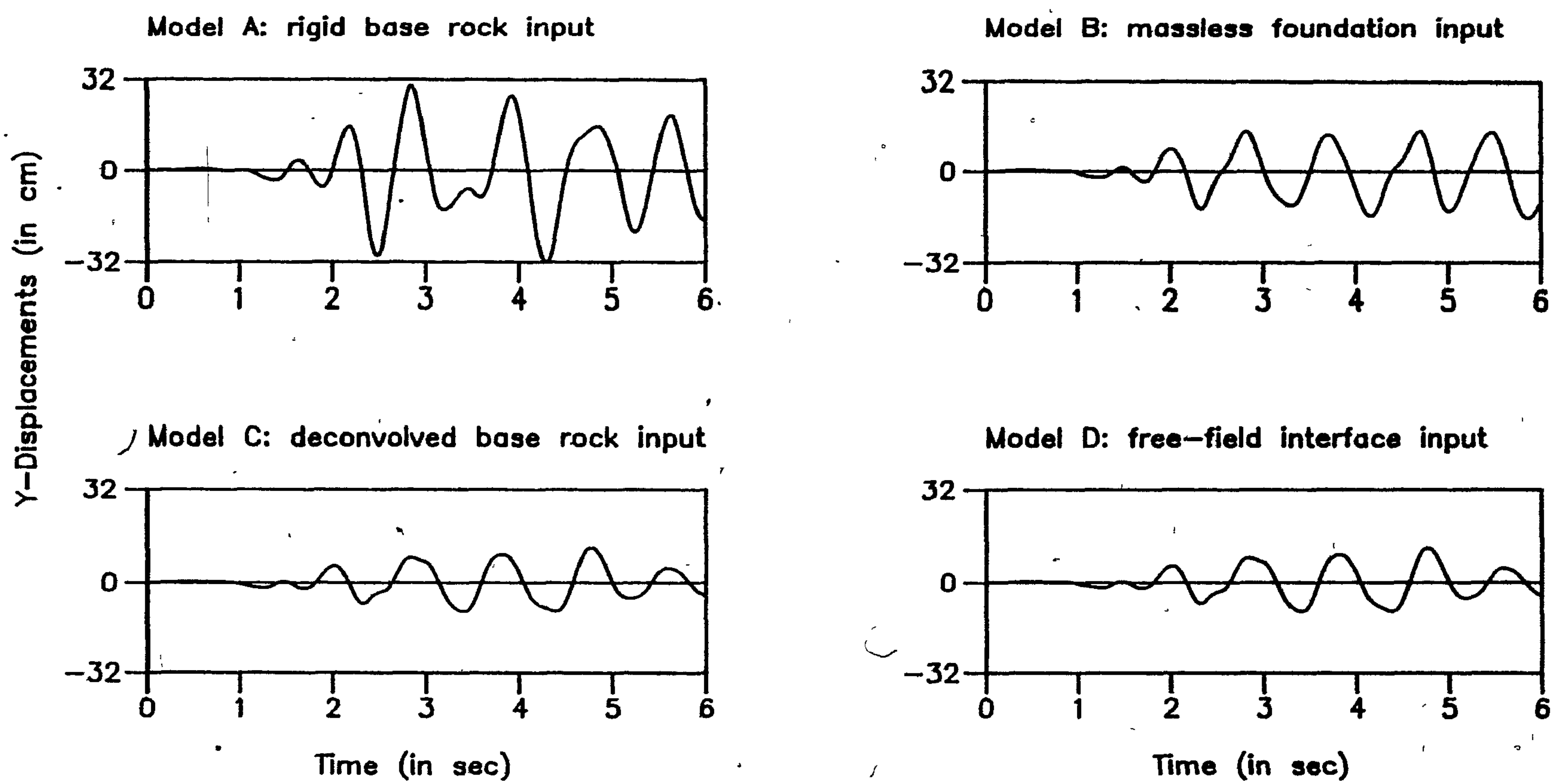

Figure 4.3a Horizontal Displacements Histories at Node 1 Derived from the Four Input Models ($E_f/E_d = 1/8$, $\xi_f = 5\%$), El Centro Earthquake.

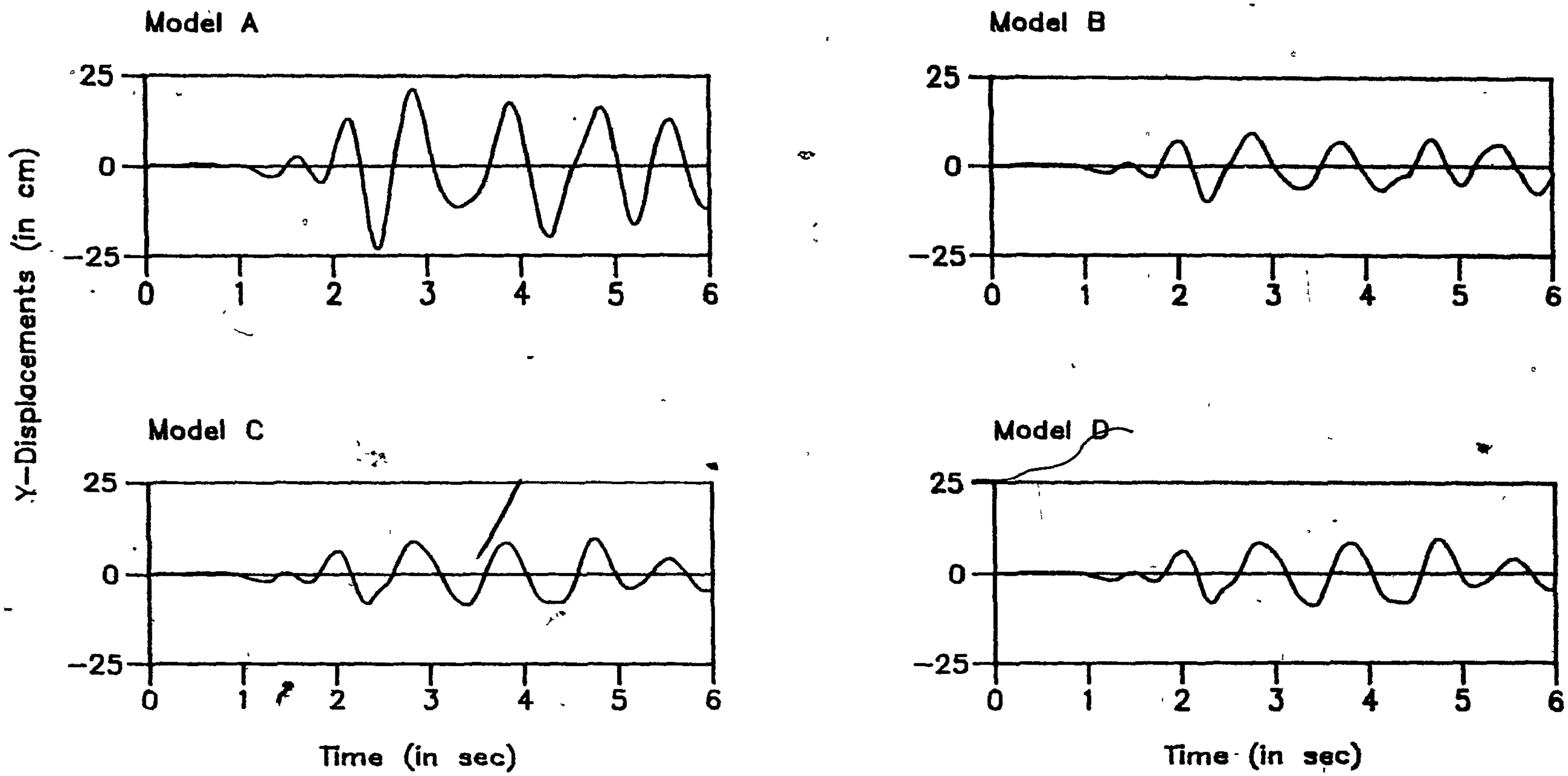

Figure 4.3b Horizontal Displacements Histories at Node 1 Derived from the Four Input Models ($E_f/E_d = 1/8$, $\xi_f = 15\%$), El Centro Earthquake.

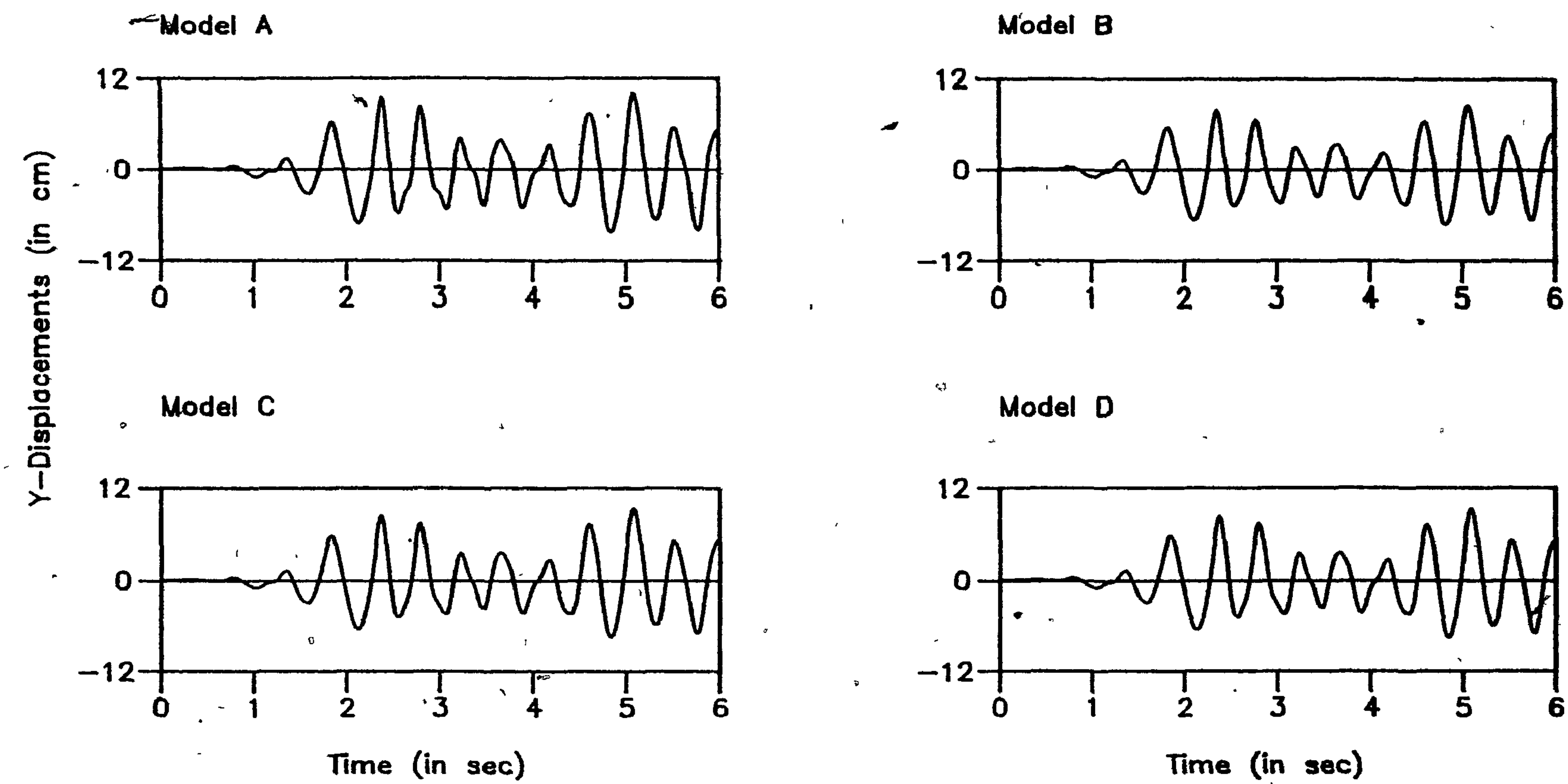

Figure 4.4a Horizontal Displacements Histories at Node 1 Derived from the Four Input Models ($E_f/E_d = 4$, $\xi_f = 5\%$), El Centro Earthquake.

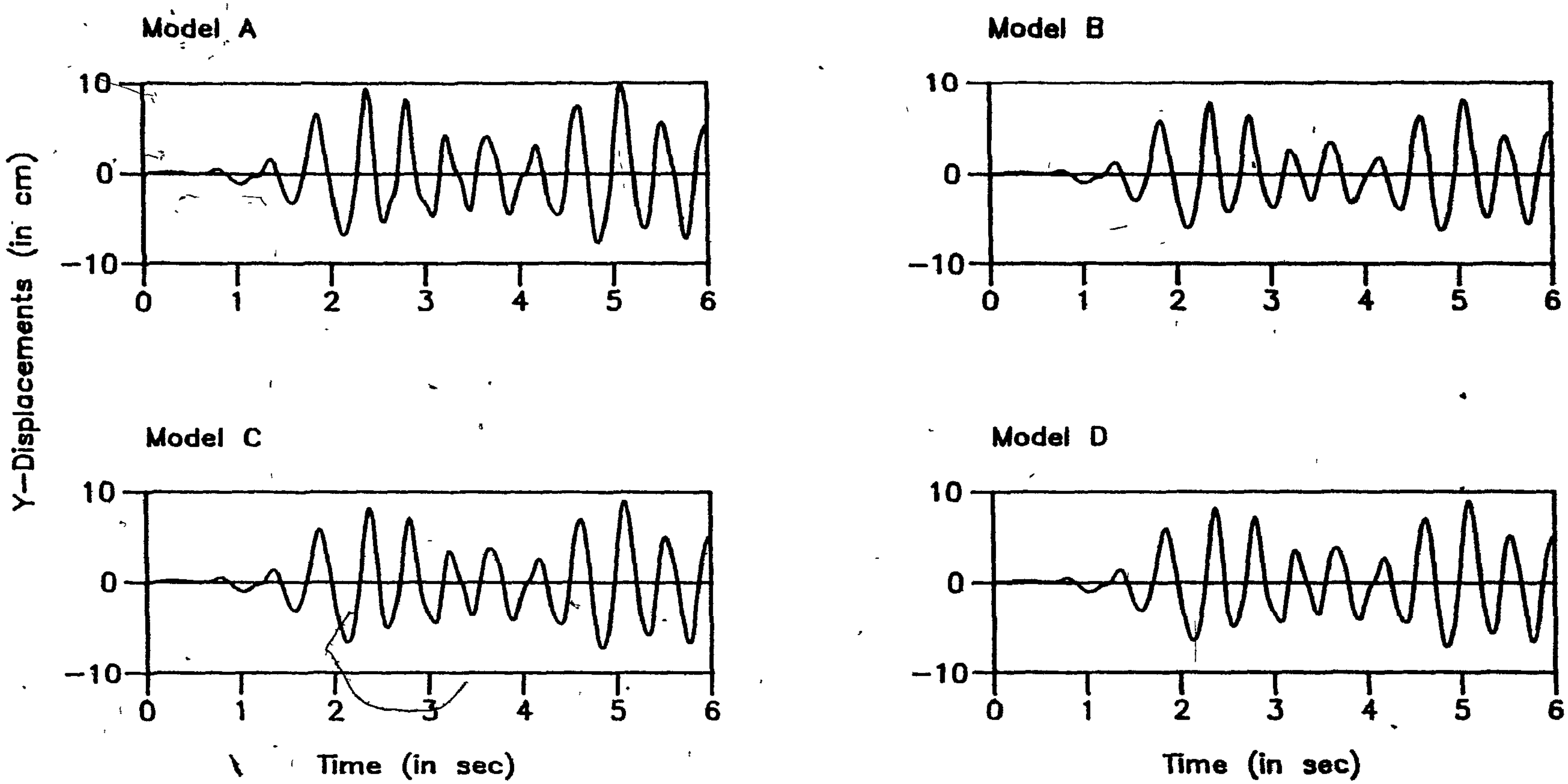

Figure 4.4b Horizontal Displacements Histories at Node 1 Derived from the Four Input Models ($E_f/E_d = 4$, $\xi_f = 15\%$), El Centro Earthquake.

models is not very significant as compared to the flexible foundation case. It should also be observed that for this case the four response histories can be approximated by harmonic functions with periods of approximately 0.5 second. The effect of increasing the damping ratio of the foundation from 5 to 15 percent is shown in Figure 4.4b. Only the amplitudes of the responses are affected by the higher damping values.

The examination of the displacements time histories has shown qualitatively the general behavior of the seismic displacement responses, obtained from the application of the four proposed earthquake input models. In order to assess the effect of the parameters retained in the analysis and to quantify the differences resulting from the different analyses, the effects of the controlling parameters will be studied in the following sections. The displacements response quantities will be represented by their maximum value (Max.D) and root mean square (R.M.S.D) values.

4.4.1.2 Influence of Controlling Parameters, E_f/E_d, ξ_f

The displacements time histories represented by their corresponding Max.D and R.M.S.D are plotted as a function of the moduli ratio E_f/E_d in Figures 4.5, 4.6 and 4.7, for the three selected values of the damping ratio, ξ_f. In order to emphasize how the displacements derived from the four input models are influenced by the variation of the damping ratio of the foundation rock, the R.M.S.D of the displacements are plotted as a function of the damping ratios in Figure 4.8, for the three different foundation flexibility conditions. From these figures the following observations can be made.

a) The displacements derived using model A are the largest in terms of the Max.D and the R.M.S.D and this is for the complete range of parameters. This was expected, since the accelerogram that was applied at the base rock was actually recorded at the surface of the foundation rock. The propagation of the ground motions through the deformable foundation rock resulted in an artificial amplification. To quantify the amount of artificial amplification, the PSa of the recorded free–field accelerogram was compared with the pseudo-spectra of the derived free–field accelerogram

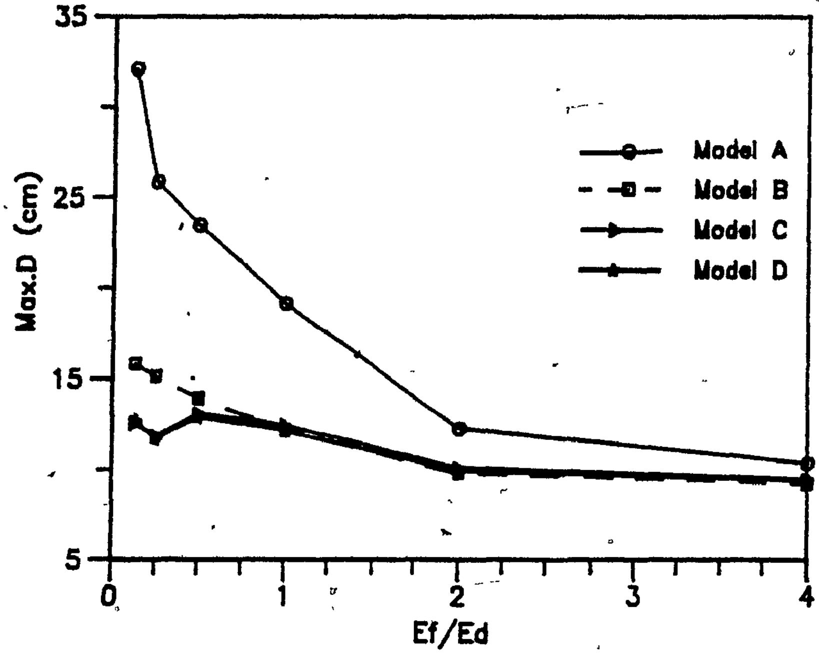

(a) Maximum Displacement as a Function of Ef/Ed

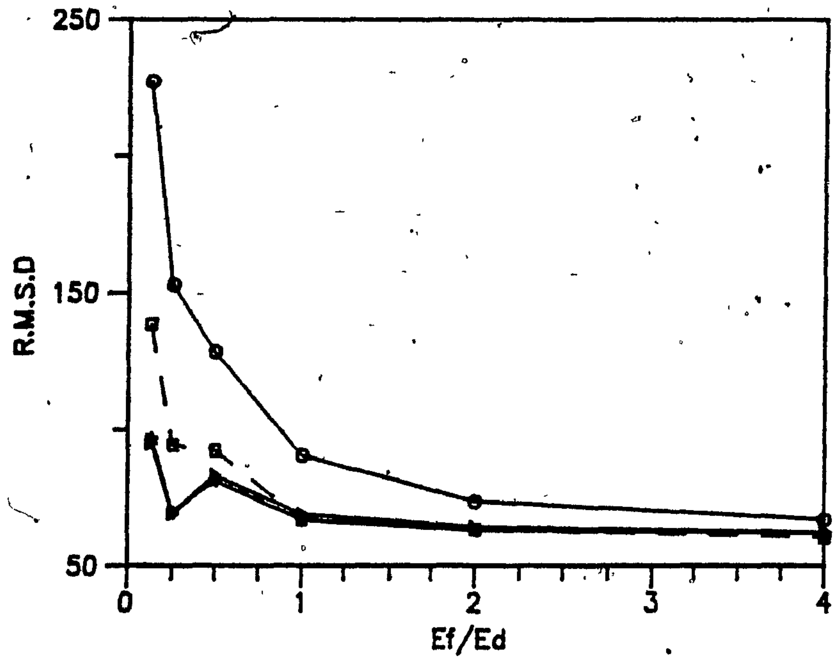

(b) R.M.S.D as a Function of Ef/Ed

Figure 4.5 Horizontal Displacements at Node 1 Derived from the Four Input Models as a Function of E_f/E_d ($\xi_f = 5\%$), El Centro Earthquake.

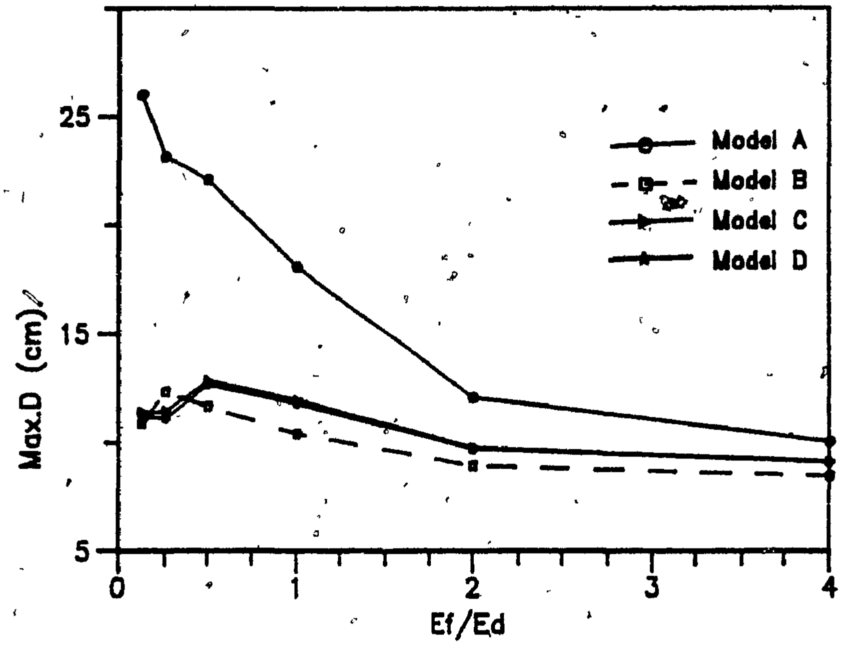

(a) Maximum Displacement as a Function of Ef/Ed.

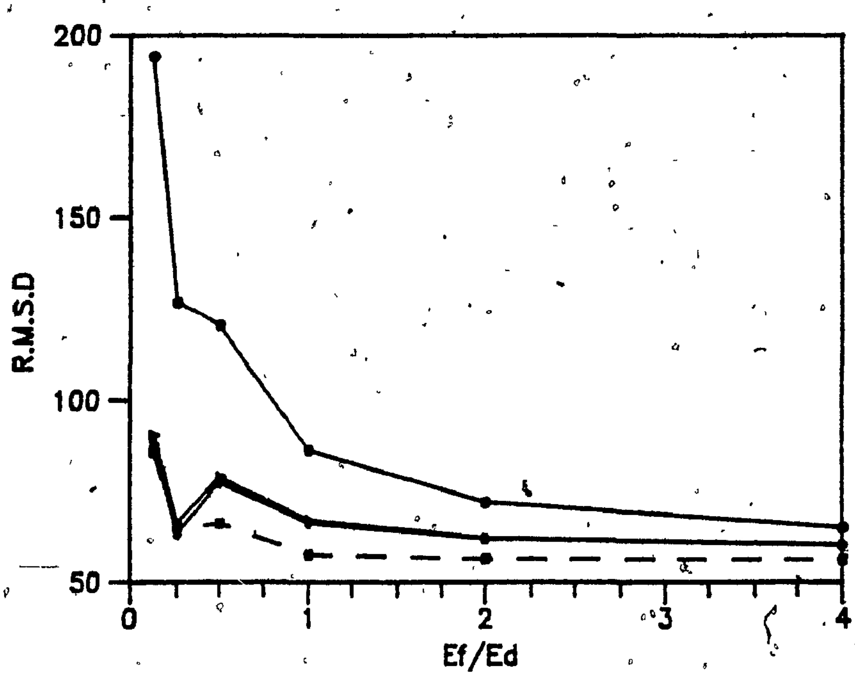

(b) R.M.S.D as a Function of Ef/Ed.

Figure 4.6 Horizontal Displacements at Node 1 Derived from the Four Input Models as a Function of E_f/E_d ($\xi_f = 10\%$), El Centro Earthquake.

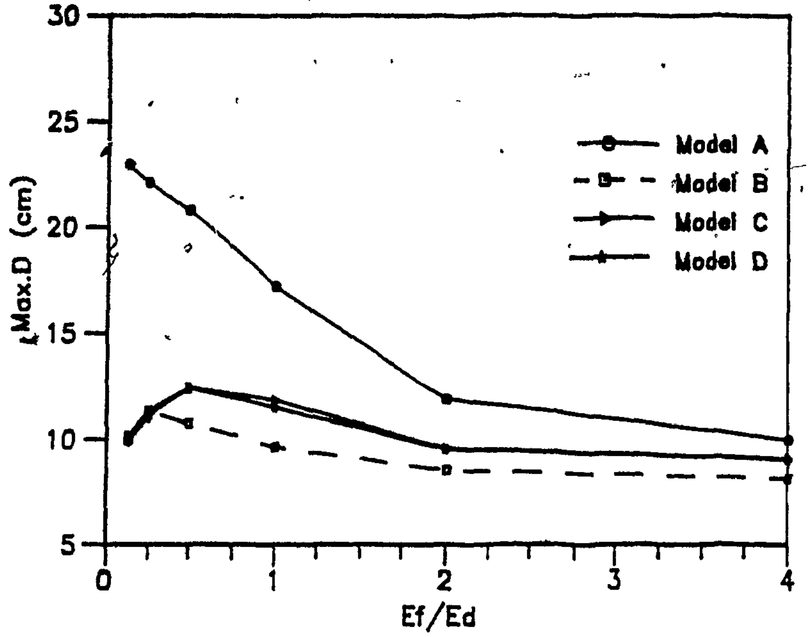

(a) Maximum Displacement as a Function of Ef/Ed

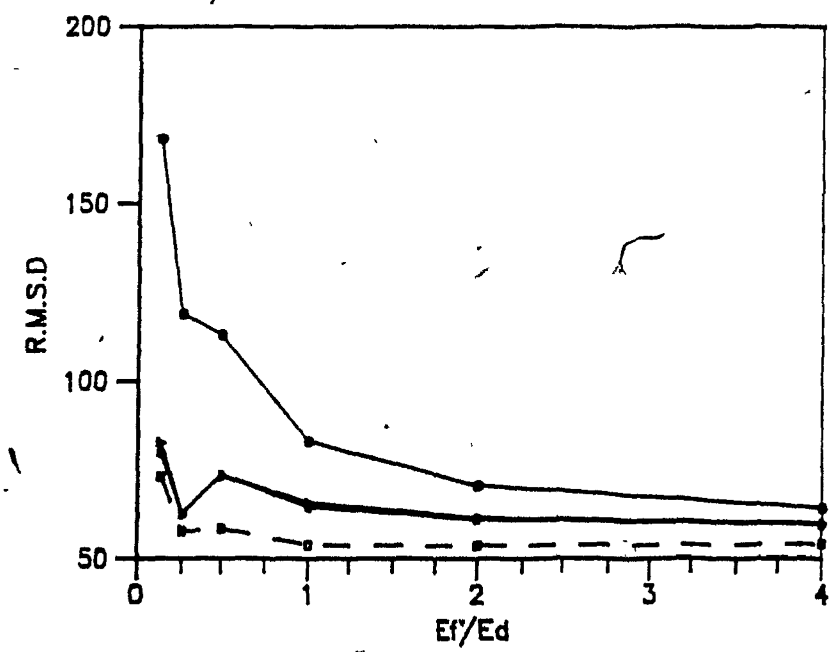

(b) R.M.S.D as a Function of Ef/Ed

Figure 4.7 Horizontal Displacements at Node 1 Derived from the Four Input Models as a Function of E_f/E_d ($\xi_f = 15\%$), El Centro Earthquake.

that resulted from the application of the recorded accelerogram at the base rock. The case shown in Figure 4.9 corresponds to $E_f/E_d = 1/2$ and $\xi_f = 5\%$. It is clear that the amplifications that the different modes of vibration of the structure will receive are larger than those that they would have received if they were subjected to the accelerogram that corresponds at the surface to the PSa shown in dashed line in Figure 4.9. It should also be noted, that the difference between the two PSa shown in Figure 4.9 will increase for a more flexible foundation rock than the one considered ($E_f/E_d = 1/2$) and it will decrease for a more rigid foundation rock where the effect of soil-structure interaction become less important.

b) For the case $E_f/E_d = 1/8$ (Fig. 4.8a)), which represents a flexible foundation rock, there is a substantial diminution in the displacements derived from model A, when the damping ratio is increased from 5 to 15 percent.

c) The displacements computed from model C, the deconvolved input model and model D, the free–field interface input model are almost identical for the complete range of the controlling parameters. It can also be noticed (Fig. 4.8a)) that the displacements derived from models C and D were not affected significantly by the increase of the damping ratio of the foundation.

d) For model B, the massless foundation input model, with $\xi_f = 5\%$, artificial amplifications of the displacements, of the order of 40 % in terms of the R.M.S.D, with respect to models C and D are observed in Figure 4.5 for the case of flexible foundations ($E_f/E_d \leq 1/4$). These amplifications are partly due to the different free–vibration characteristics of the massless foundation model as compared to models with mass foundation. It should also be noted that these results were obtained by using a proportional damping matrix computed by Rayleigh's method for the complete system.

e) Further numerical experimentation has shown that for the case discussed in d), if the damping matrix is computed by assembling the mass and stiffness proportional

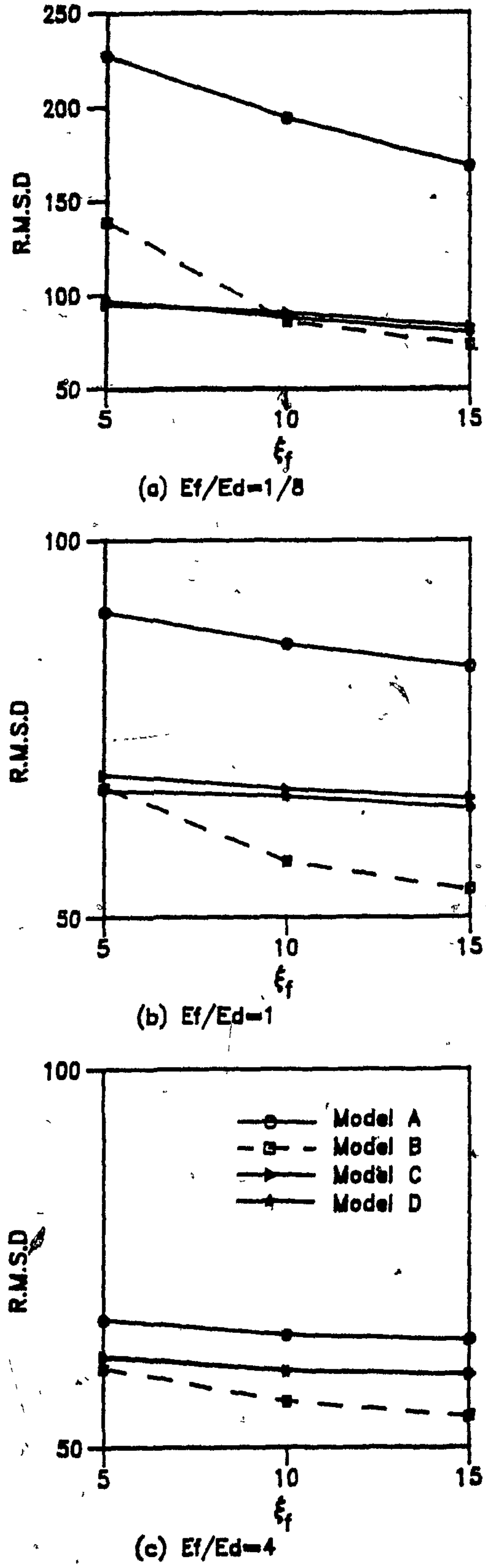

Figure 4.8 Effect of the Damping Ratio of the Foundation on the Horizontal Displacements at node 1, El Centro Earthquake.

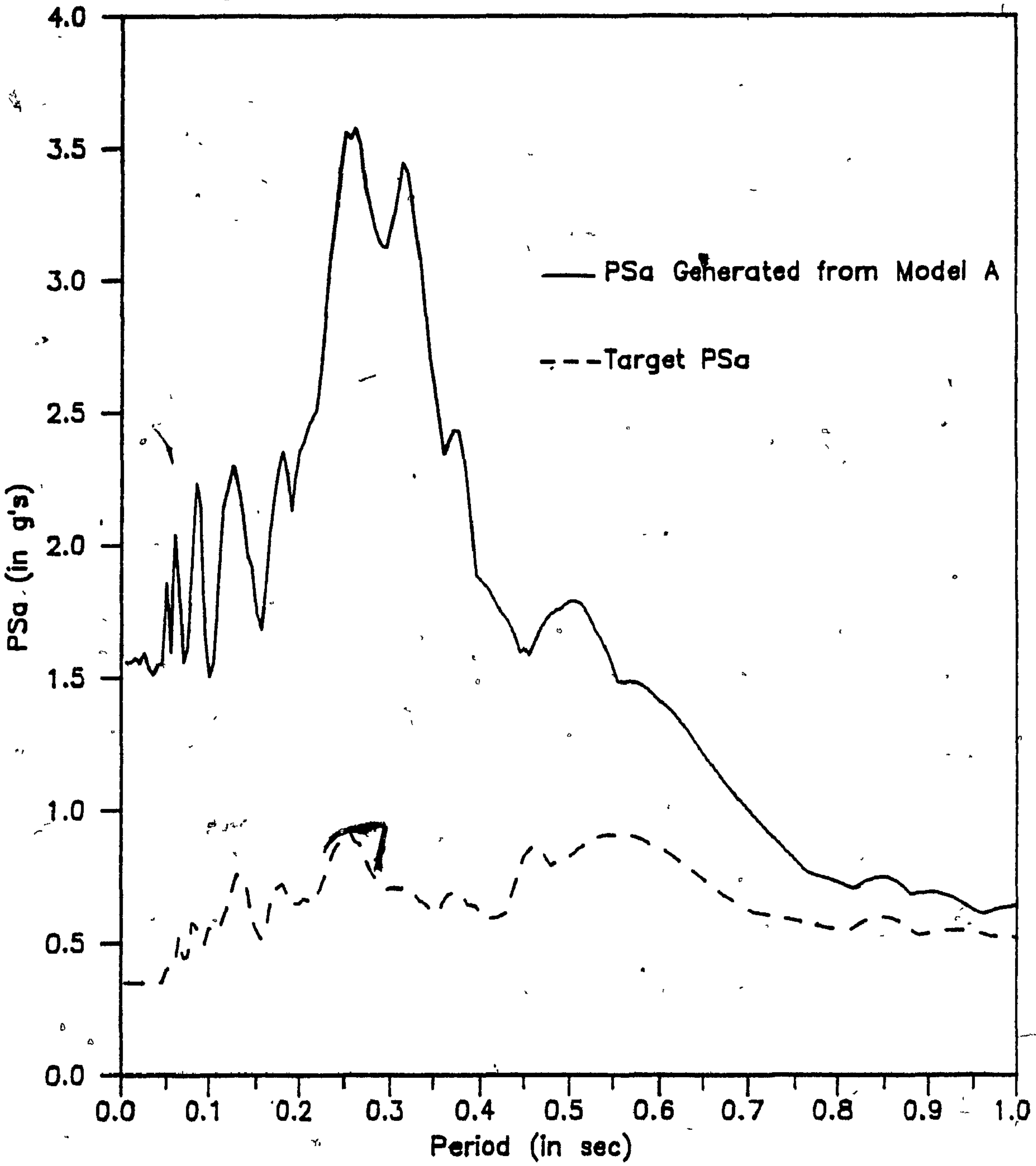

Figure 4.9 Comparison of the PSa Generated from Model A with the PSa of the Recorded Free-Field Accelerogram.

damping matrix of the dam with the stiffness proportional damping matrix of the foundation, the higher value of effective damping included in the analysis was able to reduce the maximum difference between the R.M.S.D of models B and C, D to 10%.

f) As the damping level of the massless foundation is increased (Figures 4.6 and 4.7), which corresponds to a condition of non-proportional damping, it can be noticed that the displacements derived from model B are very close to those derived from models C and D for very flexible foundation cases.

g) The displacements obtained from model B are however underestimated by an average of 15% with respect to models C and D (for $\xi_f = 15\%$), for values of E_f/E_d equal to 1/2 or higher. This can be explained by the fact that the damping for non-proportional massless foundation models was controlled only for the first mode of vibration, higher modes receiving significantly higher damping levels as explained in Section 3.2. The relative contribution of the first mode of vibration to the total response depends on the flexibility of the foundation rock. The more flexible the foundation rock, the higher is the contribution of the fundamental mode. This is significant, and explains the good agreement found for the values of E_f/E_d=1/8, 1/4, for which the first mode contributes for 86% and 68%, respectively to the total response. For relatively more rigid foundations, one should expect that the effective damping will be higher than the assigned value, since the individual modal contributions will be spread over many modes. This explains some of the discrepancies shown between models B and C, D for the stiffer foundation models.

h) The last observation is that as E_f/E_d increases, which for a fixed E_d means an increasingly rigid foundation, the displacement quantities derived from the four input models show closer agreement. The increase of the damping ratio of the foundation rock in the cases of rigid foundations does not affect significantly the displacement quantites. Furthermore, it can be noticed that as E_f/E_d increases, the displacements of the four input models converge toward a value corresponding to an infinitely rigid foundation rock.

4.4.2 Accelerations

4.4.2.1 Time Histories

The horizontal accelerations histories at node 1, resulting from the application of the El Centro accelerogram according to the four proposed input models are presented in Figures 4.10 and 4.11, respectively for $E_f/E_d = 1/8$ and 4, and for a damping ratio of the foundation equal to 5 percent. As for the displacements, model A yielded to the largest response in terms of the acceleration values. The accelerations computed from models C and D are almost identical for the complete range of parameters. The frequency content of the accelerations derived from model B is very similar to the ones derived from models C and D. The major differences between the acceleration histories of model B and those of models C and D are in their amplitudes.

For the case $E_f/E_d = 1/8$ ($\xi_f = 5\%$), the maximum acceleration is 3.1g for model A, corresponding to an amplification factor (AF) of 9.4, 1.38g for model B (AF=4.18) and .96g (AF=2.9) for models C and D. Considering the case $E_f/E_d = 4$, which represents a rigid rock foundation, it can be observed that the intensity of the accelerations has increased comparatively with the previous case, but the difference between the accelerations derived from the four input models has diminished. The maximum acceleration from model A is 3.9g (AF=11.8), from model B it is 2.4g (AF=7.27) and from model C and D it is 2.5g (AF=7.37). Therefore, as was noted for the displacements, as the stiffness of the foundation is increased, the accelerations tend to converge toward the value obtained for the dam fixed at its base.

4.4.2.2 Influence of Controlling Parameters, E_f/E_d, ξ_f

Following the same procedure as for the displacements, the effects of the modular ratio E_f/E_d and the damping ratio, ξ_f, on the accelerations are examined in this

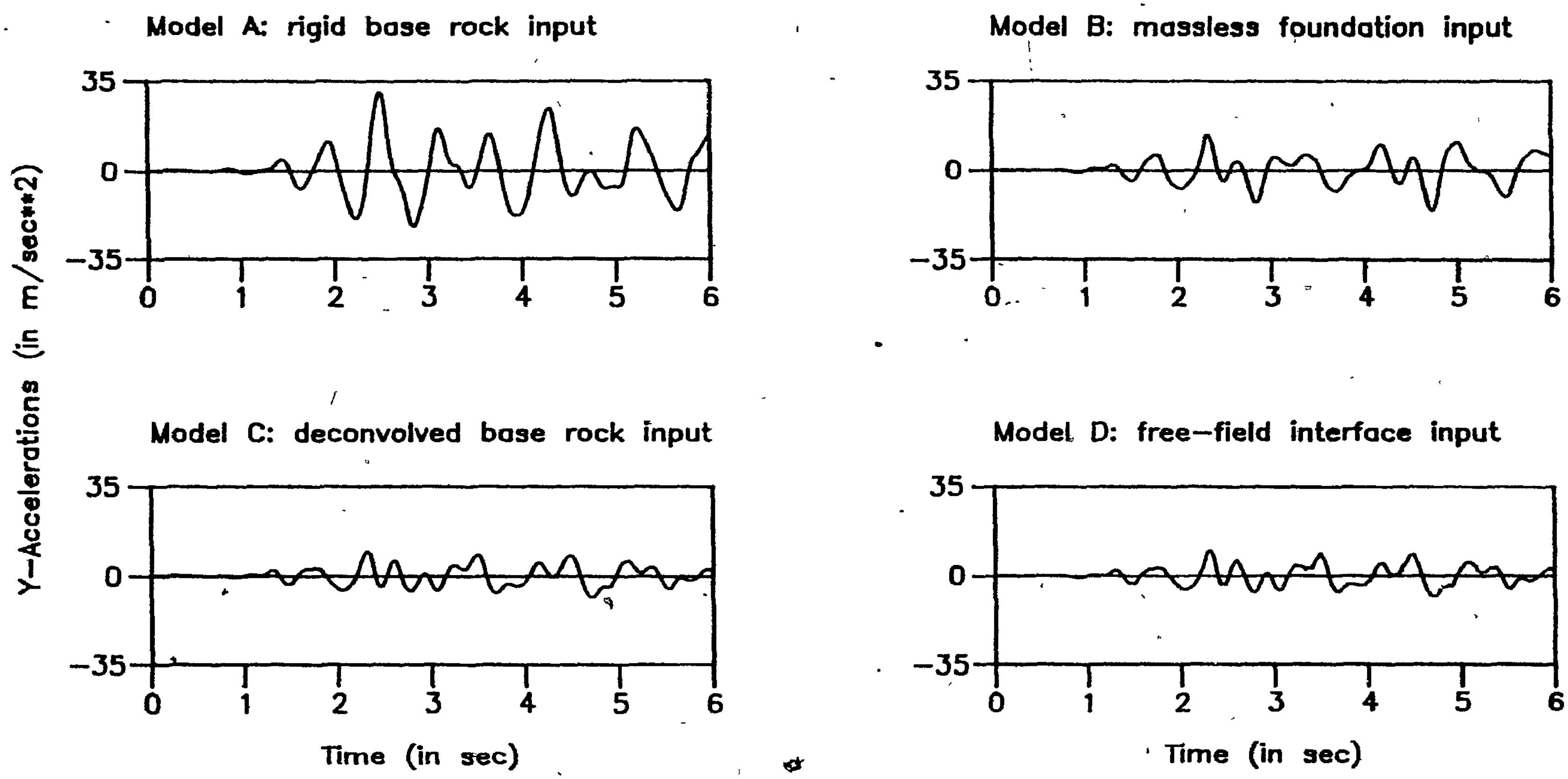

Figure 4.10 Horizontal Accelerations Histories at node 1 Derived from the Four Input Models ($E_f/E_d = 1/8$, $\xi_f = 5\%$), El Centro Earthquake.

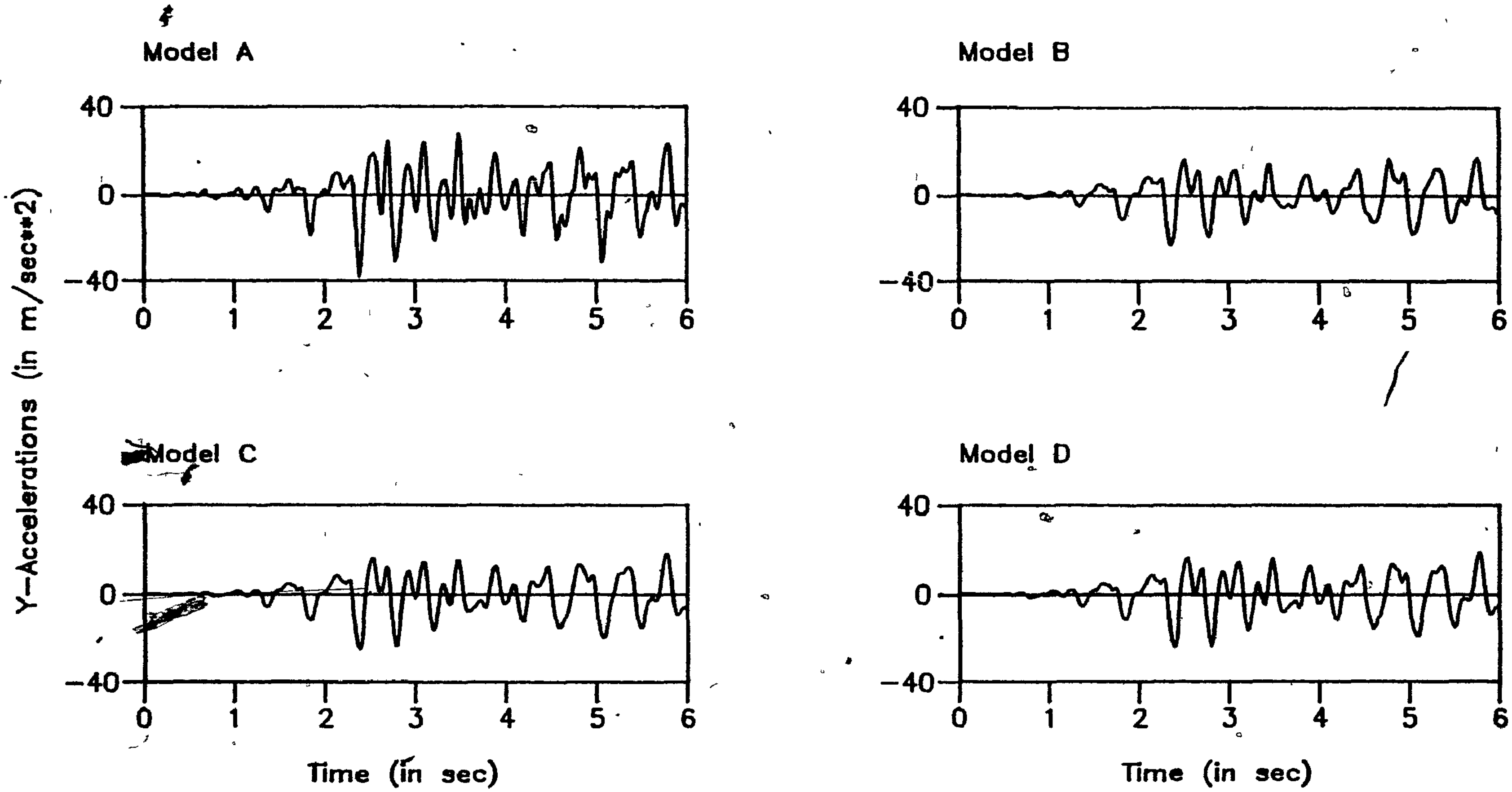

Figure 4.11 Horizontal Accelerations Histories at node 1 Derived from the Four Input Models ($E_f/E_d = 4$, $\xi_f = 5\%$), El Centro Earthquake.

section. The R.M.S.A of the accelerations, and the corresponding Max.A, are plotted as a function of the ratio E_f/E_d in Figures 4.12 to 4.14, for the three selected values of the damping ratio, ξ_f, of the foundation rock. The variation of the horizontal accelerations due to the increase in the damping ratio, ξ_f, for three different levels of foundation flexibility, is shown in Figure 4.15. These figures show that:

a) The accelerations derived from model A are larger than the ones derived from the other models for the complete range of the controlling parameters. The increase in the damping ratio, ξ_f, resulted in a substantial decrease in the accelerations derived from model A for flexible foundation cases, whereas for rigid foundations the accelerations were affected to a lesser degree.

b) The accelerations derived from models C and D are very similar, except at some points where small deviations between the two models are observed. This is mainly due to the fact that the response is more sensitive in terms of the acceleration quantities than it is in terms of the displacements. This is because the accelerations are the second derivatives of the displacements with respect to time. The increase of the damping ratio, ξ_f, did not affect significantly the accelerations of models C and D.

c) The accelerations derived from model B for the proportionally damped case, $\xi_f =$ 5% (Fig. 4.12), are close to those derived from models C and D for relatively rigid foundation cases ($E_f/E_d \geq 1$). For very flexible foundation cases, as was noted for the displacements, an artificial amplification is observed between model B and models C, D. The maximum difference in terms of the R.M.S.A which was of the order of 55% for the caseC E_f/E_d=1/8, was reduced to 20% when the damping matrix of the complete system was established by assembling the Rayleigh damped matrix of the dam and the stiffness proportional damping matrix of the foundation.

d) For the non-proportionally damped cases (ξ_f = 10%, 15%), the accelerations derived from model B were close to those of models C and D. Indeed, for E_f/E_d=1/8

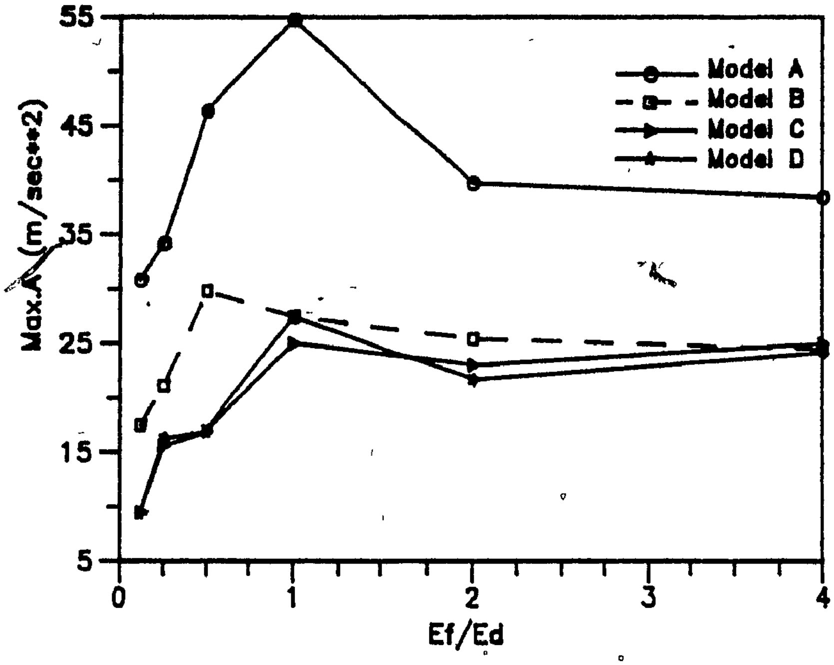

(a) Maximum Accelerations as a Function of Ef/Ed

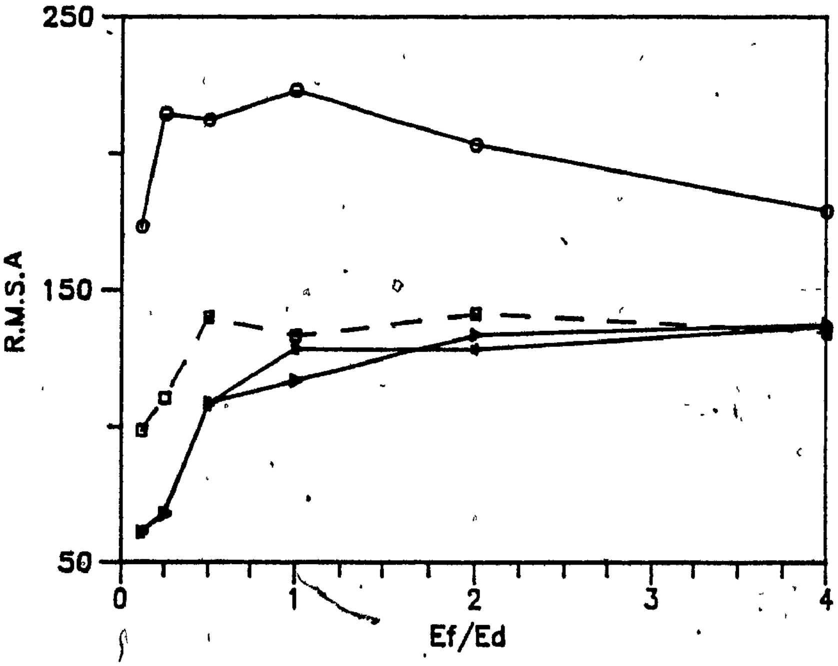

(b) R.M.S.A as a Function of Ef/Ed

Figure 4.12 Horizontal Accelerations at Node 1 Derived from the Four Input Models as a Function of E_f/E_d ($\xi_f = 5\%$), El Centro Earthquake.

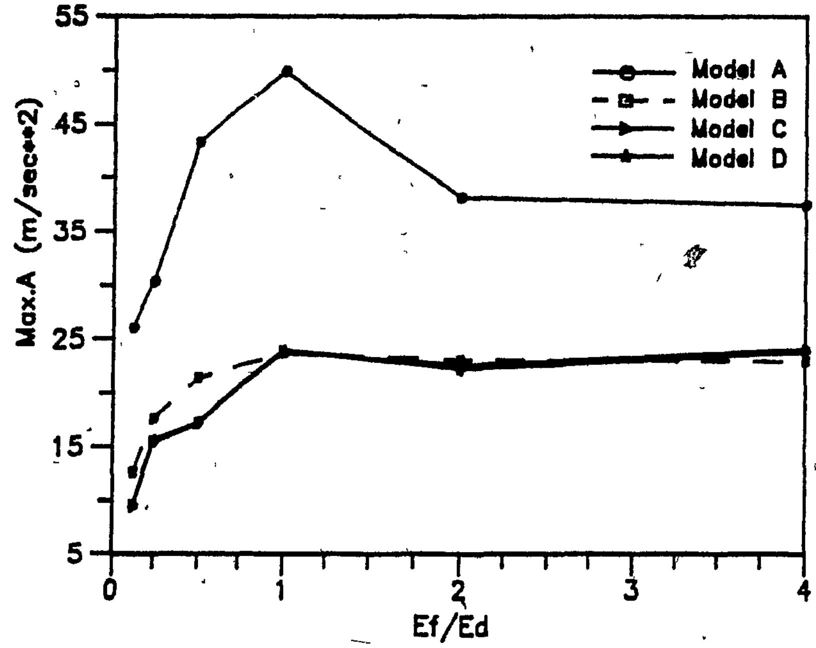

(a) Maximum Accelerations as a Function of Ef/Ed

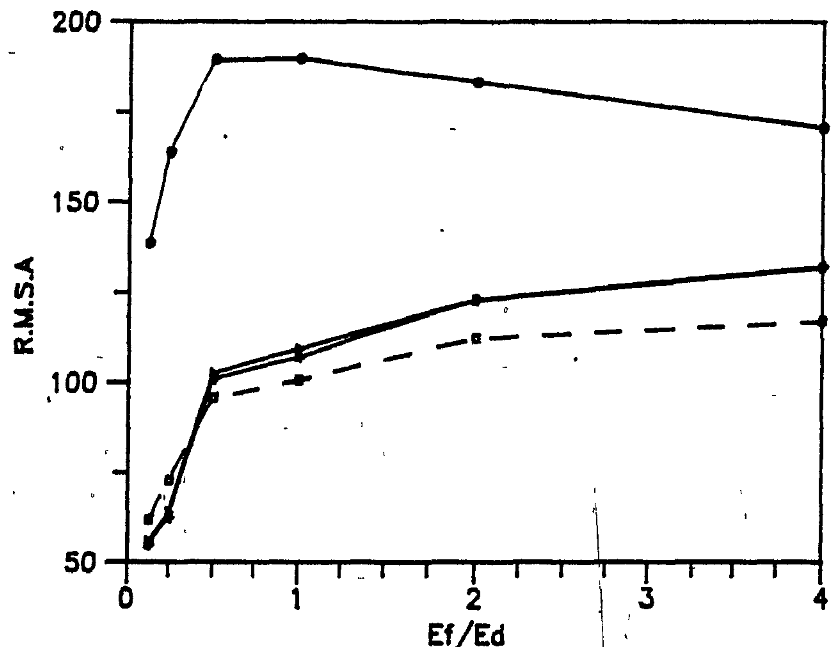

(b) R.M.S.A as a Function of Ef/Ed

Figure 4.13 Horizontal Accelerations at Node 1 Derived from the Four Input Models as a Function of E_f/E_d ($\xi_f = 10\%$), El Centro Earthquake.

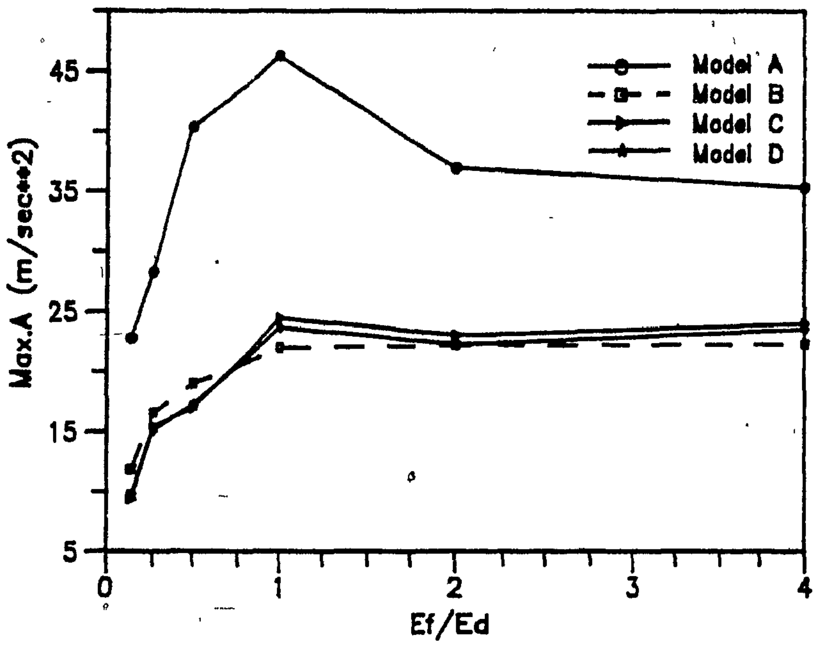

(a) Maximum Accelerations as a Function of Ef/Ed

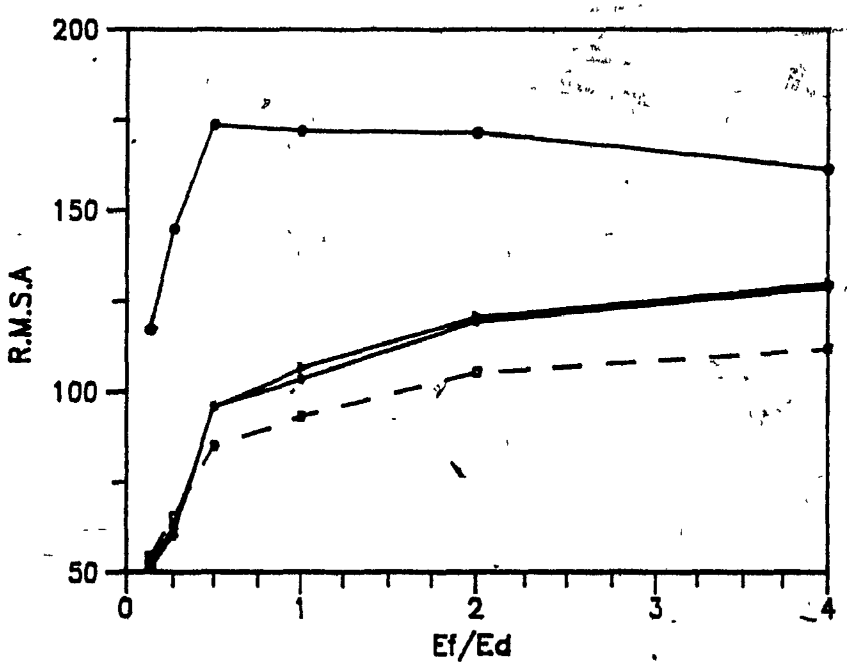

(b) R.M.S.A as a Function of Ef/Ed

Figure 4.14 Horizontal Accelerations at Node 1 Derived from the Four Input Models as a Function of E_f/E_d ($\xi_f = 15\%$), El Centro Earthquake.

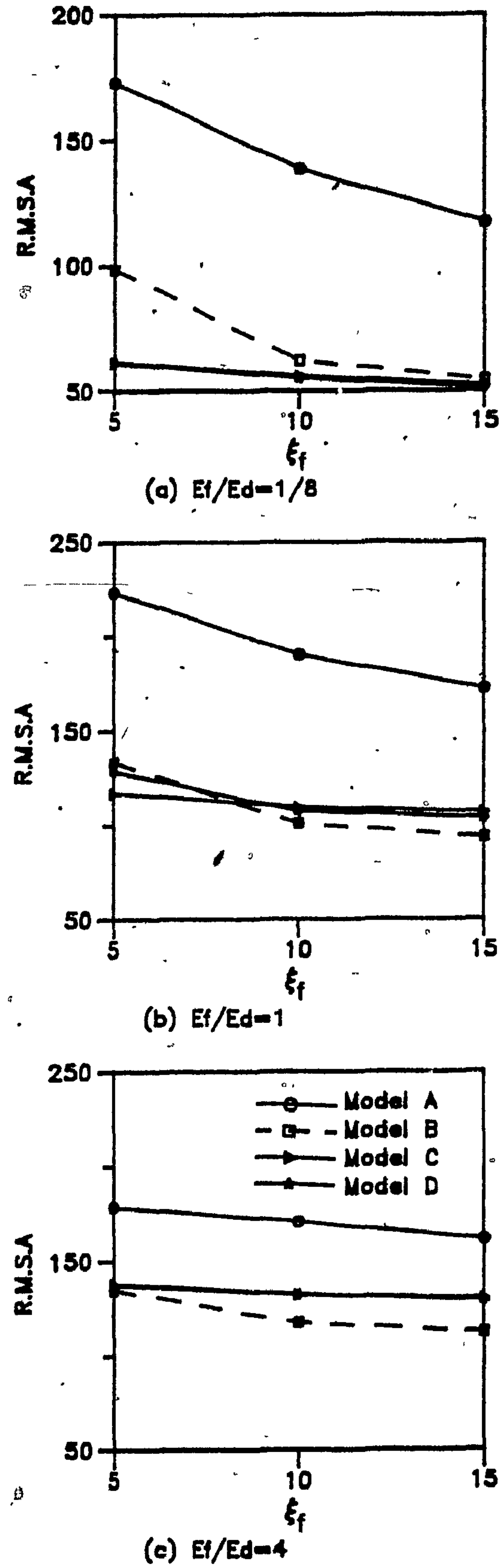

Figure 4.15 Effect of the Damping Ratio of the Foundation on the Horizontal Accelerations at Node 1, El Centro Earthquake.

the difference in the accelerations of model B, in terms of the R.M.S.A as compared to models C and D was 12% for $\xi_f = 10\%$ and 4% for $\xi_f = 15\%$. For relatively rigid foundations, deviations are observed between models B and C, D, leading to an average difference of 8% for $\xi_f = 10\%$ and 12% for $\xi_f = 15\%$.

e) It should be noted that the differences between model B and models C, D noted previously were in terms of the R.M.S.A, if the Max.A are considered the differences in the results of model B as compared to those of models C and D are less significant.

h) For the most rigid foundation case considered (Fig. 4.15c)), the accelerations derived from the four input models are quite close to each other. In this stiffer range, the increase of the damping ratio, ξ_f, does not affect the accelerations of the four models to a great extent.

4.4.3 Stresses

The stress results presented in Appendix A, consist of normal stresses in the horizontal (σ_{yy}) and vertical (σ_{zz}) directions and shear stresses (σ_{yz}). For the design of the dam, the magnitude of the normal stresses in the vertical direction will be critical. Therefore, the following discussion will be based on them. However it should be noted that qualitative observations derived for vertical stress components remain valid for the other stress components.

4.4.3.1 Time Histories

The normal stress histories ~~in~~ the vertical direction, for element 5 (point b), are shown in Figures 4.16 and 4.17 respectively for $E_f/E_d = 1/8$ and 4, and a damping ratio $\xi_f = 5\%$. It is clear from these figures that as for the displacement and the acceleration histories, model A results in the largest stresses. The stresses derived from model C and D are almost identical in terms of both the frequency content and amplitudes. The stresses derived from model B for the flexible foundation case, $E_f/E_d = 1/8$, are larger than those derived from models C and D. For the case $E_f/E_d = 4$, the frequencies content of the stress responses derived from the four input models, are almost identical. Furthermore for that case, the amplitudes of the stresses derived from model B are very close to those from models C and D.

4.4.3.2 Influence of Controlling Parameters, E_f/E_d, ξ_f

The effects of both the flexibility and damping level of the foundation on the vertical normal stresses are investigated in this section. As was done for the previous response quantites, the R.M.S.S and the Max.S of the normal stresses in the vertical direction at element 5, are plotted as a function of the moduli ratio E_f/E_d in Figures 4.18 to 4.20, for the three selected values of the damping ratio. Figure 4.21 shows the variation of the vertical normal stresses at element 5 represented by their corresponding R.M.S.S, as a function of the damping ratio of the foundation, ξ_f. From these figures the following observations can be made:

a) Model A results in the largest normal stresses and this is for the complete range of selected parameters. However, for the most rigid foundation case considered ($E_f/E_d = 4$), the difference between stresses derived from model A and the stresses derived from the three other models is not very significant.

b) In the case of the stresses also, the results derived from models C and D are similar for the complete range of parameters.

c) Model B for the case $\xi_f = 5\%$ and for flexible foundation cases, yielded vertical normal stresses which are relatively different in terms of the R.M.S.S from those of models C and D with an average relative error of about 38%. From Figure 4.21 it can be noticed that for the cases E_f/E_d=1 and 4, the normal stresses increase when the damping ratio is increased from 5 to 10 percent. This has been observed only for the stresses and can again be explained by the way the global damping matrix was established for ξ_f =5%, for which a condition of proportional damping allowed the application of the Rayleigh damping method to the complete

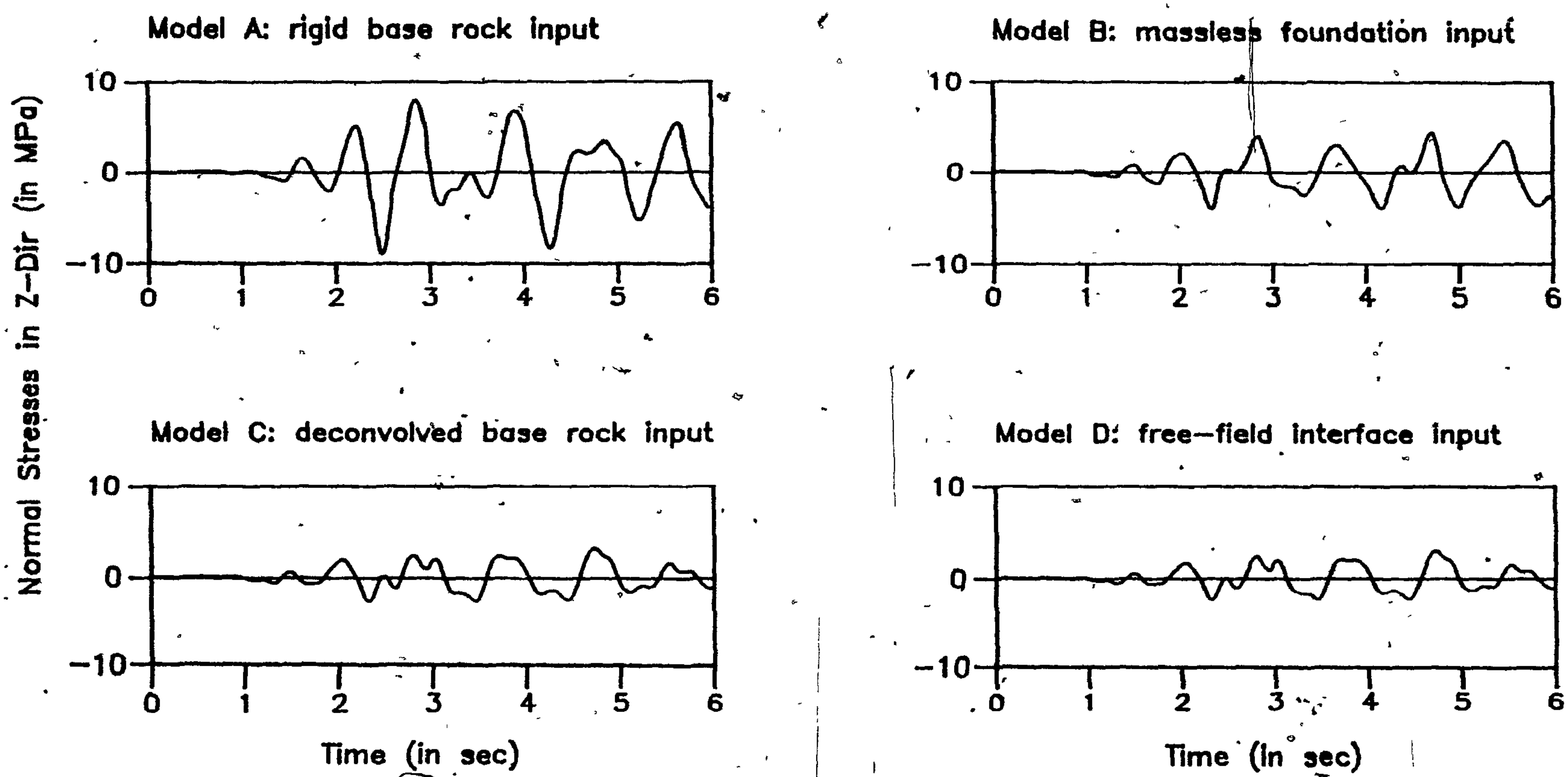

Figure 4.16 Vertical Normal Stresses Histories at Element 5 (point b) Derived from the Four Input Models ($E_f/E_d = 1/8$, $\xi_f = 5\%$), El Centro Earthquake.

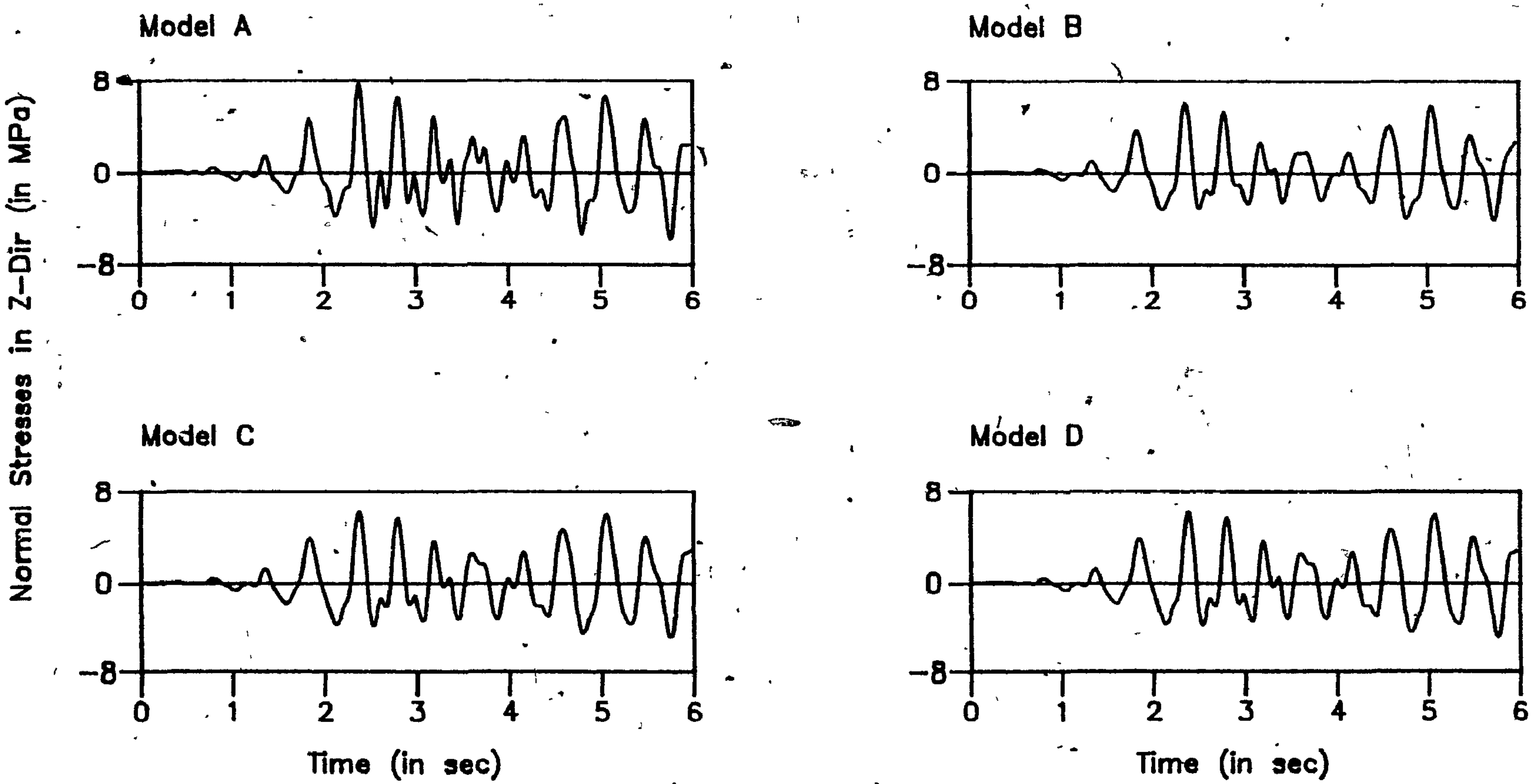

Figure 4.17 Vertical Normal Stresses Histories at Element 5 (point b) Derived from the Four Input Models ($E_f/E_d = 4$, $\xi_f = 5\%$), El Centro Earthquake.

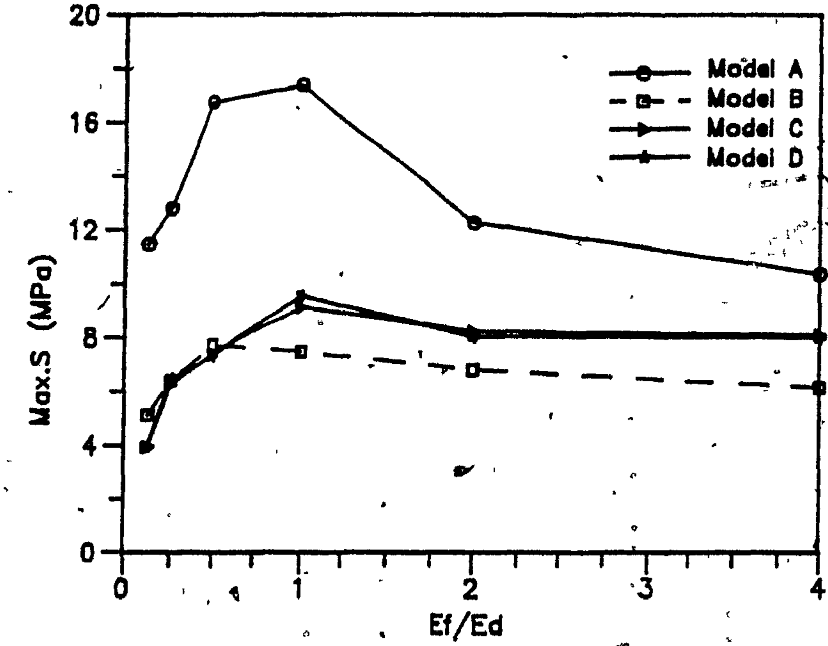

(a) Maximum Normal Stress in Z–dir as a Function of Ef/Ed

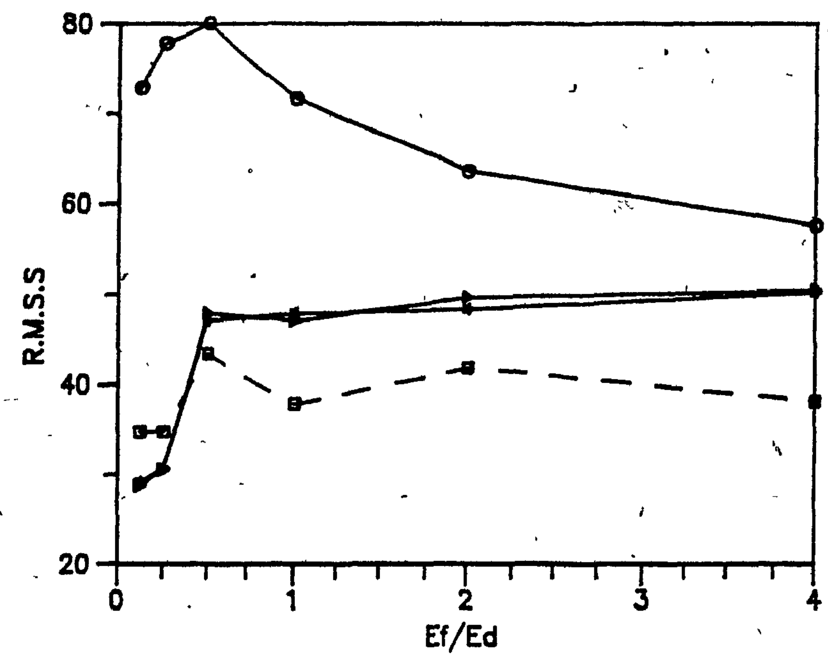

(b) R.M.S.S as a Function of Ef/Ed

Figure 4.18 Vertical Normal Stresses at Element 5 Derived from the Four Input Models as a Function of E_f/E_d ($\xi_f = 5\%$), El Centro Earthquake.

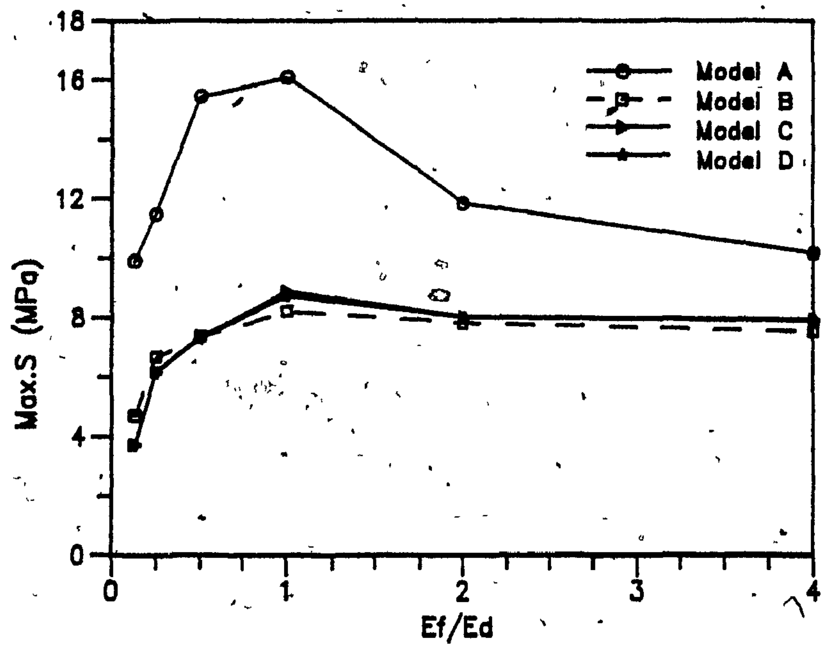

(a) Maximum Normal Stress in Z-dir as a Function of Ef/Ed

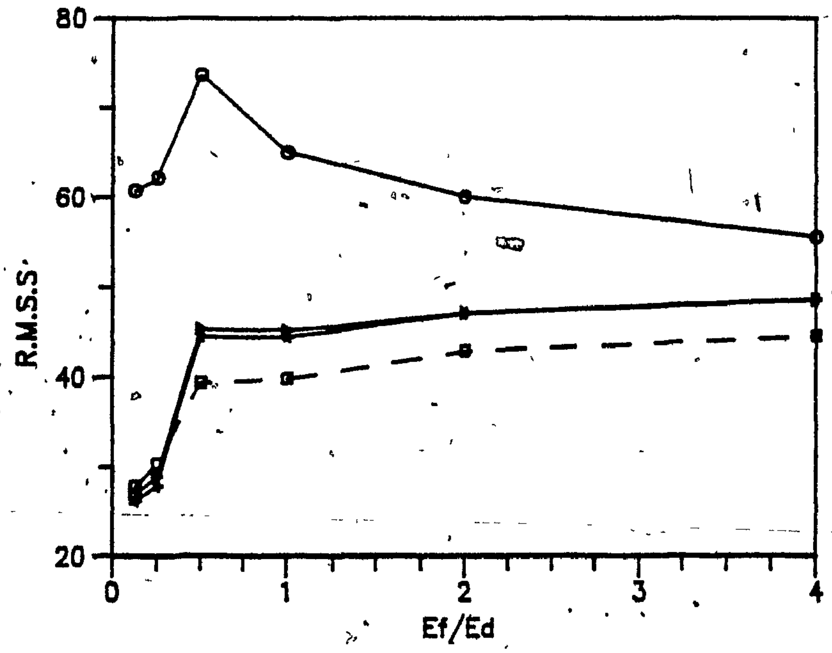

(b) R.M.S.S as a Function of Ef/Ed

Figure 4.19 Vertical Normal Stresses at Element 5 Derived from the Four Input Models as a Function of E_f/E_d ($\xi_f = 10\%$), El Centro Earthquake.

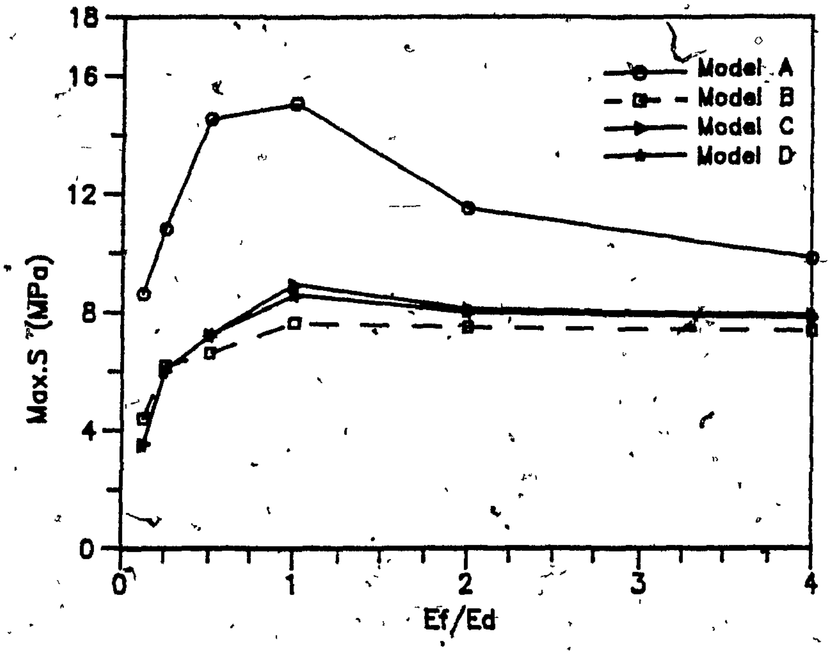

(a) Maximum Normal Stress in Z-dir as a Function of Ef/Ed

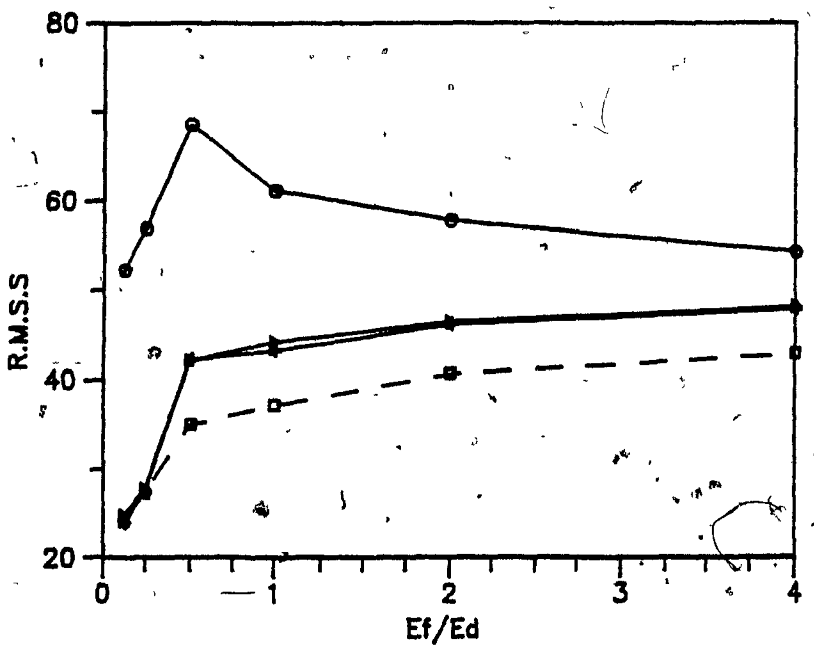

(b) R.M.S.S as a Function of Ef/Ed

Figure 4.20 Vertical Normal Stresses at Element 5 Derived from the Four Input Models as a Function of E_f/E_d ($\xi_f = 15\%$), El Centro Earthquake.

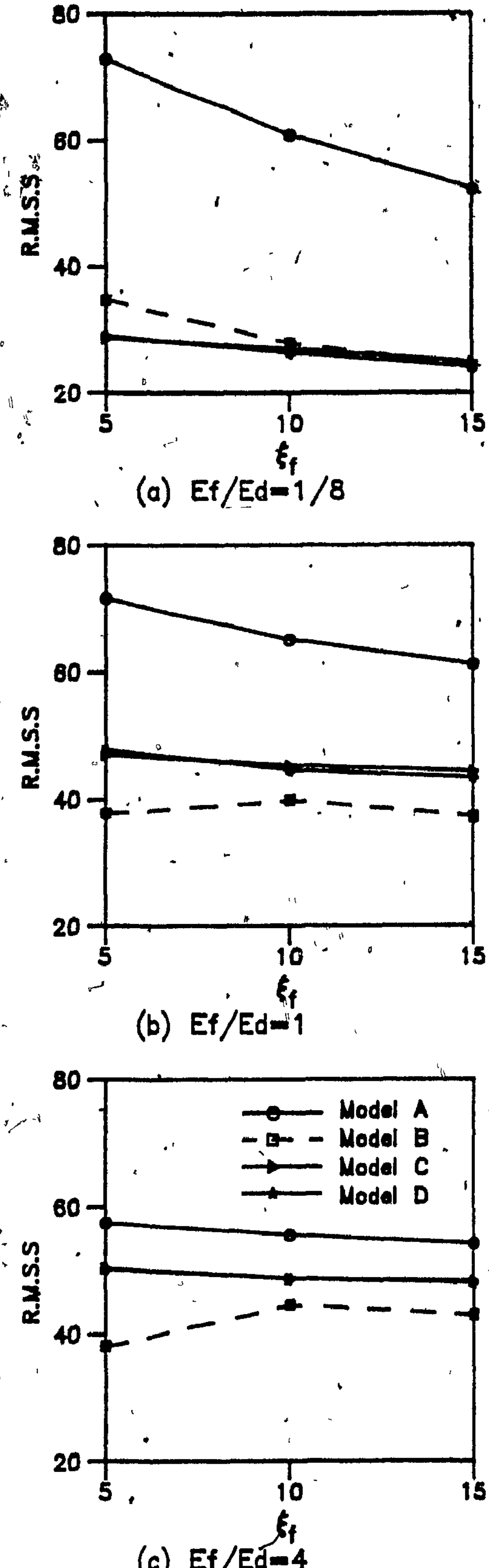

Figure 4.21 Effect of the Damping Ratio of the Foundation on the Vertical Normal Stresses at Element 5, El Centro Earthquake.

system. It has been verified that if the damping matrix corresponding to $\xi_f = 5\%$ is established by assembling the damping matrices of the two substructures, the stresses corresponding to $\xi_f = 5\%$, for the cases E_f/E_d of 1 and 4, will be larger than those corresponding to $\xi_f = 10\%$. Furthermore, the stresses for the flexible foundation cases ($E_f/E_d \leq 1/4$), derived from model B will then exhibit a relative error of the order of 15% as compared to those obtained from models C and D.

d) For higher damping ratios (ξ_f =10%, 15%), the vertical normal stresses derived from model B are very close to those of models C, D, for very flexible foundations ($E_f/E_d \leq 1/4$). For the other values of the ratio, E_f/E_d, model B underestimated the stresses by an average of 13% as compared to models C and D.

e) As was noted previously for the accelerations, the maximum values of the vertical normal stresses derived from model B and models C, D, are closer than are the corresponding R.M.S.S.

4.5 Effect of the Damping Ratio on the Massless Foundation Model

It has been shown in the previous sections that the performance of model B is closely related to the value of damping ratio assigned to the foundation rock and the computational technique used to form the global damping matrix [C]. The performance of model B can be improved by a better numerical control of the values of the damping ratio of the foundation rock. It should be noted however, that the differences in the response quantities computed from model B and those of models C and D are also due to the fact that the behavior of the massless foundation model in free-vibration is not the same as compared to the mass foundation model.

In order to illustrate the effect of the damping ratio, ξ_f, of the massless foundation model on the displacements quantities, the horizontal displacement at node 1 represented by the corresponding R.M.S.D is plotted in Figure 4.22 as a function of the modular ratio, E_f/E_d, for four selected values of the damping ratio, ξ_f =0, 5, 10 and 15 percent of critical. It should be noted that for the proportionally damped case ($\xi_f = 5\%$), two cases are shown. The first case corresponds to a damping matrix formed by applying the Rayleigh method to the complete system, while the second case corresponds to a damping matrix established by assembling the damping matrices of the dam and the foundation recognizing explicitly their different inertial characteristics. It can be noticed from Figure 4.22 that the effect of the damping ratio is dependent on the flexibility of the foundation. For very flexible foundation cases, assigning a value of zero damping to the massless foundation increases the displacement quantities significantly, whereas for relatively rigid foundation cases the value of the damping ratio does not have a significant influence on the magnitude of the displacements quantities. The use of a stiffness proportional only foundation damping matrix is also shown to reduce significantly the amplitude of the response for relatively flexible foundations.

The displacements derived from model B, with a value of zero damping for the massless foundation are compared in Figure 4.23 with the average displacements derived from models C and D in which the damping ratio of the foundation was assigned the values of ξ_f =5, 10, 15%, for the various foundation flexibility levels. It is noteworthy from Figure 4.23 that model B with $\xi_f = 0\%$ is in good agreement with models C and D for relatively rigid foundations, with $E_f/E_d \geq 1$, especially for the lightly damped foundation rock ($\xi_f = 5\%$ in models C, D). For flexible foundation cases, with $E_f/E_d \leq 1$, it can be noticed from Figure 4.23 that a damping value different from zero has to be assigned to the massless foundation in order to improve the performance of this model.

An alternative method to control the numerical damping of the dam–foundation system with a massless foundation, would be to define a weighted damping ratio for each mode expected to contribute significantly to the total response, then to combine these modal damping ratios to the prorata of the corresponding modal participation factors to end up with a unique effective damping ratio for the combined system. An

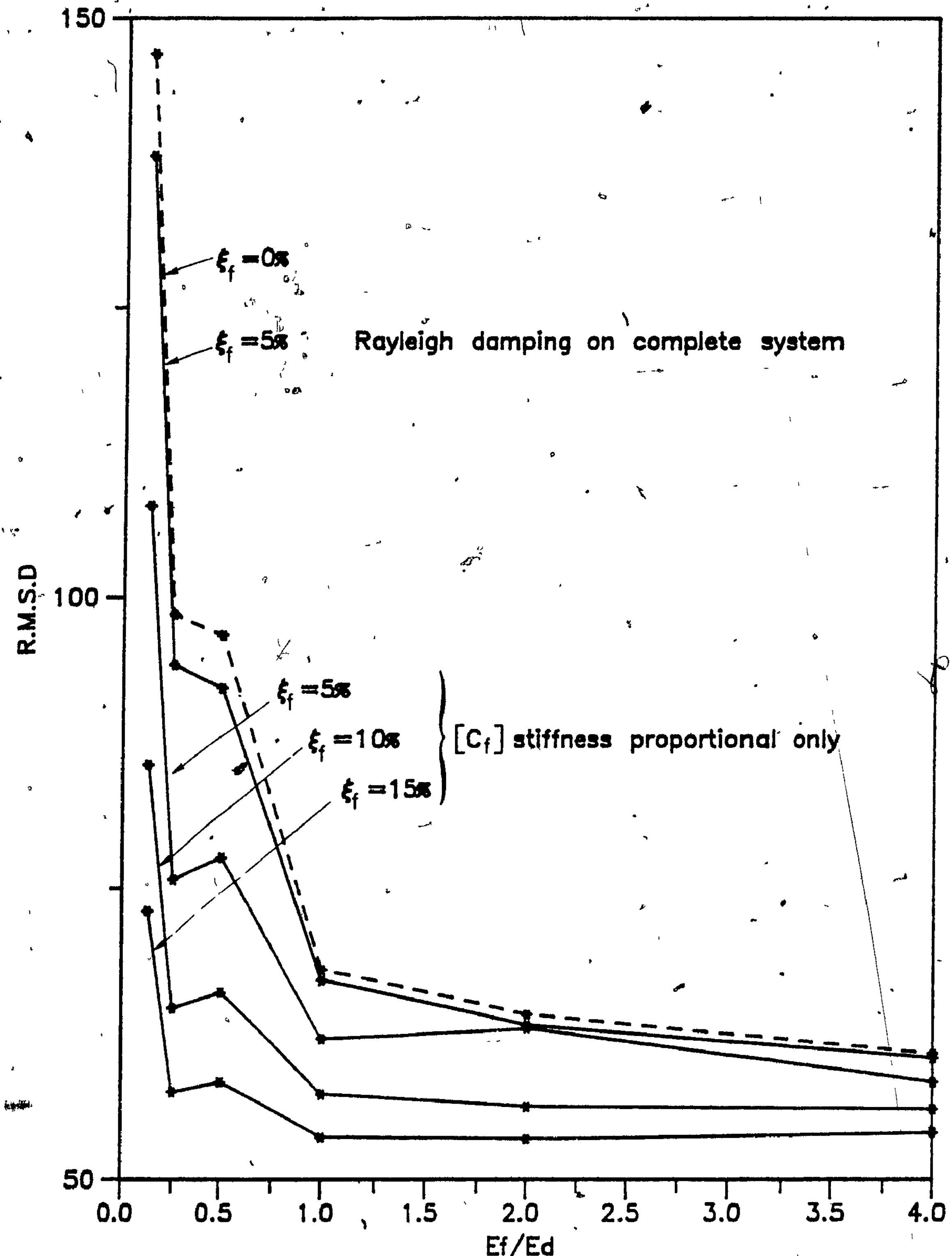

Figure 4.22 Effect of the Damping Ratio of the Massless Foundation (Model B) on the Horizontal Displacements at Node 1, El Centro Earthquake.

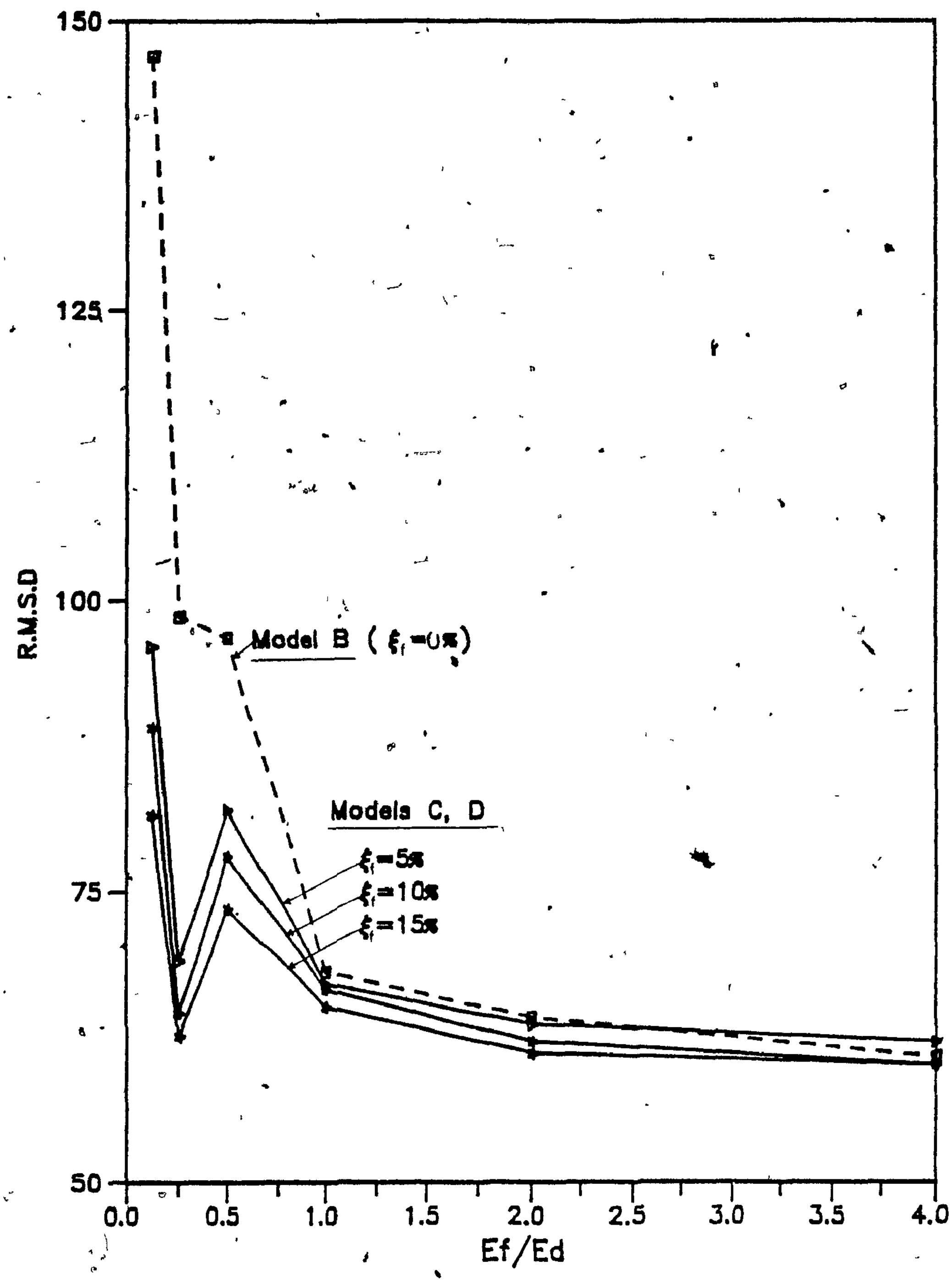

Figure 4.23 Comparison of the Dispalcements at node 1 Derived from Model B with $\xi_f = 0\%$ and Models C, D with $\xi_f = 5$, 10 and 15%, El Centro Earthquake.

example of a formula that can be used to obtain a weighted damping ratio is given in the STARDYNE computer program[45]. The weighted modal damping ratio is based on a weighted average of strain energies in each material, for each mode the weighted damping ratio $\bar{\xi}_j$ for the vector X_j is computed as:

$$\bar{\xi}_j = \frac{\sum_{i=1}^{m} \underline{X}_j^T [K_i] \underline{X}_j \xi_i}{\underline{X}_j^T [K] \underline{X}_j} \tag{4.2}$$

where m is the number of substructures, ξ_i is the percent critical damping associated with component i, $[K_i]$ is the stiffness associated with component i, [K] is the stiffness of the complete system. Having determined the weighted damping ratios of the first r modes expected to contribute significantly to the total response, the effective damping ratio of the complete system is found by the following formula:

$$\bar{\xi}_{eff} = \frac{\sum_{j=1}^{r} p_j \bar{\xi}_j}{\sum_{j=1}^{r} p_j} \tag{4.3}$$

where p_j is the participation factor of mode j (Eq. (3.12))

The main advantage of this method is that it transforms the non-proportional damping characteristics of a system to an equivalent proportional system with all ensuing advantages. In order to investigate the performance of the above procedure, the dam–foundation system considered has been reanalyzed for the case $E_f/E_d = 1$ and a foundation damping ratio, $\xi_f = 15\%$. The weighted modal damping ratios derived from equation (4.2) are listed in Table 4.2. The effective damping ratio for the complete system was derived from equation (4.3) as, $\bar{\xi}_{eff}$=8.1%. The global damping matrix was established by the Rayleigh method assuming a condition of proportional damping between the dam and the foundation. The earthquake response of the dam–foundation system, using the effective damping ratio found above has improved slightly the performance of model B with non-proportional damping as compared to models C and D. Yet, the most important feature of this method is that it allows assignment of a unique damping ratio to the complete system which implies a condition of proportional damping.

Table 4.2 Weighted Modal Damping Ratios Derived From Equation (4.2) ($E_f/E_d = 1$, $\xi_f = 15\%$, $\xi_d = 5\%$).

Mode	Computed Damping ratios (in %)
1	7.6
2	8.3
3	10.0
4	7.9

4.6 Effect of Using Different Ground Accelerations

The time history analysis is attractive in the sense that it provides completely deterministic results for specified ground motions. However, any two motions may produce quite different peak responses, even though they have the same intensity and statistical properties. Therefore, to validate the conclusions regarding the application of the four proposed input mechanisms, the dam–foundation system considered has been subjected to the Pacoima and the Parkfield accelerograms, scaled to 0.35g which represents the maximum acceleration of the El Centro accelerogram. The foundation

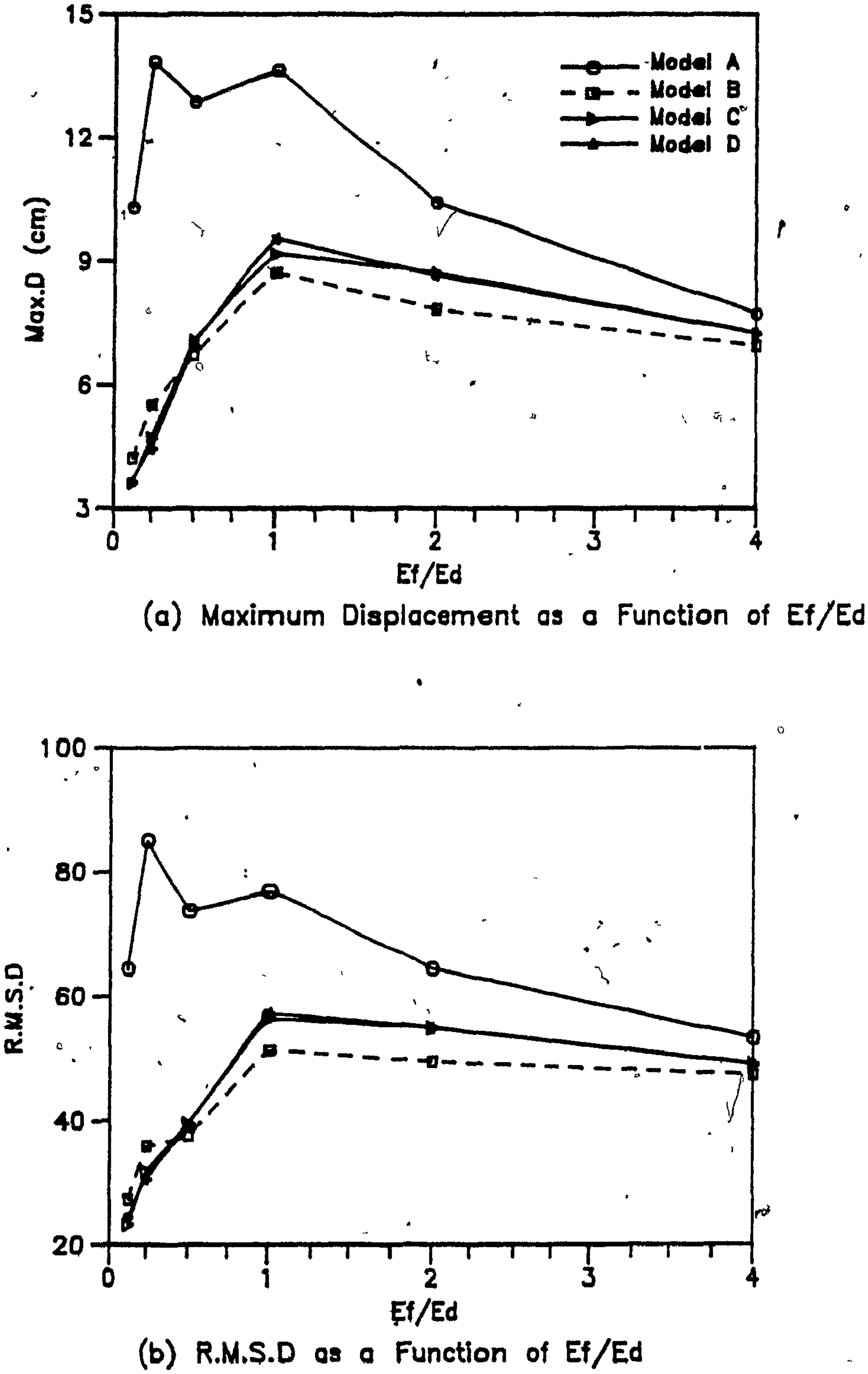

Figure 4.24 Displacements at Node 1 Derived from the Four Input Models Using the Pacoima Accelerogram as the Input Motion, ($\xi_f = 10\%$).

flexibility was varied such that the modular ratio has the same values as presented in Section 4.3, and the damping ratio of the foundation has been assigned a value of 10 percent of critical. The cases analyzed using the Pacoima accelerogram as the input motion, covered the complete range of the E_f/E_d parameter. Additional cases considering different damping ratios, and using the Parkfield accelerogram as the input motion were also analyzed.

The displacements of the dam crest (node 1) resulting from applying the Pacoima accelerogram according to the four proposed input models, are represented in Figure 4.23 as a function of the E_f/E_d ratio. It can be observed that as for the El Centro accelerogram, model A yields the largest response, models C and D are almost identical for the complete range of parameters. Model B is in good agreement with models C and D for very flexible foundation rock ($E_f/E_d = 1/8$, $1/4$). For other values model B underestimated the displacements by an average of 7% as compared to models C and D. The relative performance of model B with respect to models C and D, are very similar to the results presented in Figure 4.6 obtained from the application of the El Centro accelerogram. For the additional cases analyzed using the Parkfield accelerogram as the input motion the same trends concerning the performance of the four proposed input models have also been observed. The qualitative observations reported in Section 4.4 can thus be considered independent of the frequency content of a particular earthquake record.

4.7 Conclusions from Numerical Analyses

This section presents a summary of the conclusions that were obtained from the application of the four proposed earthquake input mechanisms to the concrete gravity dam–foundation system considered. The main conclusions were:

a) The use of different earthquake input models can lead to significant differences in the structural response of a concrete gravity dam–foundation system.

b) The application of model A, the rigid base rock input model, induced very significant artificial amplifications in the response quantities of interest. The magnitude of these artificial amplifications were shown to increase with the level of foundation flexibility. Model A is therefore recognized inadequate to evaluate time domain seismic responses of dam-foundation systems and should not be used in practice.

c) The reliability of model C, the deconvolved accelerogram input model, which is theoretically the most accurate model depends on the quality of the deconvolution analysis. The verification of the deconvolved accelerogram by computing the free-field response of the finite element foundation model is a mandatory step to ensure accurate results for model C.

d) The use of model D, the free-field input model, led to results which were almost identical to those derived from the theoretically more accurate model C and that was shown to be independent of the levels of flexibility and damping of the foundation rock. Model D can thus be considered the most efficient to evaluate the time domain responses of gravity dam–foundation systems since it is much easier to implement than model C.

e) The good performance of the free-field input model (model D), showed that the assumption of the same free-field accelerogram at all interface nodes is adequate for a concrete gravity dam.

f) The performance of model B, the massless foundation input model, was shown to be dependent on the foundation flexibility, on the level of damping of the massless foundation rock and on the computational procedure retained to form the global damping matrix.

g) For model B, in the case of a proportional damping ($\xi_f = 5\%$), it was shown that for relatively flexible foundations ($E_f/E_d \leq 1/4$), the performance of this model was improved when the damping matrix of the complete system was established by assembling the damping matrices of the dam and the massless foundation ($[C_f]$

proportional to $[K_f]$ only), which were separately formed by the Rayleigh damping method.

h) For a relatively rigid foundation ($E_f / E_d \geq 1$), and still in the case of a lightly damped foundation ($\xi_f = 5\%$), a value of zero damping for the massless foundation model led to results which were in good agreement with those derived from models C and D.

i) For higher damping ratios, $\xi_f = 10$ and 15% it was shown that in the case of model B with a relatively flexible foundation, controlling the damping at only the first mode in the foundation, led to results which were almost similar to the results derived from models C and D. For relatively rigid foundation rock ($E_f / E_d \geq 1$), model B underestimated the response and that was partly due to the poor numerical control of the damping provided in higher modes of the massless foundation model.

j) It was also shown that in the case of non–proportional damping, the use of weighted damping ratios (Eq. 4.2) for the different modes of vibration expected to contribute significantly to the total response, improved slightly the response of model B as compared to models C and D. Furthermore, this procedure eliminates the needs to consider explicitly the combined system as non–proportional.

k) Comparison of the numerical results between model B and models C , D, showed that the maximum values of the response quantities derived from these models are generally in better agreement than their corresponding root mean square.

In summary, model B although not as accurate as models C and D, do present several practical advantages allowing a significant reduction of the number of dynamic degrees-of-freedom. It can be used in time domain seismic analyses of dam-foundation systems if certain precautions are taken with regard to the mathematical idealization of the energy dissipation characteristics of the foundation;

i) The damping matrix should be constructed by considering the foundation damping characteristics to be only stiffness proportional, even when similar damping ratios are assigned to the dam and foundation.

ii) For the flexible foundation cases ($E_f/E_d \leq 1/4$), a good correlation of typical response quantites of interest has been observed between model B, in which the damping was controlled only in the first mode of vibration, and models C and D.

iii) In order to obtain a good correlation between model B and models C, D, for stiffer foundation cases the damping ratio assigned to the foundation of the massless foundation input model should be smaller than the one that would have been retained for the application of models C and D. For example, in the case where a value of $\xi_f = 15\%$ is assigned to the mass foundation in models C, D, a value of $\xi_f = 5\%$ in model. B lead to an average error of 3.6% in the R.M.S.D, for $E_f/E_d \geq 1/2$. If $\xi_f = 10\%$ is considered in models C and D then a value of $\xi_f = 0\%$ in model B lead to an average error of 6% in the R.M.S.D for the same foundation flexibility conditions as for the previous case.

CHAPTER 5

Coordinates Reduction Techniques for Dam–Foundation Interaction

5.1 Introduction

The importance of dam–foundation interaction has been emphasized in the previous chapter, illustrating the phenomenon in detail for the relatively simple two-dimensional system described in Chapter 3. In this chapter attention will be directed toward numerical methods that have been developed recently to overcome the limitations inherent to the analytical solutions of systems that requires a large number of dynamic d.o.f for their idealization such as a three–dimensional extension of dam–foundation–fluid interaction problems. The application of these methods and the development in computer hardware are already making possible the solution of highly complex problems on relatively inexpensive micro-computers. A key to this capability is obviously the minimization of the number of unknowns in the dam–foundation–fluid idealization and it is this aspect that will often govern the manner in which the interaction problem will be best formulated.

The selection of coordinates to carry out a dynamic analysis can be made using

– kinematic constraints enforced by constraint equation and proper boundary conditions,

– static constraint or static condensation,

– finite element modal coordinates,

– derived Ritz or Lanczos coordinates using load dependent transformation vectors.

Each of these techniques can be understood as Ritz analysis. Variations in the methods are related to the choice of the Ritz basis transformation vectors. Practical capabilities to apply these coordinates reduction procedures to locally non-linear systems have also been developed.[26,46]

Usually the geometry of a structure does not permit the discretization in a few finite elements but the behaviour may be perfectly characterized by a few generalized coordinates. This is generally true for structural dynamics problems such as earthquake analysis where typical modal analysis studies based on the frequency content and spatial distribution of the excitation have shown that the response is controlled by a relatively small number of low frequency modes. Therefore, the solution needs to be calculated only in these modes. This is achieved by vector superposition analysis by considering only the important modes of the system. This has the advantage of reducing drastically the computer cost of the analysis as compared to the solution where the dynamic equilibrium equations expressed in geometric coordinates are integrated simultaneously.

In this chapter coordinates reduction techniques to solve the dynamic equilibrium equations of the dam–foundation system are examined. In addition to the classical analysis technique using eigenvectors as bases for response computations, a solution technique using derived Ritz vectors to reduce the size of the system of dynamic equilibrium equations is also considered. The rate of convergence as well as the total computer time for these two solution techniques have been considered to compare their relative efficiency.

5.2 Selection of Generalized Coordinates for Dynamic Analysis

The equations of dynamic equilibrium (expressed in geometric cordinates) of the dam-foundation system subjected to an earthquake loading can be expressed as:

$$[M]\,\ddot{\underline{v}} + [C]\,\dot{\underline{v}} + [K]\,\underline{v} = \underline{f}(s)\,g(t) \tag{5.1}$$

The terms of the left hand side are the same as defined in Chapter 2, f(s) representing the spatial components of the earthquake loading and g(t) the prescribed accelerogram. The vector of nodal displacements $\underline{v}$ can be approximated by a linear combination of r linearly independent vectors,with r much less than n, as[24]:

$$\underline{v} = \sum_{i=1}^{r} \underline{X}_i\, y_i(t) \tag{5.2}$$

where $\underline{X}_i$ are the linearly independent basis vectors and $y_i(t)$ are unknown parameters, the generalized coordinates, obtained by solving a reduced system of r equations written as:

$$[M]^*\,\ddot{\underline{y}} + [C]^*\,\dot{\underline{y}} + [K]^*\,\underline{y} = \underline{f}^*(s)\,g(t) \tag{5.3}$$

where

$$[M]^* = [X]^T[M][X] \tag{5.4}$$

$$[C]^* = [X]^T[C][X] \tag{5.5}$$

$$[K]^* = [X]^T[K][X] \tag{5.6}$$

$$f^*(s) = [X]^T f(s) \tag{5.7}$$

The objectives of the transformation are to obtain new system mass, damping and stiffness matrices which are reduced to size $(r \times r)$ and have a smaller bandwidth than the original system matrices while maintaining a good accuracy for the response quantities of interest.

The success of vector superposition methods depends on proper selection of the basis vectors [X], to be used in the coordinates transformation. Ideally the vectors should:

i) be linearly independent and completely span the space of the solution to fully characterize the dynamic response,

ii) satisfy the geometric boundary conditions,

iii) form certain geometric patterns producing acceptable deformation shapes to characterize the dynamic response,

iv) be simple and computationally inexpensive to generate.

5.2.1 Finite Element Modal Coordinates

This is the classical method which consist of using as transformation vectors, the mode shapes $[\phi]$ of the system. These mode shapes are found by solving the free-vibration eigenproblem which can be written as:

$$[K]\,[\phi] = [M]\,[\phi]\,[\omega^2] \tag{5.8}$$

For large sytems such as dam–foundation, the solution of the eigenproblem is usually performed by either the subspace iteration method or the Lanczos method. For both methods there are usually three phases in the solution procedure:

1– Solve equation (5.8) for $[\phi]$ and $[\omega]$.

2– Perform a Sturm sequence check, in order to verify that no eigenvalues have been missed in the computations.

3– Evaluate the error of eigenpairs $(\omega_i{}^2,\ \phi_i)$ from

$$\frac{\left\| [K]\underline{\phi}_i - \omega_i^2 [M]\underline{\phi}_i \right\|_2}{\left\| [K]\underline{\phi}_i \right\|_2} < \text{specified error} \tag{5.9}$$

The mode shapes have the property of being orthogonal to both the mass and the stiffness matrices. Thus the reduced mass matrix $[M]^*$ and the reduced stiffnes matrix $[K]^*$ will be diagonal matrices. In the case of a proportional damping, the reduced damping matrix $[C]^*$ will also be diagonal. This will result in a set of uncoupled modal equations written as:

$$\underline{\ddot{y}} + [2\xi\omega]\,\underline{\dot{y}} + [\omega^2]\,\underline{y} = \underline{f}^*(s)\,g(t) \tag{5.10}$$

On the other hand in the case of a non-proportional damping, the matrix $[C]^*$ will not be diagonal leading to a set of coupled modal equations. The principal problem associated with the use of finite element modal coordinates are that the truncated eigen basis do not span the complete solution space and the high numerical effort required for the generation of eigenvectors for large structural systems. It should also be noted that the eigenbasis ignores important information about the structural dynamic problem related to the specified loading characteristics such that computed eigenvectors can be nearly orthogonal to the applied loading and therefore will not participate significantly in the solution.

5.2.2 The Derived Ritz Coordinates

The Ritz extension of the Rayleigh's method known as Rayleigh–Ritz analysis has been widely used to find approximate values of the lowest eigenvalues and corresponding eigenvectors of the free–vibration problem. It should be noted that the use of the derived Ritz transformation vectors is not to obtain an accurate solution of the free-vibration eigenproblem (Eq. 5.8), but rather to form an accurate load dependent vector basis to reduce the size of the original system of equation (Eq. 5.1). Recently, Wilson, et al. [47], have presented a simple numerical algorithm based on an inverse iteration type of scheme and using the spatial distribution of the dynamic load to generate a set of mass orthonormal load dependent transformation vectors to be used in Ritz type of analyses as an economic alternative to the classical modal superposition method. The algorithm used to generate the Ritz vectors in this study is a computational variant of the original algorithm presented by Wilson et al.[47]. It was shown by Léger et al.[48] that this new algorithm is numerically more stable for systems carrying massless d.o.f. Furthermore, it produces a higher degree of linear independence among the transformation vectors, and allow a better control of the static correction effects that are automatically included in the basis to approximate the participation of higher vectors not retained in the summation. Table 5.1 presents the algorithm used to generate the Ritz vectors. The vectors $\underline{X}_i$ generated by this algorithm are orthogonal to the mass matrix. The orthogonalization with respect to the stiffness matrix is optional.

5.3 Representation of Seismic Load from Truncated Vector Bases

One of the important aspect of direct vector superposition techniques for the solution of dynamic equilibrium equations, pertains to the number of vectors that must be retained in the analysis. Hansten and Bell[49] demonstrated that the inaccuracies of vector truncation are caused by the omission of load components that are orthogonal to the vectors included in the solution.

For earthquake analysis, the concept of effective modal mass (defined in Section 3.4) corresponding to the part of the total mass responding to the earthquake in each eigen or Ritz mode, is commonly used as a good indication of the relative contribution of a particular mode to the global structural response. A spatial error estimate indicating the relative percentage of the total earthquake load represented by the truncated vector basis can thus be written as:

Table 5.1 Algorithm for the Generation of the Ritz Vectors (Reference 24).

1–Given mass, stiffness matrices [M], [K]and load vector $\underline{f}(s)$.

2–Triangularized stiffness matrix.

$$[K] = [L]^T [D][L]$$

3–Solve for initial static deflected shape.

$$[K]\underline{v}_0 = \underline{f}(s) \qquad \text{solve for } \underline{v}_0$$

4–Solve for first vector.

$$[K]\underline{X}_1^* = [M]\underline{v}_0 \qquad \text{solve for } \underline{X}_1^*$$

$$b_1 = \left(\underline{X}_1^{*T}[M]\underline{X}_1^*\right)^{1/2}$$

$$\underline{X}_1 = \underline{X}_1^* \times \tfrac{1}{b_1} \qquad [M] \text{ normalize } \underline{X}_1^*$$

$$c_{v_1} = \underline{v}_0^T [M]\underline{X}_1 \qquad \text{update static vector } \underline{v}_0$$

$$\underline{v}_1 = \underline{v}_0 - c_{v_1}\underline{X}_1$$

5–Solve for additional vectors $i = 2, \cdots, r-1$.

$$\underline{X}_i^* = [M]\underline{v}_{i-1} \qquad \text{solve for } \underline{X}_i^*$$

$$c_j = \underline{X}_j^T [M]\underline{X}_i^* \qquad \text{compute for j=1, i-1}$$

$$\underline{X}_i^{**} = \underline{X}_i^* - \sum_{j=1}^{i-1} c_j \underline{X}_j \qquad [M] \text{ orthogonalize } \underline{X}_i^*$$

$$\underline{u} = \left(\underline{X}_i^{**T}[M]\underline{X}_i^{**}\right)^{1/2}$$

$$\underline{X}_i = \underline{X}_i^{**} \times \tfrac{1}{u} \qquad [M]\text{normalize}\{X_i^{**}\}$$

$$c_{v_i} = \underline{v}_{i-1}^T [M]\underline{X}_i \qquad \text{update static vector } v_{i-1}$$

$$\underline{v}_i = \underline{v}_{i-1} - c_{v_i}\underline{X}_i$$

6–Add static residual $\underline{v}_{r-1}$ as static correction vector $\underline{X}_r$ (optional)

$$\underline{v}_{r-1} = \underline{v}_{r-1} - \sum_{j=1}^{i-1} \left(\underline{X}_j^T [M]\underline{u}_{r-1}\right) \underline{X}_j$$

$$b_r = \left(\underline{v}_{r-1}^T [M]\underline{v}_{r-1}\right)^{1/2} \qquad [M] \text{ orthonormalize } \underline{v}_{r-1}$$

$$\underline{X}_r = \underline{v}_{r-1} \times \tfrac{1}{b_r}$$

7–Orthogonalization of transformation vectors with respect to [K] (optional).

$$[K]^* = [X]^T [K][X]$$

$$[M]^* = [X]^T [M][X]$$

$$[K]^*[Z] = [M]^*[Z][\bar{\omega}^2] \qquad \text{solve reduced eigenvalue problem}$$

$\bar{\omega}$ = approximate structural frequencies

$$[\bar{X}] = [X][Z] \qquad \text{compute final transformation vectors}$$

$$PEMM_y = \sum_{i=1}^{r} \frac{P_{i,y}^2}{M_T} \times 100 \tag{5.11}$$

In this section the representation of the seismic load from a truncated vector basis using either the eigenvectors or the derived load dependent Ritz transformation vectors is investigated.

To compare the number of vectors for the eigen and the Ritz solutions, required to represent adequately the seismic load, a target percentage of effective modal mass was fixed at a value of 95% and the required number of vectors to reach this value was determined for both solutions. This has been done for the horizontal and vertical directions. The effect of the inertia of the foundation block on the representation of the seismic load by a set of transformation vectors was also investigated. Two models for the foundation block were considered; the mass and the massless foundation models. The foundation flexibility was varied such that the modular ratio between the foundation rock and the concrete dam takes the lower and upper limits of the values used in the analyses presented in Chapter 4.

5.3.1 Comparison Between Derived Ritz Vectors and Exact Eigenvectors

5.3.1.1 Mass Foundation Model (Earthquake Input Models A, C, D)

The percentage effective modal mass in the Y-dir is represented as a function of the number of eigenvectors and the number of Ritz vectors in Figures 5.1a) and 5.1b) for a flexible and rigid foundation respectively. It can be noticed from these figures that for both the eigen and Ritz solutions, the contribution of the first mode of vibration to the total response increases with the flexibility of the foundation rock. Indeed for the most flexible case ($E_f/E_d = 1/8$), the contribution of the first mode to the total response is around 60% for both the eigen and Ritz solutions. This contribution drops to nearly 10% for the most rigid case ($E_f/E_d = 4$). The number of vectors needed to reach the required 95% of effective modal mass is dependent on the flexibility of the foundation rock. For $E_f/E_d = 1/8$, which represents a flexible foundation, 6 vectors for the eigensolution and 8 vectors for the Ritz solution were needed to get 95% of the $PEMM_y$. For the case $E_f/E_d = 4$, which represents a rigid foundation rock, 15 vectors were needed in the eigensolution to reach the required 95% of the $PEMM_y$, while the Ritz solution converged with 14 vectors. This shows that the eigensolution and the Ritz solution converge with very similar characteristics in the horizontal direction.

The same study has been carried out for the Z-dir, the results are presented in Figure 5.2. The first observation that can be made is that the required number of vectors for both solutions to converge , is more important as compared to the horizontal direction since axial modes of deformation are stiffer than lateral modes of deformation. It can also be noticed in this case that the derived Ritz solution achieved loading convergence with fewer vectors than the eigensolution and this is for the complete range of the selected parameters. For the case $E_f/E_d = 1/8$, 17 eigenvectors were needed to achieve 95% of the $PEMM_z$, whereas only 11 vectors were needed for the Ritz solution to converge. For the case of the relatively rigid foundation ($E_f/E_d = 4$) the eigensolution converged with 37 vectors, while only 20 vectors were needed for the Ritz solution to converge.

5.3.1.2 Massless Foundation Model (Earthquake Input Model B)

For the massless foundation model as one should expect, the convergence for both vector bases is achieved with fewer vectors than the models where the mass of the foundation block is taken into account. This is because the mass of the foundation being neglected, the foundation block will not tend to dominate the dynamic response of the dam–foundation system. The percentage effective modal masses in the horizontal and vertical directions are represented in Figures 5.3 and 5.4 respectively, as a function of the number of vectors retained in the analysis. From Figure 5.3, it can be noticed that the contribution of the first mode of vibration to the total response in the Y-dir is

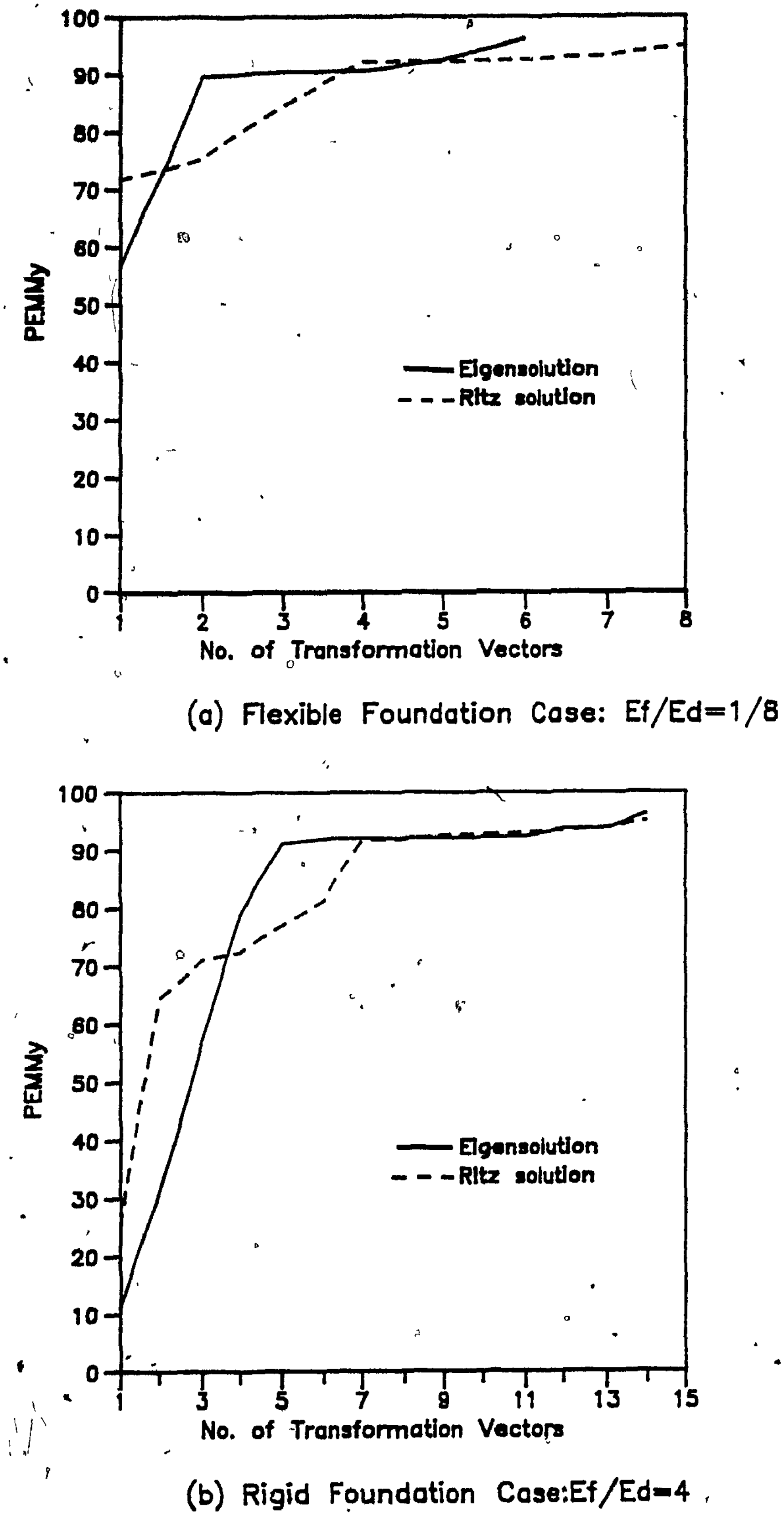

Figure 5.1 Percentage Effective Modal Mass in the Y-Dir as a Function of the Number of Vectors Retained in the Analysis (Mass Foundation Model).

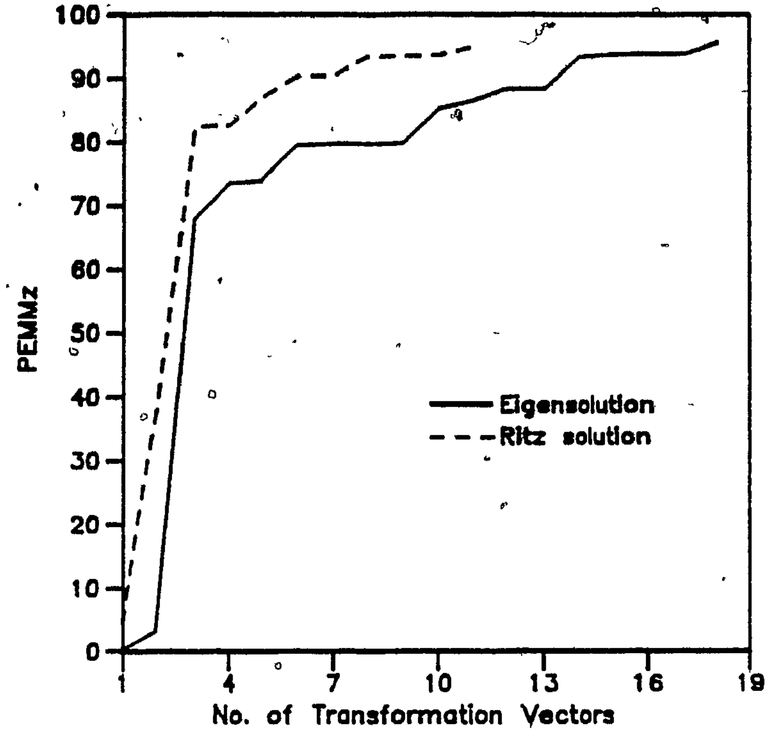

(a) Flexible Foundation Case: Ef/Ed=1/8

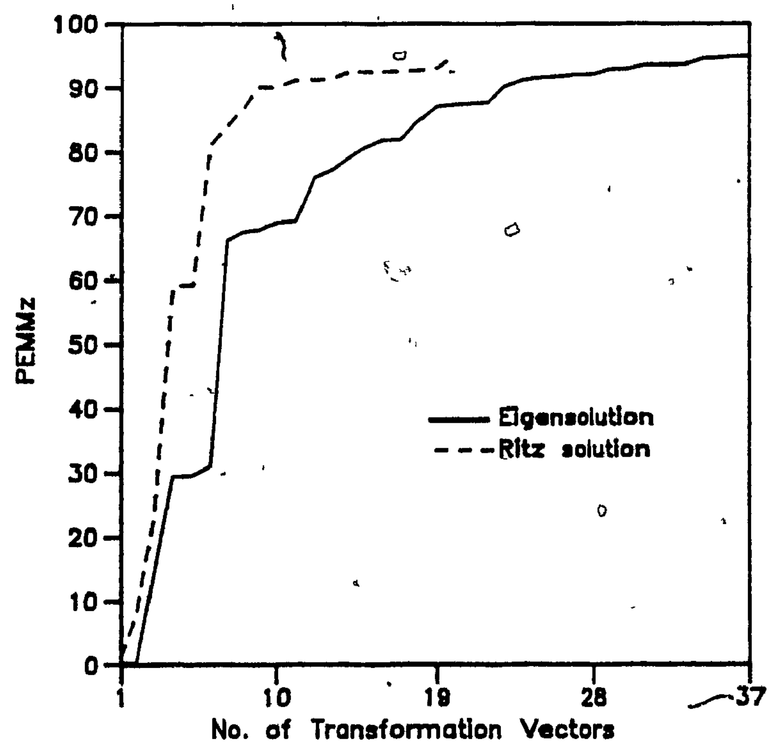

(b) Rigid Foundation Case: Ef/Ed=4

Figure 5.2 Percentage Effective Modal Mass in the Z-Dir as a Function of the Number of Vectors Retained in the Analysis (Mass Foundation Model).

more significant than in the mass foundation model. The convergence characteristics of the solution using the eigenvectors and the solution using the Ritz vectors are very similar in the horizontal direction. For the case $E_f/E_d = 1/8$, the required number of vectors to reach 95% of the $PEMM_y$ is 2 for the eigensolution and 4 for the Ritz solution. For the rigid foundation case, $E_f/E_d = 4$, the solution using the eigenvectors converged with 9 vectors while the Ritz solution converged with 7 vectors.

Considering Figure 5.4 which represents the variation of the PEMM in the vertical direction as a function of the number of vectors retained in the analysis, it can be noticed that for the case $E_f/E_d = 1/8$, the eigensolution and the Ritz solution converged with 3 and 4 vectors respectively. For the case $E_f/E_d = 4$, the convergence of the eigensolution was achieved by 11 vectors and for the Ritz solution the required number of vectors was of 10. Thus for the massless foundation model, the solution using the eigenvectors and the solution using the Ritz vectors have very similar convergence characteristics in both horizontal and vertical directions.

5.3.1.3 Relative Computational Efficiency

The study of the representation of the seismic load by a truncated vector basis showed, that for mass foundation models, if vertical excitation is to be disregarded, the eigenvectors and the Ritz vectors have very similar convergence characterististics. If vertical excitation is to be considered, it has been shown that the Ritz solution achieved loading convergence with fewer vectors than the eigensolution. For the massless foundation model, the required number of vectors for both the eigen and Ritz solutions was very close in the horizontal and vertical directions.

The required number of vectors to achieve effective modal mass convergence is not the only important factor if comparison between the performances of the eigensolution and the Ritz solution is to be made. Indeed the numerical cost in terms of computer execution time is also an important factor since low computer costs of a typical analysis cycle will allow inexpensive reanalysis to conduct reliability evaluation of the numerical

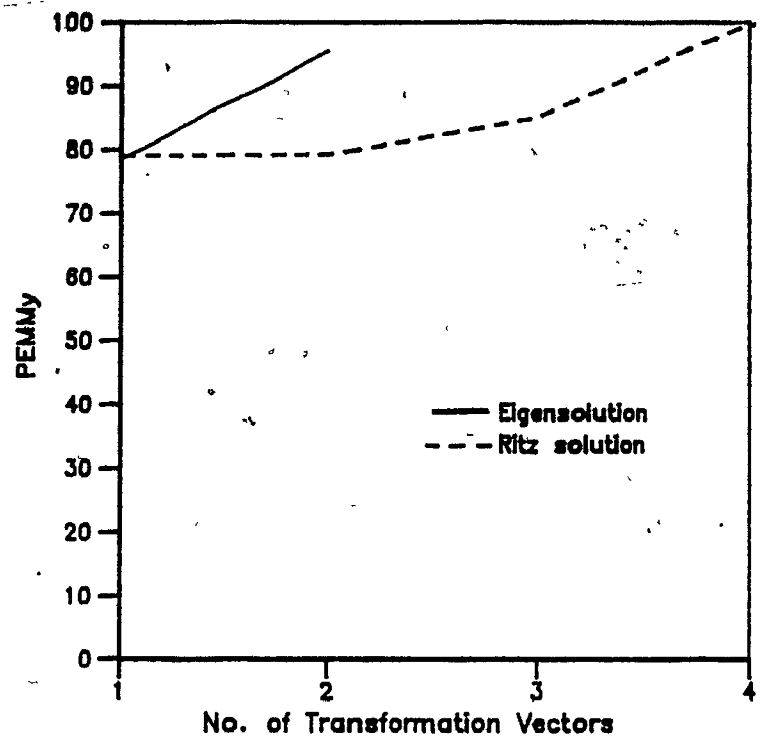

(a) Flexible Foundation Case: Ef/Ed=1/8

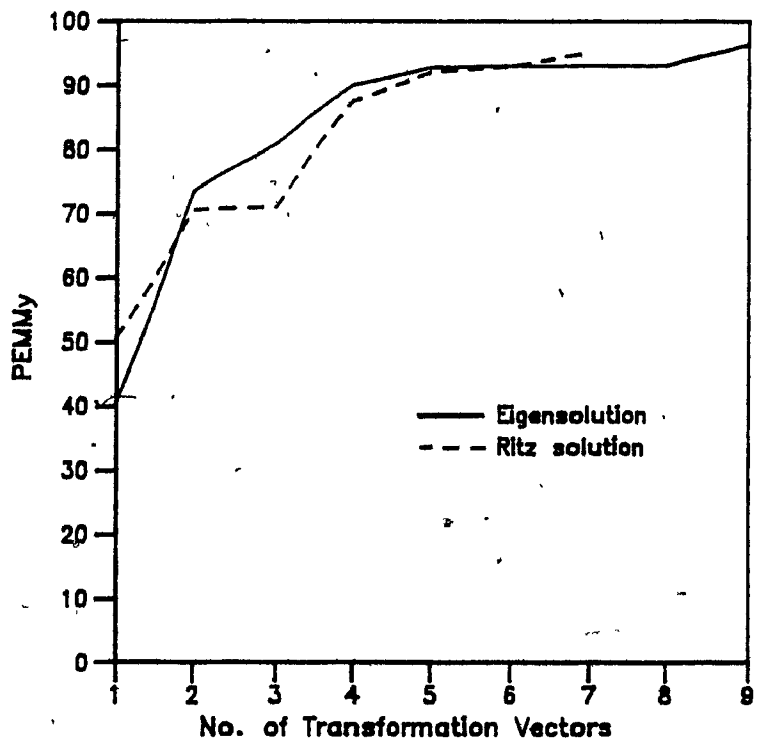

(b) Rigid Foundation Case:Ef/Ed=4

Figure 5.3 Percentage Effective Modal Mass in the Y-Dir as a Function of the Number of Vectors Retained in the Analysis (Massless Foundation Model).

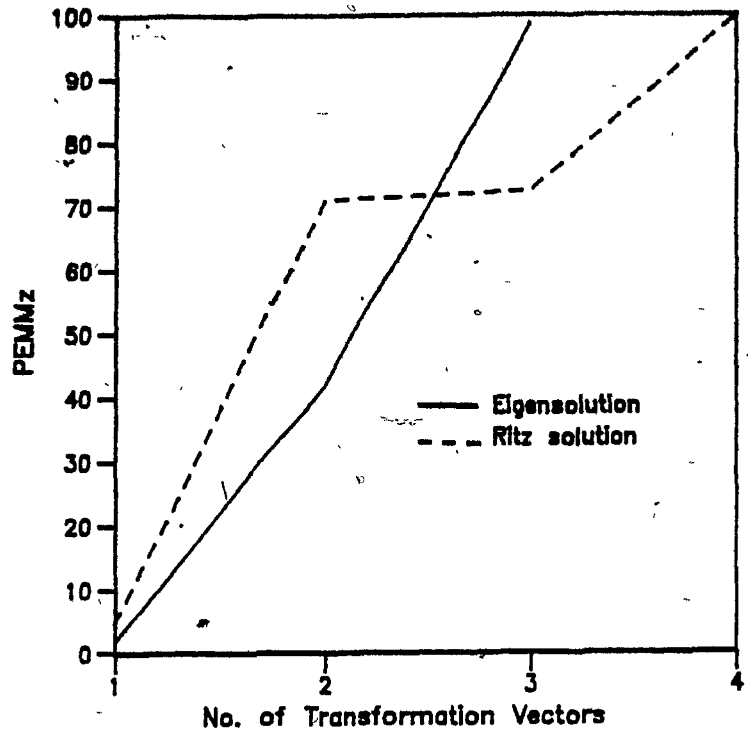

(a) Flexible Foundation Case: Ef/Ed=1/8

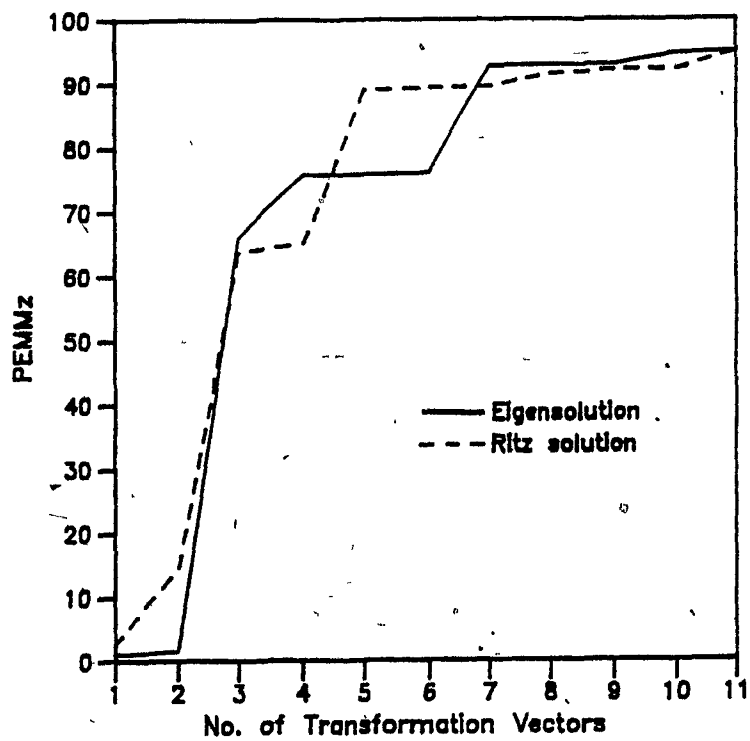

(b) Rigid Foundation Case: Ef/Ed=4

Figure 5.4 Percentage Effective Modal Mass in the Z-Dir as a Function of the Number of Vectors Retained in the Analysis (Massless Foundation Model).

results. The generation of the derived Ritz vectors was approximately 7 to 9 times more efficient than the eigensolution when a subspace iteration scheme was used and 2 to 3 times more efficient when the Lanczos method was used to generate the eigenvectors.

On the basis of the previous observations it can be stated that the use of the derived Ritz vectors for the representation of a seismic load applied to a concrete gravity dam-foundation system, is more appropriate than the use of the eigenvectors. It should also be noted that a satisfactory seismic loading representation by truncated load dependent Ritz transformation vectors has been shown to ensure convergence of typical response quantities such as stresses and displacements of typical civil engineering structures.[47,48]

5.4 Dynamic Response Analysis Procedure

Having selected the transformation vectors and the number of vectors required to represent adequately the seismic load, a solution strategy has to be adopted to solve the reduced system of dynamic equilibrium equations (Eq. 5.3). Two cases have to be considered. One with proportional damping and the other with non-proportional damping. For the case where the damping is proportional, the dynamic equilbrium equations are uncoupled and can thus be solved separately. The total response is then obtained by superposing the Ritz or eigen modal responses. In the case of a non-proportional damping, the reduced damping matrix $[C]^*$ (Eq. 5.5) is not diagonal and its off-diagonal coefficients produce coupling of the modal equations of motion. Three possible methods to solve the coupled reduced system of dynamic equilibrium equations (Eq 5.3) are:

1) Mode superposition using complex mode shapes (Method 1)

The equations of motion of a structure with non-proportional damping may also be uncoupled by the solution of the complex eigenproblem which may be written as:

$$-[\omega^2][M][\phi] + i[\omega][C][\phi] + [K][\phi] = 0 \qquad (5.12)$$

In such a case the complex mode shapes and frequencies will contain in-phase and out-of-phase components such that the eigenproblem is essentially of order 2n. The details of this method can be found in Reference (39). It should be noted that the same approach can be used to diagonalize the reduced system expressed in derived Ritz coordinates by the matrices $[M]^*$, $[C]^*$ and $[K]^*$. The order of the complex eigenproblem will then be 2r where r is the number of vectors retained in the analysis. The major drawback of the complex eigenmethod is the larger size of the eigenproblem that must be considered and the necessity of dealing with complex numbers in the dynamic response.

2) Direct integration of the reduced system (Method 2)

An interesting approach to solve the coupled equations of motion expressed in generalized eigen or Ritz coordinates (Eq. 5.3) is to integrate these equations directly. By limiting the transformation to the modes that are expected to contribute significantly to the dynamic response, an efficient solution technique is obtained. This procedure was recommended by Clough and Mojtahedi[39], a numerical example to illustrate the effectiveness of the method was presented. The major drawback of this method is that if damping coupling between one of the lower modes with a higher mode exists, this effect will not be taken into account since the solution is found by including only a small number of modes expected to contribute significantly to the total response from the consideration of the effective modal mass.

3) Vector superposition using weighted damping ratios (Method 3)

The simplest but only approximate procedure for treating the non-proportional damped case, is to ignore the off–diagonal terms of the reduced damping matrix $[C]^*$, and to assign a weighted damping ratio to each uncoupled modal equation. In practice different approaches to determine the weighted damping ratios to be assigned to each modal equation, have been proposed.

– In a first approach the non–diagonal matrix $[C]^*$ can be replaced by a diagonal matrix with the same diagonal terms as in the original matrix. Then the standard modal analysis procedure is followed in order to solve the uncoupled dynamic equilibrium equations. It is obvious that this procedure introduces errors in the solution, however Warburton and Soni[50] proposed a criterion that should be satisfied in order that neglecting the off–diagonal terms in matrix $[C]^*$ leads to a maximum error in typical response quantities, of the order of 10%.

$$\xi_i \leq 0.05 \left| \frac{c^*_{ii}}{2c^*_{is}} \left(\frac{\omega_s^2}{\omega_i^2} - 1 \right) \right|_{min\, s} \tag{5.13}$$

ξ_i is calculated from the diagonal element from $c^*_{ii} = 2\xi_i \omega_i$, ω_i and ω_s which are natural frequencies, c^*_{ii} and c^*_{is} are element of the $[C]^*$ matrix and the minimum of the expression $|\cdots|$ with respect to s is taken, s may be any integer between 1 and r $(s \neq i)$, r being the number of vectors retained in the analysis.

- Another approach to find the weighted damping ratios is based on the weighted average of strain energies in each material, presented in Chapter 4 (Section 4.5).

$$\bar{\xi}_j = \frac{\sum_{i=1}^{m} \underline{X}_j^T [K_i] \underline{X}_j \, \xi_i}{\underline{X}_j^T [K] \underline{X}_j} \tag{5.14}$$

It is clear that ignoring the off–diagonal terms of the reduced damping matrix $[C]^*$ and assigning weighted damping ratios to each modal equation will introduce errors in the solution. However this procedure is frequently used in practice, and it has been demonstrated to give acceptable results using only a few modal coordinates in the earthquake response analysis of a soil–building system.[51]

5.5 Analysis of Structural Response

In this section the performances of Method 2, the direct integration of the reduced system and Method 3 using weighted damping ratios, as presented in the previous section for the analysis of systems with non-proportional damping were tested by carrying out the earthquake response analysis of the considered concrete gravity dam–foundation system described in Chapter 3. The foundation flexibility was set to a value corresponding to $E_f/E_d = 1/2$. The damping ratio for the concrete gravity dam was taken as 5 percent of critical. For the foundation rock the damping ratios were taken as 5, 10, 15 and 40 percent of critical.

The dynamic response of the dam–foundation system to the NS component of the El Centro earthquake was determined for each of the damping case mentioned above. The earthquake input model used for these analyses was model C, the deconvolved accelerogram input mechanism. For the proportionally damped system using $\xi_f = 5\%$, the uncoupled equations of motion were integrated independently and the total response was obtained by vector superposition. These results were then compared to those obtained from the step-by-step integration of the equations of motion expressed in geometric coordinates.

For the cases $\xi_f = 10\%$ and 15%, where the equations expressed in generalized coordinates were coupled by the reduced damping matrix $[C]^*$, Methods 2 and 3 were used to solve the system of coupled equations. For each method two types of solution were obtained. For Method 2, which consists of integrating simultaneously the coupled modal equations, two types of transformation vectors were used to obtain the solution; the eigenvectors and the derived Ritz vectors. For Method 3, which consists of integrating independently the uncoupled equations of motion by ignoring the off–diagonal terms in the reduced damping matrix $[C]^*$, two types of weighted damping ratios were used. First, the weighted damping ratios were computed from equation (5.14), second the weighted damping ratios were computed directly from the diagonal terms of matrix $[C]^*$. The damping ratio of foundation was then set at 40 percent of critical to investigate a heavily damped foundation system. The same procedure as in cases of ξ_f = 10% and 15% was followed except that in Method 2 only the Ritz vectors were used as transformation vectors and in Method 3 the damping ratios were computed from the diagonal terms of the reduced damping matrix $[C]^*$. It should be noted that the results of the above analyses were also compared with the results obtained from a step-by-step integration of the coupled equations of motion expressed in geometric coordinates.

Although a complete set of stress and displacement histories was generated for each analysis, it was verified that the displacements at node 1 (Fig. 4.2) represented by their R.M.S.D and the corresponding Max.D can be considered to provide an adequate indication of the relative results given in the different analyses for typical quantities of engineering interest.

The number of vectors expected to contribute significantly to the total response, was selected by determining the required number of transformation vectors (eigenvectors or Ritz vectors) to reach a value of percentage effective modal mass of 95 percent in the horizontal direction. This requirement has lead to a number of 7 vectors when an eigensolution was used and 8 vectors for the Ritz solution.

The results of the different analyses for cases ξ_f = 5, 10, 15 and 40 percent are presented in Table 5.2. The results for ξ_f = 5% showed that for a proportionally damped system, the integration of the uncoupled modal equations lead to almost the same displacements in terms of the R.M.S.D and the Max.D, as the ones obtained from a step-by-step integration carried out in geometric coordinates. In the case of a non-proportionally damped system, it is noteworthy that the integration of the reduced coupled equations of motion lead to results which are in good agreement with those obtained from a direct integration of the equations of motion expressed in geometric coordinates and this is for cases ξ_f = 10, 15 and 40%. Furthemore, the use of the derived Ritz vectors maintains or improve the accuracy of the response as compared to the solution using the eigenvectors as bases for computations. The performance of Method 3 depends on the values of weighted damping ratios assigned to the different modes contributing significantly to the response. Indeed, it can be noticed from Table 5.2 that in the case where the weighted damping factors are computed from equation (5.14), the resulting displacements are underestimated. In other words, the use of equation (5.14) leads to damping ratios that are too high. The other alternative in Method 3, which consists of computing the damping ratios directly from the diagonal terms of the reduced damping matrix $[C]^*$, showed to give results which are in good agreement with those derived from a step-by-step integration in geometric coordinates. The largest error introduced in the results due to the neglect of the off-diagonal terms in $[C]^*$, corresponds to the heavily damped case of $\xi_f = 40\%$. It should be noted also that the Warburton criteria (Eq. 5.12) was satisfied for cases of $\xi_f = 10$ and 15%, for $\xi_f = 40\%$ this criterion was not satisfied for all the transformation vectors. This shows that this criterion can be restrictive in some cases since the maximum relative error in the displacements was approximately 3%. It should be noted that the use of the previously investigated methods can also be applied directly to a massless foundation model.

The total execution computer times required by the different methods considered above, to compute the displacements history are listed in Table 5.3. The computations were performed in double arithmetic precision, on a micro–computer working with the 80286/80287 micro–processors, no advantages were taken of symmetry and of the reduced bandwidth of stiffness and damping matrices for the step-by-step integration of the coupled system.

It should be noted that the total computer execution times shown in Table 5.3 for any method, represent the time required to derive the displacements history, given the system matrices [M], [C] and [K] and the load vector $\underline{f}(s)$, which includes the generation

Table 5.2 Horizontal Displacements at Node 1 Derived from the Different Solution Strategies.

Foundation damping, ξ_f	10%		15%		40%	
Solution method	R.M.S.D	Max.D (cm)	R.M.S.D	Max.D (cm)	R.M.S.D	Max.D (cm)
Step-by step integration	79.00	12.85	73.44	12.41	63.72	11.82
Reduced coupled equations						
a) Derived Ritz vectors	78.75	12.78	73.21	12.39	63.37	11.78
b) Eigenvectors	78.75	12.75	73.20	12.36	—	—
(Non–proportional damping)						
Assumed uncoupled equations						
$a)\bar{\xi}$ from c^*_{ii}	78.13	12.75	72.04	12.21	61.96	11.47
$b)\bar{\xi}$ from Eq.(5.14)	67.43	11.74	56.00	10.43	—	—
(Non-proportional damping)						

Damping in concrete gravity dam 5%, $E_f/E_d = 1/2$

Table 5.3 Computer Times Used in Computing the Displacements History.

Step-by-step integration coupled equations (140 x 140)	4800 sec
Direct integration of reduced system (8 x 8) (using Ritz vectors as transformation vectors)	300 sec
Independent integration of uncoupled equations (8 x 8)	450 sec

and application of transformation vectors. The advantages of using the coordinates reduction techniques for linear systems are put onto evidence by the examination of the values shown in Table 5.3. The integration of the reduced coupled system is more than ten times faster than integrating the complete system of equations.

A major advantage of integrating directly the assumed uncoupled reduced equations of motion, as compared to the reduced coupled system is that an exact closed form mathematical solution is possible if the seismic load is described by a series of straight lines between equal intervals of time. This approximate loading description is generally used for any digitized transient record. On the other hand, the direct integration of the coupled system of equations will generally exhibit period elongation and amplitude decay with time.

5.6 Conclusions

In this chapter, it was shown that a significant reduction in the computational effort involved in the time domain earthquake response analysis of a concrete gravity dam–foundation system, can be gained by the application of recently developed coordinates reduction techniques while maintaining a good accuracy of the computed response quantities. The main conclusions of this chapter can be summarized as follows:

- The number of transformation vectors required to represent the seismic load was more important for a rigid foundation than it was for a flexible foundation.
- The solutions using the the eigenvectors and the derived Ritz vectors as bases for computations had the same convergence characteristics in the horizontal direction for mass foundation models.

a) The Ritz solution converged more rapidly than the eigensolution in the stiffer vertical direction for mass foundation models.

b) Ignoring the inertial effect of the foundation reduced the number of transformation vectors required to represent adequately the earthquake load vector.

c) For the massless foundation model, the eigensolution and the Ritz solution had similar convergence characteristics in both the horizontal and vertical directions.

d) The time of generation of the derived Ritz vectors was 7 to 9 times less than the time required to generate the eigenvectors when a subspace iteration was used and 2 to 3 times faster when the Lanczos method was used.

e) The use of the effective modal mass approach provided a good guidance to monitor the number of transformation vectors to be included in the response.

f) In the case of proportional damping, the integration of the uncoupled modal equations lead to similar results as the step-by-step integration of the coupled equations expressed in geometric coordinates.

g) In the case of non-proportional damping, the direct integration of the coupled reduced system expressed in generalized coordinates led to results which were very close to the results derived from the step-by-step integration (geometric coordinates).

h) The use of the derived Ritz vectors maintained or improved the accuracy of the response as compared to the solution using the eigenvectors as bases for computations.

i) In the case of non-proportional damping, ignoring the off-diagonal terms of the reduced damping matrix $[C]^*$ and computing the weighted damping ratios from equation (5.14) underestimated the response.

j) The Warburton criterion[50] when satisfied ensured an acceptable level of errors in the response quantities derived from the solution that used the damping ratios computed from the diagonal terms of the reduced damping matrix.

CHAPTER 6

SUMMARY AND CONCLUSIONS

6.1 Summary

The importance of foundation interaction on the behavior of concrete gravity dams under earthquake ground motions has long been recognized. Previous studies[11,17] have been carried out typically in the frequency domain using foundation models based on analytical half-space solution and two-dimensional linearly elastic dam models in order to identify and quantify the effect of critical parameters. However, the need to represent non homogeneous geometrical and material foundation properties for which analytical models are not available and the need to consider non-linear behavior under severe seismic excitation require the extension of the analysis of dam-foundation systems in the time domain.

This study has presented the effect of using four different earthquake input mechanisms suitable for time domain structural analysis of concrete gravity dam-foundation-reservoir system. These were,

A) the standard rigid base input model,

B) the massless foundation input model,

C) the deconvolved base rock input model,

D) the free-field dam-foundation interface input model.

A two–dimensional linear elastic finite element model was selected to represent a typical dam–foundation system. The time domain responses were computed for a wide range of the moduli ratio, $E_{foundation}/E_{dam}$ and the damping ratio of the foundation, ξ_f.

Coordinates reduction techniques suitable for the time domain solutions of large linear or locally non linear structural models generally required to represent seismic dam–foundation interaction problems were also examined.

Two types of transformation vectors were presented, the eigenvectors and the derived load dependent Ritz vectors. Their relative performances to represent adequately the seismic load were compared in terms of the rate of convergence as well as the time required for their respective generation. The efficiency of different solution strategies in solving the reduced system of dynamic equilibrium equations in the cases of proportional and non-proportional damping were investigated.

6.2 Conclusions

The results derived from the application of the four proposed earthquake input mechanisms to the idealized dam–foundation–reservoir system have clearly shown that the use of different input models lead to significant differences in the structural response of this type structures. The performance of each of the proposed input models for a wide range of system parameters was established. The main conclusions were that,

1. Model A, the rigid base rock input model, induced very significant artificial amplifications in the response quantities of interest. These artificial amplifications were shown to increase with the level of foundation flexibility. Model A is therefore recognized to be inadequate to evaluate time domain seismic responses of dam-foundation systems and should not be used in practice.

2. The reliability of model C, the deconvolved accelerogram input model, which is theoretically the most accurate model, depends on the quality of the deconvolution analysis. The verification of the deconvolved accelerogram by computing the free-

field response of the finite element foundation model is a mandatory step to ensure accurate results for model C.

3. The use of model D, the free-field input model, led to results which were almost identical to those derived from the theoretically more accurate model C and that was shown to be independent of the levels of flexibility and damping of the foundation rock. Model D can thus be considered the most efficient to evaluate the time domain responses of gravity dam–foundation systems since it is much easier to implement than model C.
4. The good performance of the free-field input model (model D), showed that the assumption of the same free-field accelerogram at all interface nodes is adequate for a concrete gravity dam.
5. The performance of model B, the massless foundation input model, was shown to be dependent on the foundation flexibility, on the level of damping of the massless foundation rock and on the computational procedure retained to form the global damping matrix.
6. For model B, it was shown that in order to obtain a good correlation with models C, D, the damping matrix should be constructed by considering the foundation damping characteristics to be stiffness proportional only, even when similar damping ratios are assigned to the dam and the foundation.
7. For flexible foundation cases ($E_f/E_d \leq 1/4$), very similar results in typical response quantities of interest have been observed between model B, in which the damping was controlled at only the first mode of vibration, and models C, D.
8. For stiffer foundation cases, the numerical results showed that the damping ratio assigned to the foundation in model B should be smaller than the one that would have been retained for the application of models C, D, in order to get an accurate response from this massless foundation model.

The application of coordinates reduction techniques to solve the time domain dynamic equilibrium equations in Chapter 5, lead to the following conclusions:

1. For mass foundation models (models A, C, D), the convergence characteristics of the derived Ritz solution and the eigensolution were very close in the horizontal direction. In the stiffer vertical direction the derived Ritz solution converged more rapidly than the eigensolution.
2. For massless foundation model (model B), the derived Ritz solution and the eigensolution had similar convergence characteristics.
3. Ignoring the inertial effect of the foundation reduces the number of transformation vectors required to represent adequately the seismic load vector.
4. The use of the derived Ritz vectors is advantageous in terms of the cost of the analysis, since the time of generation of the Ritz vectors is approximately one seventh the time required to generate the exact eigenvectors.
5. The structural response obtained from the direct integration of the reduced coupled system of equations (non-proportional damping) expressed in generalized Ritz coordinates, is very close to the solution obtained from a step-by-step integration of the coupled equations expressed in geometric coordinates.
6. Ignoring the off-diagonal terms in the reduced damping matrix and integrating simultaneously the assumed uncoupled equations of motion, showed to be efficient when the damping ratios were computed from the diagonal terms of the reduced damping matrix, especially for cases where the Warburton criterion[50] was satisfied.

6.3 Recommendations and Suggestions for Future Research

In summary, the main recommendations that should be retained from the present study are that the use of model A is inadequate to evaluate the time domain responses of dam–foundation systems. Model D can be considered the most efficient, since it is relatively simple to implement and leads to accurate results. Model B although not as accurate as model D was shown to be able to produce numerical results with an acceptable level of confidence for typical engineering applications if it is implemented following the recommendations presented in Section 6.2. Model B present several practical advantages, first it is relatively simple to implement numerically, second the massless foundation provides a specified amount of flexibility that could be replaced by equivalent linear or non–linear springs resulting in an important reduction in the number of dynamic degrees-of-freedom. In the case where the damping is to be included, dashpots can be used to model the energy dissipation characteristics of the foundation. Concerning the time domain solution of the dynamic equilibrium equations, advantage should be taken from coordinate reduction techniques based on the derived load dependent Ritz transformation vectors that can be adapted to treat locally non linear systems, in order to reduce significantly the computational effort.

The time domain seismic response of large structural systems, such as concrete dam–foundation–reservoir systems, is an area where research is still needed in order to achieve safe and economical design. More specifically, work is needed to include the effect of local and global non–linearities such as uplift and relative slip at the interface of the dam and the foundation, concrete cracking and non–linear foundation behavior. It would be also appropriate to extend the problem to a three–dimensional representation to obtain a more realistic model of the foundation behavior. Investigation on the applicability of the free–field input model in a 3–D representation can be carried out. More work is also needed for a better idealization for time domain solution, of the resevoir system including the effect of water compressibility.

REFERENCES

1. Bureau G.J., "*Critères d'Analyse Sismique des Grands Barrages*", Proceedings of the Third Canadian Conference on Earthquake Engineering, pp. 147-176, Montreal, 1979.

2. Westergaard, H.M., "*Water Pressures on Dams During Earthquakes*", Transactions ASCE, Vol. 98, 1933.

3. Chopra, A.K. and Chakrabarti, P., "*Koyna Earthquake of December 11, 1967 and the Performance of Koyna Dam*", Report UCB/EERC-71/11, Earthquake Engineering Research Center, University of California, Berkeley, 1971.

4. "*Federal Guidelines for Earthquake Analysis and Design of Dams*", Federal Emergency Management Agency, Prepared by Interagency Committee on Dam Safety, Design Earthquake Task Group Committee, FEMA 65, March 1985.

5. "*Design Criteria for Concrete Arch and Gravity Dams*", United States Departement of the Interior, Bureau of Reclamation, Water Resources Technical Publication, Engineering Monograph No. 19.

6. "*A Review of Earthquake Resistant Design of Dams*", International Commission On Large Dams (ICOLD), Committee on earthquakes, Bulletin 27, March 1975.

7. Clough, R.W. and Chopra, A.K., "*Earthquake Response Analysis of Concrete Dams*", Structural and Geotechnical Mechanics, Editor Hall, W.J., Prentice–Hall, 1977.

8. Chopra, A.K., "*Earthquake Behavior of Reservoir–Dam Systems*", Journal of the Engineering Mechanics Division, Proceedings of the American Society of Civil Engineers, ASCE EM6, pp 1475-1500, December 1968.

9. Chopra, A.K., Wilson, E.L. and Farhoomand, I., "*Earthquake Analysis of Reservoir Dam Systems*", Proceedings of the fourth world Conference on Earthquake Engineering, Vol. 2, pp B4 1-10, Santiago, Chile, 1969.

10. Chopra, A.K. and Perumalswami, P.R., "*Dam–Foundation Interaction During Earthquakes*", Proceedings of the Fourth World Conference on Earthquake Engineering, Santiago, Chile, 1969.

11. Chakrabarti, P. and Chopra, A.K., "*Earthquake Response of Concrete Gravity Dams Including Reservoir Interaction Effects*", Report UCB/EERC-72/6 Earthquake Engineering Research Center, University of California, Berkeley, 1972.

12. Fok, K.L. and Chopra, A.K., "*Earthquake Analysis of Arch Dams Including Dam-Water Interaction, Reservoir Boundary Absorption and Foundation Flexibility*", Earthquake Enginering and Structural Dynamics, Vol. 14, No. 2, pp 155-184, 1986.

13. "*Analysis for Soil Structure Interaction Effects for Nuclear Power Plants*", Report by Soil-Structure Group of the Committee on Nuclear Structures and Materials, Structural Division, ASCE, 1979.

14. Lysmer, J., Udaka, T., Tsai, C. and Seed, H.B., "*FLUSH: A Computer Program for Approximate 3-D Analysis of Soil-Structure Interaction Problems*", Report UCB/EERC-75/30, Earthquake Engineering Research Center, University of California, Berkeley, Nov. 1975.

15. Gupta, S., Lin, T.W., Penzien, J. and Yen, C.S., "*Hybrid Modelling of Soil-Structure Interaction*", Report UCB/EERC-80/9, Earthquake Engineering Research Center, University of California, Berkeley, May 1980.

16. Gutieriez, J., "*A Substructure Method for Earthquake Analysis of Soil-Structure Interaction*", Report UCB/EERC-80/9, Earthquake Engineering Research Center, University of California, Berkeley, 1980.

17. Fenves, G. and Chopra, A.K., "*Earthquake Analysis of Concrete Gravity Dams Including Reservoir Bottom Absorption and Dam–Water–Foundation Rock Interaction*", Earthquake Engineering and Structural Dynamics, Vol. 12, pp 663-680, 1984.

18. Fenves, G. and Chopra, A.K., "*EAGD 84: A Computer Program for Earthquake Analysis of Concrete Gravity Dams*", Report UCB/EERC-4/11, Earthquake Engineering Research Center, University of California, Berkeley, August 1984.

19. Fok, K.L., Hall, J.F. and Chopra, A.K., "*EACD-3D: A Computer Program for Three Dimensional Earthquake Analysis of Concrete Dams*" Report UCB/EERC-86/09, Earthquake Engineering Research Center, University of California, Berkeley, July 1986.

20. Wilson, E.L., "*A Method of Analysis for the Evaluation of Foundation-Structure Interaction*", Proceedings of the Fourth World Conference on Earthquake Engineering, Santiago, Chile, 1969.

21. Bayo, E. and Wilson, E.L., "*Numerical Techniques for the Evaluation of Soil Structure Interaction Effects in the Time Domain*", Report UCB/EERC-83/04, Earthquake Engineering Research Center, University of California, Berkeley, February 1983.

22. Clough, R.W. and Penzien, J., "*Dynamics of Structures*", Mc Graw-Hill, 1975.

23. Wolf, J.P., "*Dynamic Soil–Structure Interaction*", Prentice-Hall, 1985.

24. Léger, P. and Wilson, E.L., "*Load Dependent Vector Bases for Earthquake Response Analysis*", Proceedings of the Fifth Canadian Conference on Earthquake Engineering, Ottawa, July 1987.

25. Bayo, E. and Wilson, E.L., "*Finite Element and Ritz Vectors Technique for the Solution of Three Dimensional Soil–Structure Interaction in the Time Domain*", Engineering Computations, Vol. 1, pp 298-311, December 1984.

26. Clough, R.W. and Wilson, E.L., "*Dynamic Analysis of Large Structural Systems with Local Non-Linearities*", Computer Methods in Applied Mechanics and Engineering, Vol. 17/18, pp 107-129, 1979.

27. Khana, J., "*Elastic Soil-Structure Interaction*", Proceedings of the Fourth World Conference on Earthquake Engineering, Santiago, Chile, 1969.

28. Roesset, J.M. and Kim, Y-S., "*Specifications of Control Motions for Embedded Foundations*", Proceedings of the Fifth Canadian Conference on Earthquake Engineering, Ottawa, July 1987.

29. Chopra, A.K., "*Earthquake Analysis, Design and Safety of Concrete Dams*", Proceedings of the Fifth Canadian Conference on Earthquake Engineering, Ottawa, July 1987.

30. Dreher, K.J., "*Seismic Analysis and Design Considerations for Concrete Dams*", Proceedings of a Conference on Dams and Earthquakes Held at the Institution of Civil Engineers, London, October 1980.

31. Reimer, R.B., "*Deconvolution of Seismic Response for Linear Systems*", Report UCB/EERC-73/10, Earthquake Engineering Research Center, University of California, Berkeley, 1973.

32. Clough, R.W., and Chang, K.T., "*Dynamic Interaction Effects in Arch Dams*", Report UCB/EERC-85/11, Earthquake Engineering Research Center, University of California, Berkeley, October 1985.

33. Clough, R.W., "*Non-Linear Mechanisms in the Seismic Response of Arch Dams*", Proceedings of the International research Conference on Earthquake Engineering, pp 669-684, Skopje, Yugoslavia, June/July 1980.

34. Hall, J.F., "*Study of the Earthquake Response of Pine Flat Dam*", Earthquake Engineering and Structural Dynamics, Vol. 14, pp 281-295, 1986.

35. Fok, K.L. and Chopra, A.K., "*Frequency Response Functions for Arch Dams: Hydrodynamic and Foundation Flexibility Effects*", Earthquake Engineering and Structural Dynamics, Vol. 14, pp 769-795, 1986.

36. Schnabel, P.B., Lysmer, J. and Seed, H.B., "*SHAKE A Computer Program for Earthquake Response of Horizontally Layered Sites*", Report UCB/EERC-72/12, Earthquake Engineering Research Center, University of California, Berkeley, 1972.

37. Fenves, G. and Chopra, A.K, "*Earthquake Analysis and Response of Concrete Gravity Dams*", Report UCB/EERC-84/10, Earthquake Engineering Research Center, University of California, Berkeley, September 1984.

38. Zienkiewicz, O.C., "*The Finite Element Method*", Mc Graw Hill, London, 1977.

39. Clough, R.W. and Mojtahedi, S., "*Earthquake response Analysis Considering Non-Proportional Damping*", Earthquake Engineering and Structural Dynamics, Vol. 4, 1976.

40. Lysmer, J. and Kuhlemeyer, R.L., "*Finite Dynamic Model for infinite Media*", Journal of the Engineering Mechanics Division, ASCE, Vol. 95, No.. EM4, pp 859-877, August 1969.

41. Wilson, E.L., "*SAP 80: Structural Analysis Program*", Computers and Structures Inc., Berkeley, California, 1986

42. Wilson, E.L., "*CAL-86: Computer Assisted Learning of Structural analysis and the CAL/SAP Development System*", Report No. UCB/SESM-86/05, University of California, Berkeley, August 1986.

43. "*SPECTR: Spectra Response Analysis*", Dames and Moore, San Fransisco, 1972

44. "*GRAPHER: A Plotting Package*", Golden Software Inc, 1986.

45. *STARDYNE*, User Information Manual, Mechanics Research Inc., Santa Monica, California, 1972

46. Bathe, K.J. and Gracewsky, S., "*On Non-Linear Dynamic Analysis Using Mode Superposition and Substructuring*", Computers and Structures, Vol. 13, 1981.

47. Wilson, E.L., Yuan,M.W. and Dickens, J.M., "*Dynamic Analysis by Direct Superposition of Ritz Vectors*",Earthquake Engineering and Structural Dynamics, Vol. 10, 1982.

48. Léger, P., Wilson, E.L. and Clough, R.W., "*The Use of Load Dependent Vectors for Dynamic and Earthquake Analyses*", Report UCB/EERC-86/04, Earthquake Engineering Research Center, University of California, Berkeley, March 1986.

49. Hansteen, O.E. and Bell, K., "*On the Accuracy of Mode Superposition Analysis in Structural Dynamics*", Earthquake Engineering and Structural Dynamics, Vol. 7, No. 5, 1979.

50. Warburton, G.B. and Soni, S., "*Errors in Reponse Calculations for Non-Classically Damped Structures*", Earthquake Engineering and Structural Dynamics, Vol. 5, pp 365-376, 1977.

51. Roesset, J., Whitman, R.V. and Dobry, R., "*Modal Analysis for Structures with Foundation Interaction*", Journal of the Structural Division, ASCE, Vol. 99, pp 399-416, 1973.

APPENDIX

This appendix includes the results derived from the application of the El Centro accelerogram to the dam–foundation system according to the four proposed earthquake input mechanisms. The horizontal and vertical displacements and accelerations are presented at nodes 1 and 11 (Fig. 4.2), the normal and shear stresses are presented at element 5 (node b). It should be noted that the response quantities are represented by their maximum values (Max) and the corresponding root mean square (R.M.S).

Table A.1 Displacements at Selected Nodal Points, Derived from the Four Input Models, El Centro Earthquake ($\xi_d = 5\%$, $\xi_f = 5\%$).

Moduli Ratio E_f/E_d		1/8		1/4		1/2		1		2		4	
Input Model		R.M.S.D	Max.D (cm)	R.M.S.D	Max.D (cm)	R.M.S.D	Max.D (cm)	R.M.S.D	Max.D (cm)	R.M.S.D	Max.D (cm)	R.M.S.D	Max.D (cm)
Node 1 /Y	A	227.2	32.1	152.7	25.8	128.2	23.4	90.3	19.1	73.5	12.2	66.8	10.3
	B	138.5	15.8	94.1	15.1	92.2	13.8	67.1	12.1	63.2	9.7	60.4	9.17
	C	95.1	12.5	69.2	11.8	93.3	13.1	68.9	12.4	64.2	10.1	62.1	9.4
	D	96.8	12.7	69.3	11.7	81.3	12.9	66.8	12.1	62.9	9.9	62.0	9.3
Node 11 /Y	A	83.9	11.7	46.5	8.2	34.3	5.3	20.8	3.5	16.2	2.3	14.1	1.8
	B	51.4	5.9	30.2	4.5	25.2	4.0	16.2	2.7	13.8	2.0	12.6	1.7
	C	36.0	4.7	22.9	3.5	23.2	3.7	16.7	2.8	13.9	1.9	12.9	1.7
	D	36.7	4.8	22.9	3.4	22.7	3.7	16.1	2.7	13.6	1.9	12.8	1.7
Node 1 /Z	A	75.3	10.8	47.8	7.9	37.8	7.1	26.1	5.8	21.0	3.6	19.0	2.8
	B	44.2	5.1	28.5	4.7	26.9	4.1	19.2	3.4	18.0	2.8	17.0	2.6
	C	30.3	4.2	20.9	3.5	24.3	3.8	19.7	3.5	18.2	2.9	17.5	2.6
	D	30.8	4.2	20.9	3.6	23.7	3.8	19.1	3.4	17.8	2.8	17.4	2.6
Node 11 /Z	A	64.4	9.2	36.3	6.2	26.0	4.5	16.0	3.2	12.4	1.8	11.0	1.7
	B	37.7	4.4	22.0	3.5	18.7	2.8	12.2	2.0	10.7	1.6	9.8	1.5
	C	26.2	3.6	16.4	2.6	17.2	2.7	12.6	2.1	10.8	1.6	10.1	1.5
	D	26.6	3.7	16.5	2.6	16.7	2.7	12.2	2.0	10.6	1.6	10.1	1.5

Table A.2 Acceleration at Selected Nodal Points, Derived from the Four Input Models, El Centro Earthquake ($\xi_d = 5\%$, $\xi_f = 5\%$).

Moduli Ratio E_f/E_d		1/8		1/4		1/2		1		2		4	
	Input Model	R.M.S.A	Max.A (m/s^2)	R.M.S.A	Max.A (m/s^2)	R.M.S.A	Max.A (m/s^2)	R.M.S.A	Max.A (m/s^2)	R.M.S.A	Max.A (m/s^2)	R.M.S.A	Max.A (m/s^2)
Node 1 /Y	A	172.9	30.7	214.3	34.1	212.1	64.3	223.0	54.7	202.9	39.6	178.4	38.3
	B	98.3	17.38	110.3	21.1	140.0	29.7	133.1	27.4	141.2	25.3	134.2	24.4
	C	61.1	9.4	67.6	15.6	108.6	16.9	116.9	24.9	133.7	23.0	137.7	25.0
	D	61.1	9.4	68.7	16.2	108.1	16.9	128.4	27.3	128.4	21.6	136.9	24.1
Node 11 /Y	A	60.0	5.6	59.2	11.1	51.6	9.0	47.6	10.3	67.9	11.8	62.4	13.8
	B	31.7	4.9	29.2	5.8	34.8	7.3	32.6	7.7	37.1	7.9	37.0	6.9
	C	19.4	2.8	20.3	3.6	31.6	6.0	26.8	5.5	29.6	5.9	36.9	7.3
	D	19.8	3.1	20.6	3.9	32.6	6.1	31.4	7.5	28.4	5.8	36.4	7.1
Node 1 /Z	A	34.4	6.8	50.0	8.6	57.4	13.2	68.6	17.1	66.4	13.9	66.7	12.1
	B	21.4	4.1	28.3	5.6	38.2	8.0	40.9	7.4	43.1	8.6	41.5	7.8
	C	13.8	2.3	17.9	4.2	27.8	4.5	32.0	6.4	39.3	7.3	41.5	7.2
	D	13.8	2.4	18.2	4.6	29.0	4.6	38.8	7.4	37.5	6.8	41.2	7.2
Node 11 /Z	A	49.5	7.3	54.2	8.6	42.6	8.7	40.3	9.0	48.0	7.9	54.9	10.5
	B	32.9	5.4	25.8	5.2	27.2	6.2	23.5	4.4	23.8	4.9	23.6	4.7
	C	14.9	2.7	14.2	2.6	22.5	4.1	21.5	4.3	20.8	3.5	24.3	4.3
	D	14.6	2.8	14.3	2.6	22.1	4.4	22.8	4.4	20.4	3.4	23.4	3.9

Table A.3 Stresses at Element 5 (Node b), Derived from the Four Input Models, El Centro Earthquake ($\xi_d = 5\%$, $\xi_f = 5\%$).

Moduli Ratio E_f/E_d		1/8		1/4		1/2		1		2		4	
Input Model		R.M.S.S	Max.S (MPa)	R.M.S.S	Max.S (MPa)	R.M.S.S	Max.S (MPa)	R.M.S.S	Max.S (MPa)	R.M.S.S	Max.S (MPa)	R.M.S.S	Max.S (MPa)
σ_{yy}	A	7.84	1.12	7.79	1.32	7.95	1.54	6.32	1.28	5.72	1.1	5.94	1.22
	B	4.85	0.64	4.63	0.80	5.69	0.94	4.73	0.89	4.80	0.74	4.79	0.78
	C	3.18	0.41	3.27	0.58	5.06	0.83	4.82	0.94	4.85	0.81	4.88	0.69
	D	3.22	0.42	3.28	0.59	4.94	0.84	4.70	0.88	4.77	0.71	4.88	0.71
σ_{zz}	A	57.04	8.99	60.96	10.03	62.39	13.11	55.66	13.58	49.06	9.43	44.36	7.72
	B	34.63	5.10	34.68	6.36	43.36	7.72	37.73	7.45	38.50	6.54	38.00	6.11
	C	22.31	3.03	23.68	4.85	37.21	5.80	36.53	7.12	38.57	6.40	39.08	6.23
	D	22.58	3.06	23.85	5.01	36.50	5.73	37.14	7.42	37.53	6.20	38.93	6.16
σ_{yz}	A	5.00	0.69	4.40	0.80	4.62	0.69	3.81	0.75	4.28	0.68	4.42	0.79
	B	3.20	0.37	2.91	0.48	3.46	0.57	2.94	0.48	3.00	0.48	3.04	0.45
	C	2.13	0.28	2.14	0.32	3.07	0.54	2.89	0.47	2.80	0.38	3.05	0.42
	D	2.17	0.29	2.15	0.32	3.07	0.54	2.89	0.47	2.80	0.38	3.05	0.42

Table A.4 Displacements at Selected Nodal Points, Derived from the Four Input Models, El Centro Earthquake ($\xi_d = 5\%$, $\xi_f = 10\%$).

Moduli Ratio E_f/E_d		1/8		1/4		1/2		1		2		4	
Input Model		R.M.S.D	Max.D (cm)	R.M.S.D	Max.D (cm)	R.M.S.D	Max.D (cm)	R.M.S.D	Max.D (cm)	R.M.S.D	Max.D (cm)	R.M.S.D	Max.D (cm)
Node 1 /Y	A	194.1	26.0	126.5	23.1	120.3	22.1	86.1	18.0	71.8	12.0	64.8	10.0
	B	85.6	10.9	64.7	12.3	66.1	11.6	57.3	10.4	56.2	8.9	56.0	8.4
	C	90.5	11.4	66.0	11.4	79.0	12.8	67.0	11.9	61.9	9.7	60.1	9.1
	D	87.9	11.2	63.0	11.1	77.5	12.7	66.0	11.8	61.9	9.7	60.1	9.1
Node 11 /Y	A	72.2	9.3	39.4	7.3	32.5	5.1	20.2	3.3	15.7	2.3	13.7	1.8
	B	31.7	3.9	20.7	3.6	18.1	3.3	13.9	2.4	12.3	1.8	11.6	1.6
	C	34.3	4.2	21.8	3.3	22.1	3.7	16.2	2.7	13.4	1.9	12.5	1.7
	D	33.3	4.2	20.8	3.2	21.7	3.6	16.1	2.7	13.4	1.9	12.5	1.7
Node 1 /Z	A	63.4	8.8	39.3	7.1	35.4	6.6	24.8	5.4	20.5	3.5	18.4	2.7
	B	27.0	3.5	19.5	3.8	19.2	3.4	16.3	3.0	15.8	2.5	15.8	2.4
	C	28.7	3.7	19.9	3.5	23.1	3.8	19.1	3.4	17.5	2.8	16.9	2.6
	D	27.9	3.6	19.0	3.4	22.6	3.7	18.8	3.4	17.5	2.8	16.9	2.6
Node 11 /Z	A	54.4	7.4	30.1	5.5	24.5	4.3	15.5	3.0	12.1	1.8	10.7	1.7
	B	22.9	2.8	15.0	2.8	13.4	2.4	10.5	1.7	9.5	1.5	9.1	1.3
	C	24.8	3.2	15.7	2.6	16.3	2.7	12.3	2.1	10.5	1.6	9.8	1.4
	D	24.1	3.1	15.0	2.5	16.0	2.6	12.1	2.0	10.5	1.6	9.8	1.4

Table A.5 Acceleration at Selected Nodal Points, Derived from the Four Input Models, El Centro Earthquake ($\xi_d = 5\%$, $\xi_f = 10\%$).

Moduli Ratio E_f/E_d		1/8		1/4		1/2		1		2		4	
	Input Model	R.M.S.A	Max.A (m/s^2)	R.M.S.A	Max.A (m/s^2)	R.M.S.A	Max.A (m/s^2)	R.M.S.A	Max.A (m/s^2)	R.M.S.A	Max.A (m/s^2)	R.M.S.A	Max.A (m/s^2)
Node 1 /Y	A	138.4	26.0	163.8	30.3	189.4	43.2	189.8	49.9	183.0	38.1	170.4	37.4
	B	61.8	12.5	72.8	17.6	95.6	21.3	100.6	23.6	112.2	23.0	117.0	22.8
	C	55.8	9.3	64.0	15.3	102.7	17.1	109.3	23.8	122.8	22.5	131.8	24.1
	D	54 9	9.6	62.5	15.6	101.7	17.2	107.1	24.0	122.9	22.1	132.1	23.8
Node 11 /Y	A	48.2	7.5	46.0	9.7	46.4	8.3	42.3	9.1	56.8	11.1	58.7	12.7
	B	20.1	2.9	20.1	4.6	24.4	5.8	24.8	5.6	28.1	6.4	30.3	7.1
	C	18.3	2.5	19.3	3.8	29.7	5.7	25.5	5.1	26.7	5.5	34.7	7.1
	D	18.2	2.7	18.9	3.7	29.7	6.0	26.3	5.6	27.3	5.9	35.0	6.9
Node 1 /Z	A	27.1	5.7	38.2	7.4	49.8	11.7	56.9	15.2	58.0	12.5	61.2	10.8
	B	13.4	3.1	18.0	4.7	25.2	5.7	28.4	6.2	32.5	6.1	35.4	6.1
	C	12.0	2.3	16.3	4.2	26.1	4.6	29.2	6.3	35.1	6.2	39.4	6.8
	D	12.0	2.4	16.4	4.4	26.1	4.7	28.8	6.2	35.2	6.2	39.6	7.0
Node 11 /Z	A	37.0	5.8	40.2	7.5	37.9	7.7	33.1	7.5	38.0	6.4	48.3	9.7
	B	14.4	2.2	15.6	3.5	18.3	4.5	17.9	4.1	19.6	3.8	20.3	3.9
	C	12.5	2.3	13.7	2.7	21.1	4.1	20.1	4.1	19.7	3.3	22.3	3.8
	D	12.5	2.3	13.3	2.6	20.7	4.2	20.2	4.4	19.7	3.3	22.3	3.9

Table A.6 Stresses at Element 5 (Node b), Derived from the Four Input Models, El Centro Earthquake ($\xi_d = 5\%$, $\xi_f = 10\%$).

Moduli Ratio E_f/E_d		1/8		1/4		1/2		1		2		4	
Input Model		R.M.S.S	Max.S (MPa)	R.M.S.S	Max.S (MPa)	R.M.S.S	Max.S (MPa)	R.M.S.S	Max.S (MPa)	R.M.S.S	Max.S (MPa)	R.M.S.S	Max.S (MPa)
σ_{yy}	A	6.63	0.97	6.35	1.19	7.43	1.43	6.02	1.21	5.52	1.00	5.66	1.09
	B	3.05	0.42	3.21	0.65	4.08	0.76	4.03	0.74	4.27	0.68	4.44	0.70
	C	3.01	0.39	3.12	0.58	4.80	0.82	4.67	0.91	4.68	0.77	4.72	0.68
	D	2.92	0.39	2.98	0.55	4.70	0.83	4.61	0.87	4.69	0.77	4.73	0.70
σ_{xx}	A	47.48	7.75	48.62	8.98	57.37	12.07	50.46	12.53	46.40	9.10	42.85	7.58
	B	21.62	3.64	23.60	5.21	30.60	5.74	30.89	6.37	33.29	6.04	34.54	5.81
	C	20.94	2.88	22.51	4.82	35.24	5.75	35.11	6.92	36.62	6.25	37.69	6.11
	D	20.38	2.89	21.65	4.77	34.60	5.72	34.53	6.79	36.61	6.22	37.70	6.08
σ_{yx}	A	4.29	0.54	3.71	0.71	4.35	0.66	3.61	0.67	3.84	0.65	4.16	0.74
	B	2.01	0.25	2.03	0.40	2.49	0.47	2.44	0.40	2.58	0.39	2.70	0.40
	C	2.03	0.25	2.04	0.31	2.95	0.52	2.76	0.48	2.71	0.38	2.94	0.41
	D	1.97	0.25	1.95	0.31	2.91	0.52	2.75	0.48	2.72	0.38	2.95	0.41

Table A.7 Displacements at Selected Nodal Points, Derived from the Four Input Models, El Centro Earthquake ($\xi_d = 5\%$, $\xi_f = 15\%$).

Moduli Ratio E_f/E_d		1/8		1/4		1/2		1		2		4	
	Input Model	R.M.S.D	Max.D (cm)	R.M.S.D	Max.D (cm)	R.M.S.D	Max.D (cm)	R.M.S.D	Max.D (cm)	R.M.S.D	Max.D (cm)	R.M.S.D	Max.D (cm)
Node 1 /Y	A	168.2	22.9	118.8	22.1	113.0	208	83.1	17.2	70.4	11.9	64.2	9.9
	B	73.0	9.9	57.5	11.3	58.4	10.7	53.6	9.6	53.3	8.5	54.0	8.1
	C	82.8	10.1	62.7	11.3	73.4	12.4	65.7	11.8	61.3	9.5	59.8	9.0
	D	79.9	9.9	62.4	11.0	73.6	12.4	64.4	11.5	61.0	9.5	59.6	9.0
Node 11 /Y	A	62.7	8.0	37.4	6.9	30.6	4.9	19.6	3.1	15.3	2.2	13.5	1.8
	B	26.9	3.4	18.4	3.3	16.0	3.1	12.9	2.3	11.7	1.7	11.2	1.6
	C	31.3	3.7	20.7	3.3	20.5	3.5	16.0	2.7	13.3	1.9	12.4	1.7
	D	30.2	3.6	20.6	3.2	20.6	3.5	15.7	2.7	13.2	1.9	12.4	1.7
Node 1 /Z	A	54.5	7.7	36.6	6.8	33.2	6.2	23.8	5.1	20.0	3.5	18.1	2.7
	B	22.9	3.2	17.2	3.4	16.9	3.1	15.25	2.8	15.1	2.4	15.2	2.3
	C	26.3	3.2	18.9	3.5	21.4	3.6	18.7	3.4	17.3	2.7	16.8	2.5
	D	25.3	3.2	18.8	3.4	21.5	3.6	18.4	3.4	17.2	2.7	16.8	2.5
Node 11 /Z	A	46.7	6.4	28.2	5.2	23.0	4.0	15.0	2.8	11.9	1.8	10.5	1.6
	B	19.4	2.5	13.3	2.5	11.8	2.2	9.7	1.6	9.1	1.4	8.8	1.3
	C	22.7	2.8	14.9	2.6	15.2	2.6	12.1	2.0	10.4	1.6	9.7	1.4
	D	21.8	2.7	14.8	2.5	15.2	2.6	11.8	2.0	10.3	1.6	9.7	1.4

Table A.8 Accelerations at Selected Nodal Points, Derived from the Four Input Models, El Centro Earthquake ($\xi_d = 5\%$, $\xi_f = 15\%$).

Moduli Ratio E_f/E_d		1/8		1/4		1/2		1		2		4	
Input Model		R.M.S.A	Max.A (m/s^2)	R.M.S.A	Max.A (m/s^2)	R.M.S.A	Max.A (m/s^2)	R.M.S.A	Max.A (m/s^2)	R.M.S.A	Max.A (m/s^2)	R.M.S.A	Max.A (m/s^2)
Node 1 /Y	A	116.9	22.7	144.7	28.2	173.6	40.3	171.8	46.2	171.3	36.9	161.3	35.3
	B	54.2	11.8	65.5	16.5	84.9	18.9	93.2	21.9	105.4	22.16	111.8	22.2
	C	52.0	9.3	62.6	15.4	95.5	16.9	106.6	24.4	120.7	22.9	130.0	24.0
	D	51.1	9.8	60.4	15.1	95.9	17.2	103.5	23.6	119.5	22.2	128.9	23.5
Node 11 /Y	A	40.8	6.5	41.1	8.8	42.8	7.8	39.2	8.5	50.7	10.6	52.5	10.7
	B	17.5	2.7	18.2	4.3	21.8	5.5	23.1	5.1	26.5	6.4	28.9	7.1
	C	17.1	2.4	18.4	3.7	27.5	5.6	25.1	5.2	26.7	5.7	34.0	6.9
	D	17.0	2.6	18.5	3.7	27.9	5.9	25.3	5.5	26.7	6.0	33.5	6.5
Node 1 /Z	A	22.8	4.9	33.3	6.7	45.2	10.9	50.6	13.8	53.3	11.7	53.9	10.0
	B	11.8	3.0	16.3	4.4	22.4	5.0	25.9	5.8	30.3	5.8	32.8	5.8
	C	11.1	2.2	15.8	3.9	24.4	4.7	28.4	6.4	34.3	6.0	38.8	6.9
	D	11.1	2.4	15.2	4.2	24.5	4.7	27.6	6.1	34.0	5.8	38.4	6.9
Node 11 /Z	A	29.8	4.8	34.5	6.7	34.6	6.9	29.7	6.5	33.2	5.6	38.2	8.0
	B	12.1	2.0	13.7	3.1	16.1	4.1	16.6	3.8	18.5	3.7	19.5	3.7
	C	11.5	2.2	13.6	2.7	19.5	4.1	19.6	4.1	19.8	3.3	21.9	3.9
	D	11.4	2.2	13.1	2.5	19.6	4.2	19.4	4.2	19.8	3.2	21.4	3.8

Table A.9 Stresses at Element 5 (Node b), Derived from the Four Input Models, El Centro Earthquake ($\xi_d = 5\%$, $\xi_f = 15\%$).

Moduli Ratio E_f/E_d		1/8		1/4		1/2		1		2		4	
	Input Model	R.M.S.S	Max.S (MPa)	R.M.S.S	Max.S (MPa)	R.M.S.S	Max.S (MPa)	R.M.S.S	Max.S (MPa)	R.M.S.S	Max.S (MPa)	R.M.S.S	Max.S (MPa)
σ_{yy}	A	5.74	0.85	5.90	1.12	6.97	1.33	5.80	1.15	5.39	0.95	5.39	1.00
	B	2.64	0.39	2.88	0.62	3.63	0.71	3.78	0.69	4.08	0.65	4.30	0.68
	C	2.76	0.35	2.98	0.57	4.46	0.80	4.58	0.88	4.63	0.75	4.70	0.71
	D	2.67	0.35	2.95	0.55	4.74	0.81	4.50	0.85	4.61	0.75	4.69	0.70
σ_{xx}	A	40.75	6.73	44.42	8.46	53.36	11.34	47.46	11.73	44.68	8.85	41.88	7.37
	B	18.73	3.41	21.18	4.80	27.15	5.15	28.84	5.93	31.54	5.78	33.23	5.68
	C	19.26	2.74	21.56	4.69	32.74	5.65	34.40	6.97	36.15	6.29	37.38	6.09
	D	18.64	2.75	21.23	4.66	32.84	5.65	33.63	6.67	35.90	6.21	37.19	6.02
σ_{yx}	A	3.73	0.47	3.52	0.67	4.09	0.65	3.47	0.61	3.61	0.63	3.80	0.69
	B	1.74	0.22	1.83	0.37	2.22	0.44	2.30	0.39	2.46	0.37	2.61	0.39
	C	1.86	0.22	1.94	0.31	2.75	0.49	2.71	0.47	2.69	0.39	2.91	0.41
	D	1.79	0.22	1.94	0.31	2.76	0.50	2.68	0.46	2.68	0.38	2.90	0.39